รายงานวิจัยฉบับสมบูรณ์

โครงการ บทบาทของอนุพันธ์ที่ว่องไวต่อลักษณะความเป็นเซลล์มะเร็งต้นกำเนิดและการดื้อต่อยาเคมีบำบัดในมะเร็งต่อมน้ำเหลือง

โดย ดร.สุดจิต ล้วนพิชญ์พงศ์ และคณะ

พฤษภาคม 2561

สัญญาเลขที่ TRG5980013

รายงานวิจัยฉบับสมบูรณ์

โครงการ บทบาทของอนุพันธ์ที่ว่องไวต่อลักษณะความเป็นเซลล์มะเร็งต้นกำเนิดและการดื้อต่อยาเคมีบำบัดในมะเร็งต่อมน้ำเหลือง

คณะผู้วิจัย	สังกัด
1. ดร.สุดจิต ล้วนพิชญ์พงศ์	มหาวิทยาลัยมหิดล
2. ศ.นพ.สุรพล อิสรไกรศีล	มหาวิทยาลัยมหิดล
3. Prof. Yon Rojanasakul	West Virginia University

สนับสนุนโดยสำนักงานกองทุนสนับสนุนการวิจัยและ
มหาวิทยาลัยมหิดล

Abstract

Project Code : TRG5980013

Project Title : Roles of reactive oxygen species in lymphoma stem cells and chemotherapeutic resistance

Investigator : Dr. Sudjit Luanpitpong
Faculty of Medicine Siriraj Hospital, Mahidol University

E-mail Address : suidjit@gmail.com

Project Period : May 16, 2016 to May 15, 2018

Mantle cell lymphoma (MCL) is an aggressive, incurable non-Hodgkin B-cell lymphoma with disappointing 5-year survival rate. While proteasomal inhibitor bortezomib (BTZ) has remarkably improved therapeutic outcome of relapsed and refractory MCL, substantial numbers of MCL patients are either intrinsic or acquired resistance to BTZ. An increased reactive oxygen species (ROS) is observed in the microenvironment of various aggressive tumors, including B-cell lymphoma, but how ROS affect MCL cellular behaviors is still limit. Superoxide anion ($^{\bullet}O_2^-$), hydrogen peroxide (H_2O_2) and hydroxyl radical ($^{\bullet}OH$) are the primary ROS generated from aerobic cellular metabolism of tumor cells themselves and/or neighboring cells. In the present study, we investigated the roles of $^{\bullet}O_2^-$, H_2O_2 and $^{\bullet}OH$ in the regulation of MCL response to BTZ. Using various known inhibitors and donors of $^{\bullet}O_2^-$, H_2O_2 and $^{\bullet}OH$, we revealed for the first time their distinct roles in BTZ sensitivity through the regulation of cancer stem cells (CSCs). While $^{\bullet}O_2^-$ inhibits CSC-like cells and sensitizes BTZ-induced apoptosis, H_2O_2 conversely enriches CSC-like cells and protects against apoptosis and $^{\bullet}OH$ has minimal effect. We further observed that an anti-apoptotic Mcl-1 and a transcription factor Zeb-1 are favorable targets of O_2^- and H_2O_2, respectively. In addition, we demonstrated that MCL response to BTZ could be sensitized by manipulation of *O*-GlcNAcylation through the inhibition of *O*-GlcNAcase enzyme in the hexosamine biosynthetic pathway. Together, our findings identify the important roles of redox status of the cells and metabolic pathway in MCL drug response, which is imperative to a better understanding of therapeutic resistance of aggressive B-cell lymphoma and could benefit the development of new treatment strategies to achieve long-term control of the disease.

Keywords : apoptosis, cancer stem cells, chemotherapeutic resistance, lymphoma, reactive oxygen species.

บทคัดย่อ

รหัสโครงการ : TRG5980013

ชื่อโครงการ : บทบาทของอนุพันธ์ออกซิเจนที่ว่องไวต่อลักษณะความเป็นเซลล์มะเร็งต้นกำเนิดและการดื้อยาเคมีบำบัดในมะเร็งต่อมน้ำเหลือง

ชื่อนักวิจัย : ดร.สุดจิต ล้วนพิชญ์พงศ์
คณะแพทยศาสตร์ศิริราชพยาบาล มหาวิทยาลัยมหิดล

E-mail Address : suidjit@gmail.com

ระยะเวลาโครงการ : 16 พฤษภาคม 2559 ถึง 15 พฤษภาคม 2561

มะเร็งต่อมน้ำเหลืองชนิดนอน-ฮอดจ์กิน เป็นมะเร็งระบบโลหิตวิทยาที่พบบ่อยที่สุดในประเทศไทย ถึงแม้ว่าผู้ป่วยบางส่วนจะมีการตอบสนองต่อยาเคมีบำบัดเป็นอย่างดี ผู้ป่วยบางส่วนโดยเฉพาะอย่างยิ่งผู้ป่วยมะเร็งต่อมน้ำเหลืองเซลล์เมนเทิลกลับไม่ตอบสนองต่อการรักษาด้วยยาเคมีบำบัดหรือประสบปัญหาการดื้อต่อยาเคมีบำบัด ส่งผลให้ผู้ป่วยมีอัตราการรอดชีวิตระยะห้าปีที่ต่ำมาก งานวิจัยนี้ทำการศึกษาบทบาทของอนุพันธ์ออกซิเจนที่ว่องไวที่พบได้ในสภาวะแวดล้อมบริเวณรอบมะเร็ง ได้แก่ อนุพันธ์ซุปเปอร์ออกไซด์ ไฮโดรเจนเปอร์ออกไซด์ และไฮดรอกซิลเรดิเคิลต่อการตอบสนองค่อยา Bortezomib ของเซลล์มะเร็งต่อมน้ำเหลืองเซลล์เมนเทิล คณะผู้วิจัยใช้สารโมเลกุลขนาดเล็กและสารเคมีหลายชนิดในการควบคุมระดับอนุพันธ์ออกซิเจนที่ว่องไวประเภทต่างๆภายในเซลล์ ผลการวิจัยพบว่าอนุพันธ์ซุปเปอร์ออกไซด์ทำให้เซลล์มีผลยับยั้งประชากรเซลล์มะเร็งต้นกำเนิดต่อมน้ำเหลือง ทำให้เซลล์มะเร็งตอบสนองต่อยา Bortezomib ผ่านการตายแบบอะพอพโทซิสมากขึ้น ในขณะที่อนุพันธ์ไฮโดรเจนเปอร์ออกไซด์กระตุ้นการเพิ่มจำนวนประชาการเซลล์มะเร็งต้นกำเนิดต่อมน้ำเหลืองและเหนี่ยวนำให้เซลล์มะเร็งดื้อต่อยา และอนุพันธ์ไฮดรอกซิลเรดิเคิลไม่ส่งผลอย่างมีนัยสำคัญต่อเซลล์ โปรตีน Mcl-1 และ Zeb-1 ถูกค้นพบว่าเป็นชีวโมเลกุลเป้าหมายหลักของอนุพันธ์ซุปเปอร์ออกไซด์และไฮโดรเจนเปอร์ออกไซด์ในการศึกษานี้ ตามลำดับ นอกจากนี้คณะผู้วิจัยพบว่าเซลล์มะเร็งต่อมน้ำเหลืองเซลล์เมนเทิลจะตอบสนองต่อยา Bortezomib ดีขึ้นเมื่อกระบวนการ *O*-GlcNAcylation ของโปรตีนถูกกระตุ้น ผ่านการยับยั้งเอนไซม์ *O*-GlcNAcase ใน Hexosamine biosynthetic pathway องค์ความรู้พื้นฐานเหล่านี้ช่วยให้เข้าใจถึงปัจจัยสนับสนุนที่ทำให้เซลล์มะเร็งต่อมน้ำเหลืองเซลล์เมนเทิลดื้อต่อยาเคมีบำบัด ซึ่งคาดว่าจะมีประโยชน์ต่อการวางแผนการรักษาโรคมะเร็งแบบโจมตีเป้าหมายในอนาคต

คำหลัก : อะพอพโทซิส, เซลล์มะเร็งต้นกำเนิด, การดื้อต่อยาเคมีบำบัด, มะเร็งต่อมน้ำเหลือง, อนุพันธ์ออกซิเจนที่ว่องไว

Exclusive Summary

โรคมะเร็งต่อมน้ำเหลืองชนิดนอน-ฮอดจ์กิน โดยเฉพาะมะเร็งต่อมน้ำเหลืองเซลล์เมนเทิลเป็นมะเร็งระบบโลหิตที่ผู้ป่วยประสบปัญหาการดื้อต่อยาเคมีบำบัด การศึกษาข้อมูลเชิงลึกเกี่ยวกับปัจจัยทางชีวภาพที่ควบคุมกลุ่มประชากรเซลล์มะเร็งต้นกำเนิดต่อมน้ำเหลืองซึ่งเป็นอุปสรรคสำคัญในการรักษามะเร็งอาจนำไปสู่ประโยชน์ทางคลินิกของการรักษามะเร็งแบบโจมตีเป้าหมาย คณะผู้วิจัยค้นพบอนุพันธ์ออกซิเจนที่ว่องไวที่เฉพาะเจาะจงที่ส่งผลต่อการตอบสนองของเซลล์มะเร็งต่อมน้ำเหลืองเซลล์เมนเทิลต่อยา Bortezomib ผ่านการควบคุมกลุ่มประชากรเซลล์มะเร็งต้นกำเนิดต่อมน้ำเหลือง กล่าวคือ อนุพันธ์ซุปเปอร์ออกไซด์ส่งผลยับยั้งกลุ่มประชากรเซลล์มะเร็งต้นกำเนิดต่อมน้ำเหลืองและช่วยให้เซลล์มะเร็งตอบสนองต่อยาดีขึ้น และอนุพันธ์ไฮโดรเจนเปอร์ออกไซด์กระตุ้นกลุ่มประชากรเซลล์มะเร็งต้นกำเนิดต่อมน้ำเหลืองส่งผลให้เซลล์มะเร็งดื้อต่อยา พร้อมทั้งเสนอแนวทางในการเพิ่มการตอบสนองต่อยา Bortezomib ของเซลล์มะเร็งต่อมน้ำเหลืองเมนเทิลโดยการใช้สารโมเลกุลขนาดเล็กที่กระตุ้นอนุพันธ์ซุปเปอร์ออกไซด์ ยับยั้งอนุพันธ์ไฮโดรเจนเปอร์ออกไซด์ หรือยับยั้งสารชีวโมเลกุล Mcl-1 หรือ Zeb-1 โดยตรง และโดยการใช้สารโมเลกุลขนาดเล็กที่ส่งผลต่อกระบวนการ *O*-GlcNAcylation ผ่านการยับยั้งเอนไซม์ *O*-GlcNAcase

ความสำคัญและที่มาของปัญหา

ในระยะเวลา 30 ปีที่ผ่านมา อุบัติการณ์การเกิดโรคมะเร็งต่อมน้ำเหลืองในประเทศไทยเพิ่มมากขึ้นถึง 150% โดยพบว่ามะเร็งต่อมน้ำเหลืองชนิดนอน-ฮอดจ์กิน (non-Hodgkin lymphoma; NHL) โดยเฉพาะประเภท B-cell มีอุบัติการณ์มากที่สุด ทำให้มะเร็งต่อมน้ำเหลืองชนิด NHL เป็นมะเร็งระบบโลหิตที่พบได้มากที่สุดในประเทศไทย [1,2] ถึงแม้ว่าผู้ป่วย NHL บางส่วนจะมีการตอบสนองที่ดีต่อการรักษาด้วยยาเคมีบำบัด ผู้ป่วยบางส่วนกลับประสบปัญหาการดื้อต่อยาเคมีบำบัด ทำให้ไม่สามารถหายขาดจากโรคได้ [3,4] การศึกษาวิจัยพบว่าระดับ Signaling molecule เช่น อนุพันธ์ออกซิเจนที่ว่องไว (reactive oxygen species; ROS) ที่อยู่ในสภาวะแวดล้อมบริเวณรอบมะเร็ง (tumor microenvironment) มีความสัมพันธ์ต่อลักษณะพฤติกรรมที่รุนแรงของเซลล์มะเร็งและอัตราการรอดชีวิตผู้ป่วย [5] ในเซลล์มะเร็งระบบโลหิต อาทิเช่น มะเร็งเม็ดเลือดขาว ประเภท Acute และ Chronic lymphocytic leukemia และมะเร็งต่อมน้ำเหลืองพบว่าระดับของอนุพันธ์ออกซิเจนที่ว่องไวส่งผลต่อการตอบสนองต่อยาเคมีบำบัดของเซลล์ [6-8] ทั้งนี้เซลล์มะเร็งต้นกำเนิด (cancer stem cells หรือ tumor-initiating cells) ซึ่งเป็นกลุ่มประชากรย่อยของมะเร็งอาจเป็นตัวกลางที่ทำให้เกิดการดื้อต่อยาเคมีบำบัดในมะเร็งประเภทต่างๆ เนื่องจากมันมีความสามารถในการแบ่งตัวเองและเพิ่มจำนวนอย่างไม่มีขีดจำกัด [9-11] การค้นหาปัจจัยที่มีผลต่อจำนวนประชากรเซลล์มะเร็งต้นกำเนิดและกลไกการควบคุมทางชีวโมเลกุลอาจนำไปสู่ประโยชน์ทางคลินิกของการรักษามะเร็งแบบโจมตีเป้าหมาย (target cancer therapy)

การศึกษาพบว่าอนุพันธ์ออกซิเจนที่ว่องไวมีผลต่อการควบคุมจำนวนประชากรของเซลล์ต้นกำเนิดทั้งแบบปกติและแบบมะเร็ง โดยอนุพันธ์ออกซิเจนที่ว่องไวที่ระดับปกติ (physiological level) มีความสำคัญต่อการแบ่งตัวและการเปลี่ยนแปลงไปเป็นเซลล์โลหิตของเซลล์โลหิตต้นกำเนิด (hematologic stem cells; HSCs) ในขณะที่อนุพันธ์ออกซิเจนที่ว่องไวที่ระดับสูงจะยับยั้งการแบ่งตัวและเหนี่ยวนำให้เซลล์เกิดความชรา [12] กระบวนการ Hypomethylation ของยีน Gpx3 ซึ่งทำหน้าที่ควบคุมระดับอนุพันธ์ออกซิเจนที่ว่องไว และระดับของ Gpx3 ที่สูงขึ้นมีความสัมพันธ์กับการเพิ่มจำนวนของเซลล์มะเร็งต้นกำเนิดในมะเร็งเม็ดเลือดขาว [13] แสดงให้ถึงความเกี่ยวข้องของอนุพันธ์ออกซิเจนที่ว่องไวในกระบวนการดังกล่าว อย่างไรก็ตามองค์ความรู้ที่เกี่ยวข้องกับเซลล์มะเร็งต้นกำเนิดต่อมน้ำเหลือง (lymphoma stem cells; LSCs) และการดื้อต่อยาเคมีบำบัดยังมีข้อจำกัด โดยเฉพาะอย่างยิ่งความรู้ความเข้าใจในกลไกทางชีวโมเลกุลที่ควบคุมเซลล์มะเร็งต้นกำเนิดต่อมน้ำเหลือง กลไกที่ควบคุมการดื้อต่อยาเคมีบำบัดที่ถูกเหนี่ยวนำให้เกิดขึ้นภายหลัง (acquired apoptosis resistance) และความเกี่ยวข้องของอนุพันธ์ออกซิเจนที่ว่องไวที่เฉพาะเจาะจง

วัตถุประสงค์

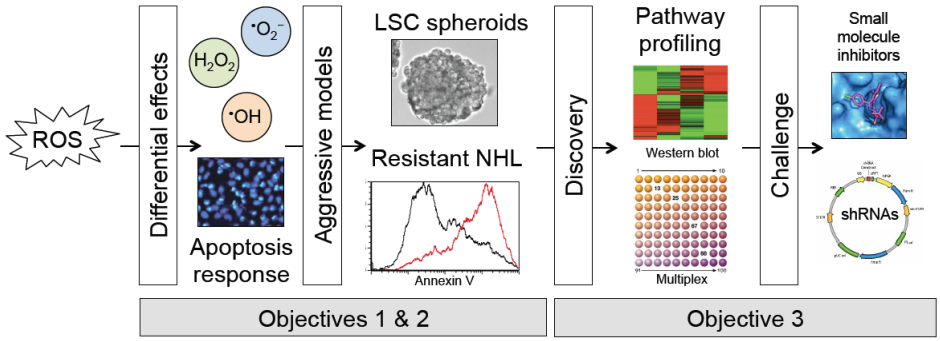

(1) เพื่อศึกษาบทบาทของอนุพันธ์ออกซิเจนที่ว่องไวที่เฉพาะเจาะจงต่อการตอบสนองต่อยาเคมีบำบัดของมะเร็งต่อมน้ำเหลือง

(2) เพื่อศึกษาบทบาทของเซลล์มะเร็งต่อมน้ำเหลืองต้นกำเนิดต่อการดื้อต่อยาเคมีบำบัดที่ถูกเหนี่ยวนำให้เกิดขึ้นภายหลัง

(3) เพื่อศึกษากลไกทางชีวโมเลกุลที่เกี่ยวข้องกับกระบวนการตายแบบอะพอพโทซิสและกระบวนการรอดชีวิตของเซลล์มะเร็งต่อมน้ำเหลืองที่ควบคุมโดยอนุพันธ์ออกซิเจนที่ว่องไว

วิธีการทดลอง

วัตถุประสงค์ที่ (1) เพื่อศึกษาบทบาทของอนุพันธ์ออกซิเจนที่ว่องไวที่เฉพาะเจาะจงต่อการตอบสนองต่อยาเคมีบำบัดของมะเร็งต่อมน้ำเหลือง

ในวัตถุประสงค์นี้ เซลล์มะเร็งต่อมน้ำเหลืองจะได้รับสารที่กระตุ้นหรือยับยั้งอนุพันธ์ออกซิเจนที่ว่องไวที่เฉพาะเจาะจงประเภทต่างๆ และทำการเปรียบเทียบการตอบสนองของยาในกลุ่มที่ได้รับสารต่างๆเทียบกับกลุ่มควบคุม

1.1 การเพาะเลี้ยงเซลล์

เซลล์มะเร็งต่อมน้ำเหลืองชนิดรุนแรง ชนิด Mantle cell lymphoma ซึ่งเป็นมะเร็งต่อมน้ำเหลืองที่รักษาได้หายขาดได้ยากมากที่สุดและเป็นหนึ่งมะเร็งที่มีอุบัติการณ์การดื้อยามากที่สุด [14,15] ได้แก่ เซลล์ Jeko-1 ซึ่งได้รับมาจาก American Type Culture Collection (ATCC, Manassas, VA) และ เซลล์ Granta-519 และ SP-49 ซึ่งได้รับมาจาก อ. ดร.ภก.ศิวนนท์ จิรวัฒโนทัย จะถูกนำมาใช้เป็นโมเดลในการศึกษานี้

1.2 การกระตุ้นหรือยับยั้งอนุพันธ์ออกซิเจนที่ว่องไว

สารที่กระตุ้นหรือยับยั้งอนุพันธ์ออกซิเจนที่ว่องไวที่เฉพาะเจาะจงประเภทต่างๆ แบ่งออกเป็น 3 กลุ่ม ประกอบด้วย: (1) สารกระตุ้นอนุพันธ์ซุปเปอร์ออกไซด์ ($^{\bullet}O_2^-$) ได้แก่ สาร DMNQ และสารยับยั้งอนุพันธ์ $^{\bullet}O_2^-$ ได้แก่ สาร SOD และ MnTBAP; (2) สารกระตุ้นอนุพันธ์ไฮโดรเจนเปอร์ออกไซด์ (H_2O_2) ได้แก่ สาร H_2O_2 และสารยับยั้งอนุพันธ์ H_2O_2 ได้แก่ สาร catalase; และ (3) สารกระตุ้นอนุพันธ์ไฮดรอกซิลเรดิเคิล ($^{\bullet}OH$) ได้แก่ สาร H_2O_2 ควบคู่กับ $FeSO_4$ เพื่อกระตุ้นปฏิกิริยา Fenton reaction และสารยับยั้งอนุพันธ์ $^{\bullet}OH$ ได้แก่ สาร sodium formate (NaFM) ระดับของอนุพันธ์ออกซิเจนที่ว่องไวภายในเซลล์จะถูกตรวจสอบโดยใช้สี Florescent ที่มีความเฉพาะเจาะจงกับอนุพันธ์ประเภทต่างๆ ได้แก่ สี H_2DCF-DA สี DHE และ สี HPF [16,17]

1.3 การให้สารการกระตุ้นหรือยับยั้งอนุพันธ์ออกซิเจนที่ว่องไว

เซลล์จะถูกบ่มด้วยสารที่กระตุ้นหรือยับยั้งอนุพันธ์ออกซิเจนที่ว่องไวที่เฉพาะเจาะจงประเภทต่างๆตามที่ระบุข้างต้นที่ความเข้มข้นไม่เป็นพิษต่อเซลล์เป็นเวลา 3 วัน ซึ่งเป็นระยะเวลาที่นานพอที่จะก่อให้เกิดการเปลี่ยนแปลงของอัตราส่วนประชากรเซลล์มะเร็งต่อมน้ำเหลืองต้นกำเนิด จากนั้นเซลล์ที่ได้รับสารแล้วได้ถูกนำไปทดสอบการตอบสนองต่อยาเคมีบำบัด Bortezomib ซึ่งเป็นยามาตรฐานที่ใช้ในการรักษาโรคมะเร็งต่อมน้ำเหลืองชนิด Mantle cell lymphoma ที่ดื้อต่อยาเคมีบำบัดหรือโรคมะเร็งกลับคืน (relapse) [18] ความเป็นพิษต่อเซลล์ถูกตรวจสอบด้วยการตรวจวัดการตายแบบอะพอพโทซิส โดย Hoechst 33342 assay และ Annexin V-FITC/PI assay

1.4 การตรวจวัดประชากรเซลล์มะเร็งต่อมน้ำเหลืองต้นกำเนิด

ประชากรเซลล์มะเร็งต่อมน้ำเหลืองต้นกำเนิดจะถูกตรวจสอบผ่านความสามารถในการแบ่งตัวทดแทนตัวเอง (self-renewal) ของเซลล์โดย Methylcellulose clonogenicity assay และการตรวจวัด ALDH activity โดยใช้ ALDEFLUOR^{TM} assay

วัตถุประสงค์ที่ (2) เพื่อศึกษาบทบาทของเซลล์มะเร็งต่อมน้ำเหลืองต้นกำเนิดต่อการดื้อต่อยาเคมีบำบัดที่ถูกเหนี่ยวนำให้เกิดขึ้นภายหลัง

การตอบสนองของยาเคมีบำบัดจะถูกเปรียบเทียบระหว่างกลุ่มเซลล์มะเร็งต่อมน้ำเหลืองต้นกำเนิดและกลุ่มเซลล์ปกติ อีกทั้งเปรียบเทียบสัดส่วนของเซลล์มะเร็งต้นกำเนิดในกลุ่มเซลล์ดื้อยาเทียบกับกลุ่มควบคุม

2.1 การคัดแยกประชากรเซลล์มะเร็งต่อมน้ำเหลืองต้นกำเนิด

สามารถทำได้โดยใช้เทคนิคการเพาะเลี้ยงเซลล์มะเร็งต้นกำเนิดต่อมน้ำเหลืองในสภาวะเพาะเลี้ยงพิเศษของ Methylcellulose culture และเทคนิคแยกเซลล์ด้วยเครื่องมือ Fluorescence Activated Cell Sorting จากหลักการที่ว่าเซลล์มะเร็งต่อมน้ำเหลืองต้นกำเนิดจะมี ALDH activity สูงกว่าเซลล์มะเร็งต่อมน้ำเหลืองปกติ

2.2 การตอบสนองต่อยาของเซลล์มะเร็งต่อมน้ำเหลืองต้นกำเนิด

การตอบสนองต่อยา Bortezomib ของเซลล์มะเร็งต้นกำเนิดต่อมน้ำเหลืองที่เพาะเลี้ยงใน Methylcellulose (3D culture) จะถูกเปรียบเทียบกับเซลล์มะเร็งต่อมน้ำเหลืองที่เพาะเลี้ยงในสภาะปกติ (cell suspension) ผ่านการตรวจสอบการตายของเซลล์แบบอะพอพโทซิส

2.3 การสร้างเซลล์มะเร็งต่อมน้ำเหลืองที่ดื้อต่อยาเคมีบำบัด

เซลล์มะเร็งต่อมน้ำเหลืองจะถูกบ่มเพาะด้วยยา Bortezomib ที่ความเข้มข้นที่เพิ่มขึ้นเรื่อยๆเป็นระยะเวลานานกว่า 6 เดือน เซลล์ที่รอดชีวิตจากยา Bortezomib ความเข้มข้นสูงจะถูกเพาะเลี้ยงและได้ตรวจสอบว่ามีความดื้อต่อยาเคมีบำบัดมากกว่า 20 เท่าจะถูกนำมาใช้ในการทดลองต่อไป

วัตถุประสงค์ที่ (3) เพื่อศึกษากลไกทางชีวโมเลกุลที่เกี่ยวข้องกับกระบวนการตายแบบอะพอพโทซิสและกระบวนการรอดชีวิตของเซลล์มะเร็งต่อมน้ำเหลืองที่ควบคุมโดยอนุพันธ์ออกซิเจนที่ว่องไว

การเปลี่ยนแปลงระดับชีวโมเลกุลภายในเซลล์ที่ได้รับสารกระตุ้นหรือยับยั้งอนุพันธ์ออกซิเจนที่ว่องไวที่เฉพาะเจาะจงประเภทต่างๆใช้วิธีการตรวจวิเคราะห์โปรตีนด้วยวิธี Western blot analysis และการตรวจวิเคราะห์ mRNA ด้วยวิธี Real-time PCR arrays

3.1 ชีวโมเลกุลที่เกี่ยวข้องกับการตายของเซลล์แบบอะพอพโทซิส (Apoptosis regulatory pathways)

ชีวโมเลกุลที่เกี่ยวข้องกับการตายแบบอะพอพโทซิส ซึ่งเป็นกลไกหลักของยาเคมีบำบัดในการฆ่าเซลล์มะเร็ง ที่ถูกตรวจสอบแบ่งเป็นชีวโมเลกุลที่เกี่ยวข้องกับการตายผ่าน Mitochondrial pathway ได้แก่ Bcl-2, Bcl-xL, Mcl-1, Bax, Bak, Bim, Noxa และ Puma และชีวโมเลกุลที่เกี่ยวข้องกับการตายผ่าน Death receptor pathway ได้แก่ Fas, c-FLIP, RIP, TNFR, Bid, FADD, TRADD, และ DR5

3.2 ชีวโมเลกุลที่เกี่ยวข้องกับการรอดชีวิตของเซลล์ (Survival signaling pathways)

ชีวโมเลกุลที่เกี่ยวข้องกับการรอดชีวิตที่ถูกตรวจสอบแบ่งเป็นชีวโมเลกุลใน Classical pathways ได้แก่ PI3K/Akt, MAP kinases ERK1/2, JNK, และ p38, และ Hippo signaling pathway เช่น YAP และชีวโมเลกุลกลุ่มใหม่ที่มีรายงานว่าเกี่ยวข้องกับการเจริญของเซลล์มะเร็งต่อมน้ำเหลือง ได้แก่ Epithelial-mesenchymal transition และ Wnt signaling pathways

3.3 การสืบหาวิธีลดการดื้อต่อยาเคมีบำบัดโดยอ้างอิงจากกลไกทางชีวโมเลกุลที่ค้นพบ

เมื่อสืบหาชีวโมเลกุลหลักที่เหนี่ยวนำให้เกิดการดื้อต่อยาเคมีบำบัดแล้ว ผู้วิจัยจะทำการคัดเลือกสารโมเลกุลขนาดเล็ก (Small molecule inhibitors) ที่ยับยั้งการทำงานของชีวโมเลกุลเหล่านั้นเพื่อนำมาทดสอบฤทธิ์การเพิ่ม

ประสิทธิภาพยา Bortezomib (sensitizing effect) ในเซลล์มะเร็งต่อมน้ำเหลืองปกติ เซลล์มะเร็งต่อมน้ำเหลืองต้นกำเนิด และเซลล์มะเร็งต่อมน้ำเหลืองดื้อยา

หมายเหตุ: การวิเคราะห์สถิติของงานวิจัยนี้ จะยึดจากข้อมูลค่าเฉลี่ย Mean ± S.D. ที่ได้จากการทำการทดลองซ้ำสามการทดลองขึ้นไป และเปรียบเทียบกับกลุ่มควบคุม โดยใช้ two-sided Student t test ที่ระดับความน่าเชื่อถือ $p < 0.05$

ผลการทดลอง

มะเร็งต่อมน้ำเหลือง ชนิด Mantle cell lymphoma เป็นมะเร็งที่มีการตอบสนองต่อการรักษาทางคลินิกเป็นอย่างดีในช่วงแรก จากนั้นจะมีการดื้อต่อการรักษาและมีการดำเนินไปของโรคที่รุนแรง ซึ่งรูปแบบของการตอบสนองแล้วดื้อต่อการรักษานี้ชี้ให้เห็นความเป็นไปได้ในการมีอยู่ของประชากรเซลล์มะเร็งต่อมน้ำเหลืองต้นกำเนิด ซึ่งไม่สามารถถูกกำจัดได้ด้วยยาเคมีบำบัด การเปลี่ยนแปลงของกลุ่มประชากรเซลล์มะเร็งต้นกำเนิดต่อมน้ำเหลืองอาจเกิดจากผลกระทบของสารชีวภาพที่พบในสภาวะแวดล้อมของเซลล์มะเร็ง ซึ่งอาจเป็นผลสืบเนื่องจากการได้รับยาเคมีบำบัด [19,20] และส่งผลกระทบต่อเซลล์มะเร็งต้นกำเนิดต่อมน้ำเหลืองหรือเซลล์มะเร็งปกติให้มีความเป็นเซลล์มะเร็งต้นกำเนิดเพิ่มขึ้นหรือลดลงได้ ความเข้าใจในกลไกระดับโมเลกุลและผลของสารชีวภาพที่อยู่ในสภาวะแวดล้อมรอบเซลล์มะเร็งต่อความเป็นเซลล์มะเร็งต้นกำเนิดอาจนำไปสู่การค้นพบเป้าหมายในการออกฤทธิ์ของยาต้านมะเร็งที่มีประสิทธิภาพสูงและอาจแก้ปัญหาการดื้อต่อยาเคมีบำบัดได้ โครงการวิจัยนี้ตรวจพบการมีอยู่ของประชากรเซลล์มะเร็งต้นกำเนิดต่อมน้ำเหลืองชนิด Mantle cell lymphoma ที่มีลักษณะสำคัญของเซลล์มะเร็งต้นกำเนิด ได้แก่ การมี ALHD activity สูง [21-23] มีความสามารถเจริญในสภาวะ semisolid ในรูปแบบของ 3D lymphoma spheroids [24] และการดื้อต่อยาเคมีบำบัด [25,26] โดยสัดส่วนกลุ่มประชากรเซลล์มะเร็งต้นกำเนิดต่อมน้ำเหลืองที่ตรวจพบนี้มีความสัมพันธ์กับระดับสารอนุพันธ์ออกซิเจนที่ว่องไวที่เฉพาะเจาะจงภายในเซลล์

คณะผู้วิจัยใช้สารโมเลกุลขนาดเล็กและสารเคมีหลายชนิดในการควบคุมระดับอนุพันธ์ออกซิเจนที่ว่องไวที่เฉพาะเจาะจงประเภทต่างๆภายในเซลล์ ได้แก่ อนุพันธ์ $^{\cdot}O_2^-$ อนุพันธ์ H_2O_2 และอนุพันธ์ $^{\cdot}OH$ ผลการวิจัยพบว่าอนุพันธ์ออกซิเจนที่ว่องไวที่เฉพาะเจาะจงประเภทต่างๆมีอิทธิพลต่อการตอบสนองต่อยา Bortezomib ของเซลล์แตกต่างกัน โดยการตอบสนองต่อยานี้มีความสัมพันธ์แบบผกผันกับจำนวนกลุ่มประชากรเซลล์มะเร็งต่อมน้ำเหลืองต้นกำเนิด กล่าวคือ ในขณะที่อนุพันธ์ $^{\cdot}O_2^-$ มีผลลดสัดส่วนประชากรเซลล์มะเร็งต้นกำเนิดต่อมน้ำเหลืองและทำให้เซลล์มะเร็งต่อมน้ำเหลืองตอบสนองต่อยามากขึ้น อนุพันธ์ H_2O_2 มีผลเพิ่มสัดส่วนประชากรเซลล์มะเร็งต้นกำเนิดต่อมน้ำเหลืองและทำให้เซลล์มะเร็งต่อมน้ำเหลืองตอบสนองต่อยาลดลง หรือดื้อต่อยาเคมีบำบัด และอนุพันธ์ $^{\cdot}OH$ ไม่มีผลต่อกลุ่มประชากรเซลล์มะเร็งต้นกำเนิดต่อมน้ำเหลืองหรือการตอบสนองต่อยาเมื่อเทียบกับกลุ่มควบคุม เมื่อศึกษากลไกในระดับโมเลกุลพบว่าโปรตีน Mcl-1 และ Zeb-1 เป็นสารชีวโมเลกุลหลักที่ถูกเหนี่ยวนำให้เกิดการเปลี่ยนแปลงโดยอนุพันธ์ $^{\cdot}O_2^-$ และอนุพันธ์ H_2O_2 ตามลำดับ โปรตีน Mcl-1 ซึ่งเป็น Anti-apoptotic protein จะลดระดับลงเมื่อเซลล์มะเร็งต่อมน้ำเหลืองอยู่ในสภาวะที่มีอนุพันธ์ $^{\cdot}O_2^-$ ในระดับที่ไม่เป็นพิษต่อเซลล์ และโปรตีน Zeb-1 ซึ่งเป็น Transcription factor จะถูกเหนี่ยวนำให้เพิ่มขึ้นเมื่อ เซลล์มะเร็งต่อมน้ำเหลืองอยู่ในสภาวะที่มีอนุพันธ์ H_2O_2 โดยที่คณะผู้วิจัยไม่พบการเปลี่ยนแปลงในระดับยีนของ Mcl-1 และ Zeb-1

คณะผู้วิจัยใช้เทคนิคการตัดต่อพันธุกรรมและสารโมเลกุลขนาดเล็กมาช่วยในการยืนยันผลของ Mcl-1 และ Zeb-1 ต่อจำนวนประชากรเซลล์มะเร็งต้นกำเนิดต่อมน้ำเหลือง กล่าวคือ เมื่อเซลล์มีการแสดงออกของโปรตีน Zeb-1 และ Mcl-

1 มากขึ้น กลุ่มประชากรมะเร็งต้นกำเนิดต่อมน้ำเหลืองจะเพิ่มขึ้น และเซลล์จะตอบสนองต่อยา Bortezomib ลดลง เมื่อระดับ Mcl-1 ถูกยับยั้ง กลุ่มประชากรมะเร็งต้นกำเนิดต่อมน้ำเหลืองจะลดลง และเซลล์จะตอบสนองต่อยา Bortezomib ได้ดีขึ้น ทั้งนี้คณะผู้วิจัยไม่สามารถยับยั้งการแสดงออกของโปรตีน Zeb-1 ในเซลล์ได้เนื่องจากโปรตีนชนิดนี้มีการแสดงออกที่ต่ำมากในสภาวะปกติที่ไม่ได้รับการกระตุ้นด้วยอนุพันธ์ H_2O_2

นอกจากระดับของสารอนุพันธ์ออกซิเจนที่ว่องไวที่เฉพาะเจาะจง คณะผู้วิจัยยังพบปัจจัยสำคัญอื่นที่ส่งผลต่อการตอบสนองต่อยา Bortezomib ได้แก่ การเปลี่ยนแปลงภายในเซลล์ที่สืบเนื่องจากการเปลี่ยนแปลงของกระบวนการเมตาบอลิซึมผ่าน Hexosamine biosynthetic pathway ซึ่งเหนี่ยวนำให้เกิดการเปลี่ยนแปลงของโมเลกุลโปรตีนหลังแปลรหัส (Post-translational modification) ที่เรียกว่ากระบวนการ *O*-GlcNAcylation [27,28] กล่าวคือ เมื่อเซลล์มะเร็งต่อมน้ำเหลืองชนิด Mantle cell lymphoma อยู่ในภาวะที่มีระดับ *O*-GlcNAcylation หรือการเติมโมเลกุลน้ำตาล GlcNAc ไปบนโปรตีนสูง เช่น เมื่อบ่มเพาะเซลล์ในสภาวะที่มีน้ำตาลสูง หรือเมื่อเอนไซม์ *O*-GlcNAcase ที่มีหน้าที่ย้ายโมเลกุลน้ำตาลออกจากโปรตีนถูกยับยั้งด้วยสารโมเลกุลขนาดเล็กหรือ CRISPR interference เซลล์มะเร็งต่อมน้ำเหลืองจะตอบสนองต่อยา Bortezomib ได้ดีขึ้นอย่างมีนัยสำคัญ ผ่านกลไกเหนี่ยวนำสัญญาณที่กระตุ้นให้เกิดการตายแบบอะพอพโทซิส ผ่านการยับยั้งการทำลายโปรตีน truncated Bid (tBid) ซึ่งเป็น apoptotic signaling ซึ่งในสภาวะปกติ tBid จะถูกย่อยสลายด้วย Ubiquitin-mediated proteasomal degradation คณะผู้วิจัยยังค้นพบอีกว่ากระบวนการ *O*-GlcNAcylation ส่งผลต่อการตอบสนองต่อยาเคมีบำบัดของมะเร็งชนิดอื่น คือ มะเร็งปอด ซึ่งแม้จะมีผลกระทบไปในทิศทางตรงกันข้ามกับการค้นพบในมะเร็งต่อมน้ำเหลืองชนิด Mantle cell lymphoma แต่แสดงให้ตระหนักถึงความสำคัญของกระบวนการ *O*-GlcNAcylation ต่อการตอบสนองต่อยาและการดำเนินของโรคมะเร็งหลากหลายชนิด

สรุปและวิจารณ์ผลการทดลอง

อนุพันธ์ออกซิเจนที่ว่องไวเป็นสารชีวภาพที่ได้รับการศึกษาและยอมรับว่ามีความสำคัญต่อการแบ่งตัวและการเปลี่ยนแปลงไปเป็นเซลล์โลหิตของเซลล์โลหิตต้นกำเนิด ในงานวิจัยนี้คณะผู้วิจัยได้แสดงให้เห็นเป็นครั้งแรกว่ากลุ่มประชากรเซลล์มะเร็งต้นกำเนิดต่อมน้ำเหลืองสามารถถูกควบคุมด้วยอนุพันธ์ออกซิเจนที่ว่องไว โดยที่อนุพันธ์ออกซิเจนที่ว่องไวที่เฉพาะเจาะจงต่างชนิดกันมีผลแตกต่างกัน ดังที่แสดงให้เห็นในแผนภาพสรุปที่ 1 การเชื่อมโยงอนุพันธ์ H_2O_2 กับการเพิ่มจำนวนประชากรเซลล์มะเร็งต้นกำเนิดต่อมน้ำเหลืองและการดื้อต่อยาเคมีบำบัดแสดงให้เห็นถึงความเข้าใจในกลไกใหม่ที่นำไปสู่การกลับคืนของโรคมะเร็งต่อมน้ำเหลืองชนิดรุนแรง Mantle cell lymphoma ที่พบอุบัติการณ์การกลับคืนของโรคในผู้ป่วยมากกว่าครึ่งหนึ่ง องค์ความรู้ที่ได้จากการวิจัยนี้อาจมีความสำคัญต่อการคาดการณ์การดำเนินของโรคและนำไปสู่การพัฒนาแนวทางในการแก้ปัญหาโรคมะเร็งต่อมน้ำเหลืองดื้อยาแบบโจมตีเป้าหมาย อาทิ การสืบหาสารโมเลกุลขนาดเล็กที่กระตุ้นอนุพันธ์ $^{\bullet}O_2^-$ ยับยั้งอนุพันธ์ H_2O_2 หรือยับยั้งสารชีวโมลกุล Mcl-1 หรือ Zeb-1 โดยตรง

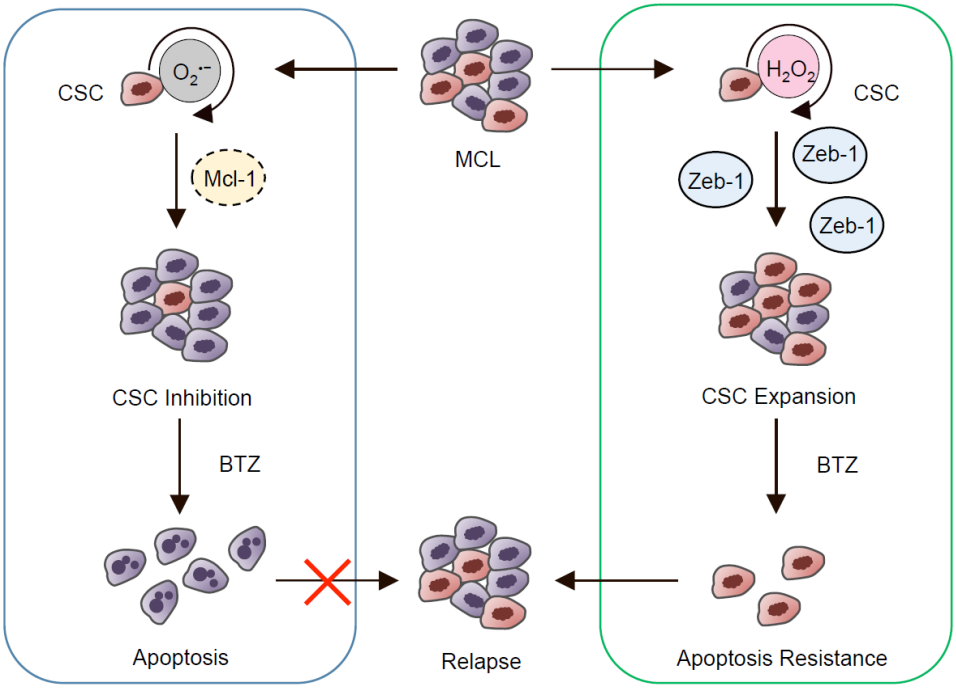

แผนภาพที่ 1 แสดงโมเดลจำลองบทบาทที่ต่างกันของอนุพันธ์ออกซิเจนที่ว่องไวที่เฉพาะเจาะจงต่อประชากรเซลล์มะเร็งต้นกำเนิดต่อมน้ำเหลืองและการตอบสนองต่อยา Bortezomib (BTZ)

การเพิ่มการตอบสนองต่อยา Bortezomib ในเซลล์มะเร็งต่อมน้ำเหลืองชนิด Mantle cell lymphoma อีกแนวทางหนึ่งอาจทำได้โดยการยับยั้งเอนไซม์ *O*-GlcNAcase ที่จะส่งผลยับยั้งกระบวนการ *O*-GlcNAcylation ภายในเซลล์ โดยคณะผู้วิจัยได้เสนอแนวทางการยับยั้งเอนไซม์ *O*-GlcNAcase ด้วยสารโมเลกุลขนาดเล็ก Ketoconazole ซึ่งมีการใช้อย่างแพร่หลายเป็นยาต้านเชื้อรา เนื่องจากมีข้อมูลด้านความปลอดภัยและชีวประสิทธิผลเป็นที่แน่ชัดอยู่แล้ว จึงมีแนวโน้มที่จะสามารถนำมาใช้ในคลินิกได้ในอนาคตอันใกล้

หนังสืออ้างอิง

1. Sukpanichnant S, Sonakul D, Piankijagum A, Wanachiwanawin W, Veerakul G, Mahasandana C, Tanphaichitr VS, Suvatte V.Malignant lymphoma in Thailand: changes in the frequency of malignant lymphoma determined from a histopathologic and immunophenotypic analysis of 425 cases at Siriraj Hospital. Cancer 1998;83:1197-1204.
2. Sukpanichnant S. Analysis of 1983 cases of malignant lymphoma in Thailand according to the World Health Organization classification. Hum Pathol. 2004;35:224-230.
3. Mato AR, Feldman T, Goy A. Proteasome inhibition and combination therapy for non-Hodgkin's lymphoma: from bench to bedside. Oncologist 2012;17:694-707.
4. Maxwell SA, Mousavi-Fard S. Non-Hodgkin's B-cell lymphoma: advances in molecular strategies targeting drug resistance. Exp Biol Med (Maywood). 2013;238:971-990.
5. Quail DF, Joyce JA. Microenvironmental regulation of tumor progression and metastasis. Nat Med. 2013;19:1423-1437.
6. Bossis G, Sarry JE, Kifagi C, Ristic M, Saland E, Vergez F, et al. The ROS/SUMO axis contributes to the response of acute myeloid leukemia cells to chemotherapeutic drugs. Cell Rep. 2014;7:1815-823.
7. Jitschin R, Hofmann AD, Bruns H, Giessl A, Bricks J, Berger J, et al. Mitochondrial metabolism contributes to oxidative stress and reveals therapeutic targets in chronic lymphocytic leukemia. Blood 2014;123:2663-2672.
8. Shacter E, Williams JA, Hinson RM, Sentürker S, Lee YJ. Oxidative stress interferes with cancer chemotherapy: inhibition of lymphoma cell apoptosis and phagocytosis. Blood 2000;96:307-313.
9. Iannolo G, Conticello C, Memeo L, De Maria R. Apoptosis in normal and cancer stem cells. Crit Rev Oncol Hematol. 2008;66:42-51.
10. Tang C, Ang BT, Pervaiz S. Cancer stem cell: target for anti-cancer therapy. FASEB J. 2007;21:3777-3785.
11. Levina V, Marrangoni AM, DeMarco R, Gorelik E, Lokshin AE. Drug-selected human lung cancer stem cells: cytokine network, tumorigenic and metastatic properties. PLoS One 2008 27;3:e3077.
12. Shao L, Li H, Pazhanisamy SK, Meng A, Wang Y, Zhou D. Reactive oxygen species and hematopoietic stem cell senescence. Int J Hematol. 2011;94:24-32.
13. Herault O, Hope KJ, Deneault E, Mayotte N, Chagraoui J, Wilhelm BT, et al. A role for GPx3 in activity of normal and leukemia stem cells. J Exp Med. 2012;209:895-901.
14. Perez-Galan P, Dreyling M, Wiestner A. Mantle cell lymphoma: biology, pathogenesis, and the molecular basis of treatment in the genomic era. Blood 2011;117:26-38.
15. Shah BD, Martin P, Sotomayor EM. Mantle cell lymphoma: a clinically heterogeneous disease in need of tailored approaches. Cancer Control 2012;19:227-235.

16. Luanpitpong S, Talbott SJ, Rojanasakul Y, Nimmannit U, Pongrakhananon V, Wang L, et al. Regulation of lung cancer cell migration and invasion by reactive oxygen species and caveolin-1. J Biol Chem. 2010;285:38832-38840.
17. Chanvorachote P, Luanpitpong S. Iron induces cancer stem cells and aggressive phenotypes in human lung cancer cells. Am J Physiol Cell Physiol. 2016;310:C728-C739.
18. Kouroukis CT, Fernandez LA, Crump M, Gascoyne RD, Chua NS, Buckstein R, et al. A phase II study of bortezomib and gemcitabine in relapsed mantle cell lymphoma from the National Cancer Institute of Canada Clinical Trials Group (IND 172). Leuk Lymphoma. 2011;52:394-399.
19. Al-Gayyar MM, Eissa LA, El-Gayar AM. Measurements of oxidative stress status and antioxidant activity in chronic leukaemia patients. J Pharm Pharmacol. 2007;59:409-417.
20. Battsti V, Maders LDK, Bagatini MD, Santos KF, Spanevello RM, Maldonado PA, et al. Measurement of oxidative stress and antioxidant status in acute lymphoblastic leukemia patients. Clin Biochem. 2008;41:511-518.
21. Brennan SK, Meade B, Wang Q, Merchant AA, Kowalski J, Matsui W. Mantle cell lymphoma activation enhances bortezomib sensitivity. Blood 2010;116:4185-4191.
22. Zhou W, Yang Y, Gu Z, Wang H, Xia J, Wu X, et al. ALDH1 activity identifies tumor-initiating cells and links to chromosomal instability signatures in multiple myeloma. Leukemia. 2014;28:1155-1158.
23. Sullivan JP, Spinola M, Dodge M, Raso MG, Behrens C, Gao B, et al. Aldehyde dehydrogenase activity selects for lung adenocarcinoma stem cells on Notch signaling. Cancer Res. 2010;70:9937-9948.
24. Ikram M, Lim Y, Baek SY, Jin S, Jeong YH, Kwak JY, et al. Co-targeting of Tiam1/Rac1 and Notch ameliorates chemoresistance against doxorubicin in a biomimetic 3D lymphoma model. Oncotarget 2018;9:2058-2075.
25. Kruyt FA, Schuringa JJ. Apoptosis and cancer stem cells: implications for apoptosis targeted therapy. Biochem Pharmacol. 2010;80:423-430.
26. Luanpitpong S, Wang L, Castranova V, Rojanasakul Y. Induction of stem-like cells with malignant properties by chronic exposure of human lung epithelial cells to single-walled carbon nanotubes. Part Fibre Toxicol. 2014;11:22.
27. Bond MR, Hanover JA. A little sugar goes a long way: the cell biology of O-GlcNAc. J Cell Biol. 2015;208:869-880.
28. Józwiak P, Forma E, Brys' M, Krzes'lak A. O-GlcNAcylation and metabolic reprograming in cancer. Front Endocrinol (Lausanne). 2014;5:145.

Output จากโครงการวิจัยที่ได้รับทุนจาก สกว.

ผลงานวิจัยที่ได้รับการสนับสนุนจากโครงการ ได้รับการตีพิมพ์ในวารสารวิชาการระดับนานาชาติ จำนวน 2 เรื่อง

1. **Luanpitpong S**, Chanthra N, Janan M, Poohadsuan J, Samart P, U-Pratya Y, Rojanasakul Y, Issaragrisil S. Inhibition of O-GlcNAcase sensitizes apoptosis and reverses bortezomib resistance in mantle cell lymphoma through modification of truncated Bid. Mol Cancer Ther. 2018;17:484-496.
   ISI Impact Factor (2016/2017): 5.764; Quartile 1 for Cancer Research and Oncology
2. **Luanpitpong S**, Angsutararux P, Samart P, Chanthra N, Chanvorachote P, Issaragrisil S. Hyper-O-GlcNAcylation induces cisplatin resistance via regulation of p53 and c-Myc in human lung carcinoma. Sci Rep. 2017 Sep 6;7:10607.
   ISI Impact Factor (2016/2017): 4.259; Quartile 1 for Multidisciplinary

และผลงานวิจัยที่รอการพิจารณาตอบรับตีพิมพ์ในวารสารวิชาการระดับนานาชาติ จำนวน 1 เรื่อง

1. **Luanpitpong S**, Poohadsuan J, Samart P, Rojanasakul Y, Issaragrisil S. Reactive oxygen species mediate cancer stem-like cells and determine bortezomib sensitivity via Mcl-1 and Zeb-1 in mantle cell lymphoma. [Submitted]

การนำผลงานวิจัยไปใช้ประโยชน์

เชิงสาธารณะ

มีเครือข่ายความร่วมมือและการเชื่อมโยงทางวิชาการกับนักวิชาการท่านอื่นๆ ได้แก่ การร่วมโครงการวิจัยกับ รศ.ภก.ดร.ปิติ จันทร์วรโชติ คณะเภสัชศาสตร์ จุฬาลงกรณ์มหาวิทยาลัย และ ดร.กาญจนา ธรรมนู สถาบันวิจัยแสงซินโครตรอน

เชิงวิชาการ

ใช้ในกระบวนการพัฒนาความรู้ ฝึกกระบวนการคิดและทักษะในห้องปฏิบัติการเพื่อสร้างนักวิจัยรุ่นใหม่ที่มีคุณภาพ จำนวน 2 คน ได้แก่ นางสาวจิรารัตน์ ภูหัดสวน และนางสาวปวีณ์อร อังศุธรารักษ์ และใช้ในการเรียนการสอนนักศึกษาระดับปริญญาเอก จำนวน 1 คน ได้แก่ นายปริญญา สามารถ

กิจกรรมอื่น ๆที่เกี่ยวข้อง

การเสนอผลงานในที่ประชุมวิชาการ

การเสนอผลงานแบบบรรยาย จำนวน 3 ครั้ง

<u>ระดับนานาชาติ</u>

1. หัวข้อ Targeting O-GlcNAcylation for the treatment of mantle cell lymphoma นำเสนอในงานประชุม The University of Texas MD Anderson Cancer Center 2017 Global Academic Programs (GAP) ระหว่างวันที่ 9-11 พฤษภาคม 2560 ณ The University of Texas MD Anderson Cancer Center ประเทศสหรัฐอเมริกา (นำเสนอผลงานวันที่ 11 พฤษภาคม 2560)

2. หัวข้อ Targeting the sweet side of mantle cell lymphoma นำเสนอในงานประชุม The 2nd CU FPhS-RIKEN CBD Symposium and 34th International Annual Meeting in Pharmaceutical Sciences ระหว่างวันที่ 8-9 มีนาคม 2561 ณ โรงแรมอโนมา จังหวัดกรุงเทพมหานคร (นำเสนอผลงานวันที่ 9 มีนาคม 2561)

ระดับชาติ

3. หัวข้อ Redox regulation of bortezomib-induced cell death in mantle cell lymphoma นำเสนอในงานประชุม นักวิจัยรุ่นใหม่ พบ เมธีวิจัยอาวุโส สกว. ครั้งที่ 17 ระหว่างวันที่ 10-12 มกราคม 2561 ณ โรงแรมเดอะรีเจนท์ ชะอำ บีช รีสอร์ท จังหวัดเพชรบุรี (นำเสนอผลงานวันที่ 11 มกราคม 2561)

การเสนอผลงานแบบโปสเตอร์ จำนวน 2 ครั้ง

ระดับนานาชาติ

1. หัวข้อ Redox status dictates the susceptibility of mantle cell lymphoma to bortezomib นำเสนอในงานประชุม The 5th JCA-AACR Special Joint Conference on the Latest Advances in Hematologic Cancer Research: From Basic Science to Therapeutics ระหว่างวันที่ 13-15 กรกฎาคม 2559 ณ Tokyo Bay Maihama Hotel Club Resort ประเทศญี่ปุ่น (นำเสนอผลงานวันที่ 14 กรกฎาคม 2559)
2. หัวข้อ Zeb-1 contributes to the development of chemotherapeutic resistance in mantle cell lymphoma นำเสนอในงานประชุม AACR Annual Meeting 2018 ระหว่างวันที่ 14-18 เมษายน 2561 ณ McCormick Place ประเทศสหรัฐอเมริกา (นำเสนอผลงานวันที่ 15 เมษายน 2561)

รางวัลที่ได้รับ

1. ได้รับทุนสนับสนุน (Travel grant) จาก JCA-AACR เพื่อนำเสนอผลงานและร่วมงานประชุม The 5th JCA-AACR Special Joint Conference on the Latest Advances in Hematologic Cancer Research: From Basic Science to Therapeutics ระหว่างวันที่ 13-15 กรกฎาคม 2559 ณ Tokyo Bay Maihama Hotel Club Resort ประเทศญี่ปุ่น
2. ได้รับทุนวิจัยลอรีอัล ประเทศไทย “เพื่อสตรีในงานวิทยาศาสตร์” (For Women in Science) ประจำปี 2559 สาขาวิทยาศาสตร์ชีวภาพ

ภาคผนวก

Published OnlineFirst November 22, 2017; DOI: 10.1158/1535-7163.MCT-17-0390

Small Molecule Therapeutics

Molecular Cancer Therapeutics

Inhibition of *O*-GlcNAcase Sensitizes Apoptosis and Reverses Bortezomib Resistance in Mantle Cell Lymphoma through Modification of Truncated Bid

Sudjit Luanpitpong[1], Nawin Chanthra[1], Montira Janan[1], Jirarat Poohadsuan[1], Parinya Samart[1,2], Yaowalak U-Pratya[3], Yon Rojanasakul[4], and Surapol Issaragrisil[1,3,5]

Abstract

Aberrant energy metabolism represents a hallmark of cancer and contributes to numerous aggressive behaviors of cancer cells, including cell death and survival. Despite the poor prognosis of mantle cell lymphoma (MCL), due to the inevitable development of drug resistance, metabolic reprograming of MCL cells remains an unexplored area. Posttranslational modification of proteins via *O*-GlcNAcylation is an ideal sensor for nutritional changes mediated by *O*-GlcNAc transferase (OGT) and is removed by *O*-GlcNAcase (OGA). Using various small-molecule inhibitors of OGT and OGA, we found for the first time that *O*-GlcNAcylation potentiates MCL response to bortezomib. CRISPR interference of *MGEA5* (encoding OGA) validated the apoptosis sensitization by *O*-GlcNAcylation and OGA inhibition. To identify the potential clinical candidates, we tested MCL response to drug-like OGA inhibitor, ketoconazole, and verified that it exerts similar sensitizing effect on bortezomib-induced apoptosis. Investigations into the underlying molecular mechanisms reveal that bortezomib and ketoconazole act in concert to cause the accumulation of truncated Bid (tBid). Not only does ketoconazole potentiate tBid induction, but also increases tBid stability through *O*-GlcNAcylation that interferes with tBid ubiquitination and proteasomal degradation. Remarkably, ketoconazole strongly enhances bortezomib-induced apoptosis in *de novo* bortezomib-resistant MCL cells and in patient-derived primary cells with minimal cytotoxic effect on normal peripheral blood mononuclear cells and hepatocytes, suggesting its potential utility as a safe and effective adjuvant for MCL. Together, our findings provide novel evidence that combination of bortezomib and ketoconazole or other OGA inhibitors may present a promising strategy for the treatment of drug-resistant MCL. *Mol Cancer Ther; 17(2); 484–96. ©2017 AACR.*

Introduction

Metabolic reprogramming is a hallmark of cancer that has emerged as an attractive target in novel therapeutic strategies for cancer treatment (1, 2). Mantle cell lymphoma (MCL), an aggressive non-Hodgkin lymphoma (NHL) arising from pregerminal center mature B cells, is typically incurable due to the inevitable development of drug resistance, and thus has the worst prognosis among NHL subtypes (3, 4). However, overcoming MCL resistance particularly through metabolic signaling remains largely an unexplored area.

O-GlcNAcylation is an abundant, dynamic, and nutrient-sensitive posttranslational modification (PTM) that describes an addition of *O*-linked β-*N*-acetylglucosamine (*O*-GlcNAc) moiety to the serine or threonine residues in proteins in response to changes of the sugar donor UDP-GlcNAc from hexosamine biosynthetic pathway (5, 6). As the hexosamine pathway consumes various essential nutrients and metabolic intermediates, for example, glucose and glutamine, acetyl coenzyme A, and nucleotide uridine-5′-triphosphate (UTP), it provides an ideal machinery for cells to sense and respond to a variety of microenvironmental conditions. Alterations in the levels of cycling enzymes *O*-GlcNAc transferase (OGT) and *O*-GlcNAcase (OGA) that catalyzes and removes *O*-GlcNAc, and the levels of *O*-GlcNAcylated proteins themselves, have been linked to many different human malignancies, including breast, lung, colon, prostate, bladder, and leukemia (7–11). In chronic lymphocytic leukemia (CLL), a recent study has shown that indolescent and aggressive clinical behaviors of CLL cells correlate well with the higher and lower levels of *O*-GlcNAc respectively, suggesting the potential involvement of *O*-GlcNAcylation in CLL pathogenesis (11).

Bortezomib has demonstrated impressive clinical efficacy and is FDA-approved for the treatment of relapse/refractory MCL. However, innate and acquired clinical resistance to bortezomib is frequently observed (12, 13). Because many nucleocytoplasmic proteins involved in the proliferation and survival of tumor cells are dramatically modified by *O*-GlcNAcylation, including p53, NFκB, and c-Myc (7, 14, 15), targeting

[1]Siriraj Center of Excellence for Stem Cell Research, Faculty of Medicine Siriraj Hospital, Mahidol University, Bangkok, Thailand. [2]Department of Immunology, Faculty of Medicine Siriraj Hospital, Mahidol University, Bangkok, Thailand. [3]Division of Hematology, Department of Medicine, Faculty of Medicine Siriraj Hospital, Mahidol University, Bangkok, Thailand. [4]WVU Cancer Institute, West Virginia University, Morgantown, West Virginia. [5]Bangkok Hematology Center, Wattanosoth Hospital, BDMS Center of Excellence for Cancer, Bangkok, Thailand.

Note: Supplementary data for this article are available at Molecular Cancer Therapeutics Online (http://mct.aacrjournals.org/).

Corresponding Author: Surapol Issaragrisil, Mahidol University, 2 Siriraj Hospital, Bangkoknoi, Bangkok 10700, Thailand. Phone: 662-419-4446; Fax: 662-411-2012; E-mail: surapolsi@gmail.com

doi: 10.1158/1535-7163.MCT-17-0390

Published OnlineFirst November 22, 2017; DOI: 10.1158/1535-7163.MCT-17-0390

O-GlcNAcylation might represent a rational approach to modulate MCL drug response. In this study, we used small-molecule inhibitors of OGT and OGA cycling enzymes to modify intracellular *O*-GlcNAcylation and to investigate its effect on bortezomib-induced apoptosis. We found that well known OGA inhibitors, including PugNAc and thiamet G (16, 17), sensitize MCL cells to bortezomib-induced apoptosis, while OGT inhibitor alloxan (18, 19) inhibits it. In an attempt to identify potential drug candidates for clinical utility, we further tested the effect of a drug-like OGA inhibitor, ketoconazole (20), on MCL response. Here, we showed that a conventional antifungal drug ketoconazole enhances the susceptibility of multiple parental and *de novo* bortezomib-resistant MCL cells as well as patient-derived primary cells to bortezomib-induced apoptosis. We also unveil the underlying mechanism of sensitization that is OGA inhibitors induce *O*-GlcNAcylation of truncated Bid (tBid) and strengthen apoptosis signaling by abrogating tBid ubiquitin-mediated proteasomal degradation, thus stabilizing tBid and prolonging its action. Our findings also suggest the role of hexosamine metabolic pathway in MCL drug response, which could be important in predicting therapeutic response and in developing new treatment strategies for drug-resistant MCL to achieve long-term control of the disease.

Materials and Methods

Reagents

Bortezomib was obtained from Jannsen-Cilag. Small-molecule inhibitors of OGA PugNAc and thiamet G were obtained from Abcam and Tocris Bioscience, while ketoconazole was obtained from Crosschem Intercontinental Company (Lugano, Switzerland). A small-molecule inhibitor of OGT alloxan and a small-molecule inhibitor of tBid BI-6C9 (21) were obtained from Sigma-Aldrich. Antibodies for ubiquitin and *O*-GlcNAc were obtained from Abcam, while antibody for tBid was from Santa Cruz Biotechnology. All other antibodies and reagents including MG132 and cycloheximide were from Cell Signaling Technology.

Cell lines and patient-derived primary cells

Human MCL-derived Jeko-1 cells were obtained from ATCC, while Granta-519 and SP49 cells were kind gifts of Dr. Siwanon Jirawatnotai (Systems Pharmacology, Faculty of Medicine Siriraj Hospital, Bangkok, Thailand; refs. 22, 23). Mycoplasma contamination was checked every eight weeks using MycoAlert mycoplasma detection kit (Lonza) and any cell lines found positive were discarded. Cells were cultured in RPMI1640 medium containing 10% FBS, supplemented with 2 mmol/L L-glutamine, 100 U/mL penicillin, and 100 μg/mL streptomycin, and maintained in a humidified atmosphere of 5% CO_2 environment at 37° C. Patient-derived primary cells were from fresh biopsy-derived lymphoma tissues (lymph nodes) after informed consent and after approval by the Siriraj Institutional Review Board (#733/2557 EC1). Tissues were diced and forced through a fine metal sieve into RPMI culture medium. Mononuclear cells were then isolated by Ficoll–Hypaque gradient centrifugation and cultured in RPMI medium containing 20% FBS and 10% conditioned medium from MCL Granta-519 cells, as described previously (24). Peripheral blood mononuclear cells (PBMC) from healthy donors were used as normal control cells.

Apoptosis assays

Apoptosis was determined by Hoechst 33342 and Annexin V/propidium iodide (PI) assays. In the Hoechst assay, cells were incubated with 10 μg/mL Hoechst 33342 (Molecular Probes) for 30 minutes and analyzed for apoptosis by scoring the percentage of cells having condensed chromatin and/or fragmented nuclei by fluorescence microscopy (Eclipse Ti-U with NiS-Elements, Nikon). The apoptotic index was calculated as the percentage of cells with apoptotic nuclei over total number of cells. For Annexin V/PI assay, cells were harvested, washed and stained with Annexin V-FITC in binding buffer supplemented with 5 mmol/L calcium chloride for 15 minutes at room temperature and costained with PI (5 μg/mL). Samples were immediately analyzed by BD LSRFortessa flow cytometer (BD Biosciences) using a 488-nm excitation beam and 530-nm and 670-nm band-pass filter with CellQuest software.

Combination index analysis

Combination index (CI) was analyzed by the fixed-ratio model using CompuSyn software (ComboSyn Inc.), which is a computerized analytical simulation using the median-effect principle of the mass-action law and its combination index theorem (25). Cells were treated with 12 concentrations of bortezomib each in combination with 12 concentrations of ketoconazole at the ratio of 1 to 10,000 or 1 to 5,000, and Fa (fraction affected) on cell apoptosis was determined by Hoechst 33342 assay. Each drug was also used alone and each data point was performed in triplicates.

CRISPR interference design and vector construction

CRISPR interference system containing catalytically inactive version of Cas9 (deactivated Cas9; dCas9) and a single guided RNA (sgRNA) was used to induce transcriptional repression of *MGEA5* (encoded OGA). Briefly, sgRNA targeting *MGEA5* (CGCAAGCGCAGTGCGGATAAAC) was designed using CRISPR Design tool (http://crispr.mit.edu/) and cloned into human sgRNA expression vector containing a mouse U6 promoter and a constitutive CMV promoter driving an *mCherry* gene (Addgene, #44248; ref. 26), as described previously (27). The constructed sgRNA plasmid was then transfected into Jeko-1 cells stably expressing human dCas9 vector (Addgene, #44246; ref. 26) by nucleofection using 4D-Nucleofector (Lonza) with EW113 device program. Two weeks after nucleofection, mCherry-positive cells were sorted using flow cytometry–based cell sorter (FACS; BD FACSAria, BD Biosciences), recovered for at least three passages, and analyzed for *MGEA5* by RT-PCR and OGA by Western blotting prior to use.

RNA isolation and RT-PCR

Total RNA was prepared using TRIzol reagent (Invitrogen). cDNA was prepared using SuperScript III first-strand synthesis system and oligo (dT) primers (Invitrogen). qPCR analysis was carried out on a 7500 Fast real-time PCR using a Power SYBR Green PCR master mix (Applied Biosystems). Initial enzyme activation was performed at 95°C for 10 minutes, followed by 40 cycles of denaturation at 95°C for 15 seconds and primer annealing/extension at 60°C for 1 minute. Relative expression of each gene was normalized against the housekeeping *GAPDH* gene product.

Published OnlineFirst November 22, 2017; DOI: 10.1158/1535-7163.MCT-17-0390

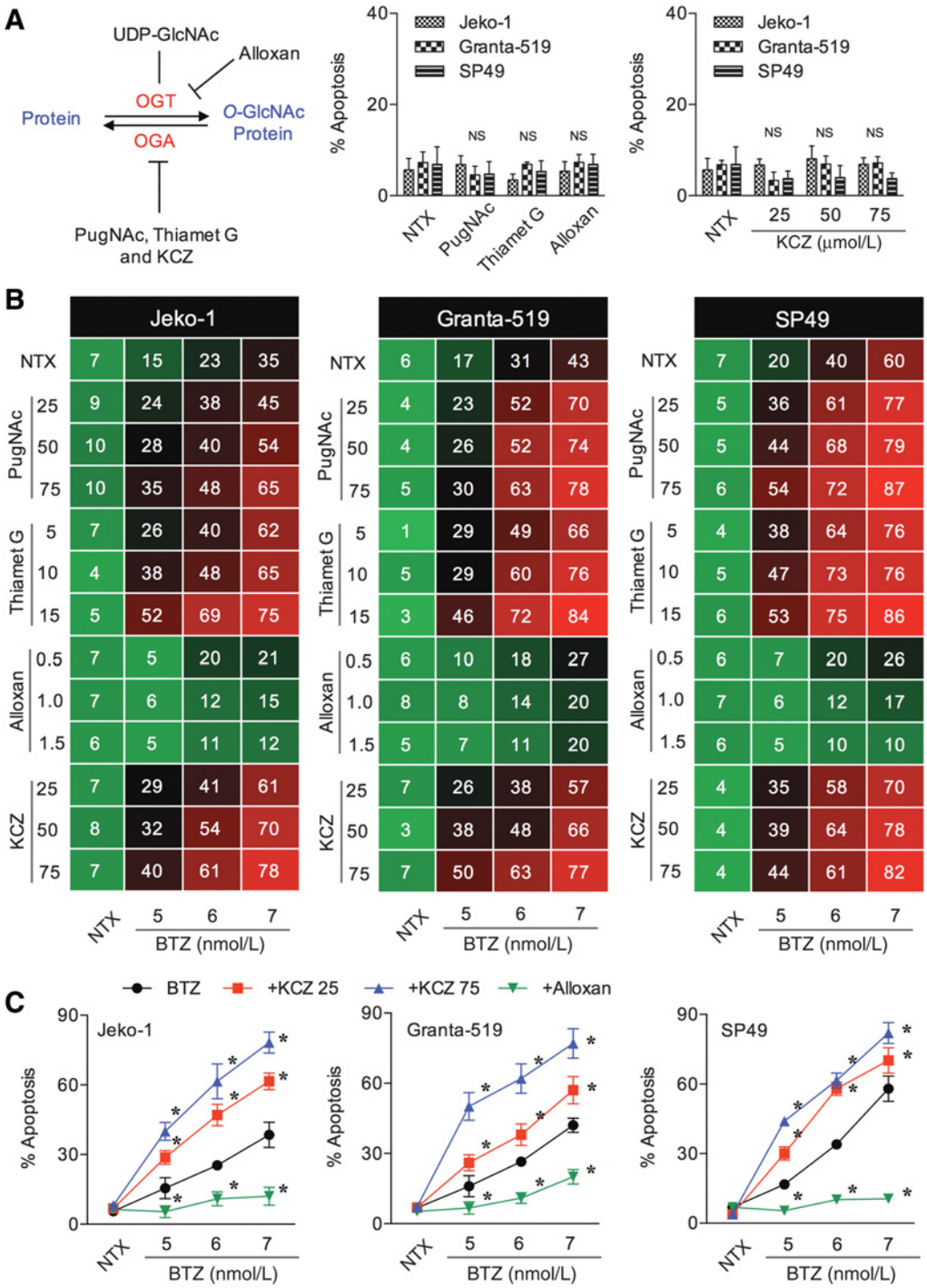

Figure 1.

O-GlcNAcase inhibitors increase the sensitivity of MCL cells to bortezomib (BTZ). **A,** (left) Schematic diagram for the *O*-GlcNAcylation, showing cycling enzymes OGT and OGA, and small-molecule inhibitors that modulate OGA, including PugNAc, thiamet G and ketoconazole (KCZ), and that modulate OGT, including alloxan. (right) Effect of OGT and OGA inhibitors on cell apoptosis to ensure their subcytotoxic concentrations. Data are mean ± SD ($n = 3$). NS, not significance versus nontreated cells; NTX, nontreatment. **B,** Effect of small-molecule OGA or OGT inhibitors on bortezomib-induced MCL cell apoptosis. Cells were treated with bortezomib (0–7 nmol/L) in the presence or absence of PugNAc (25–75 μmol/L), thiamet G (5–15 μmol/L), alloxan (0.5–1.5 mmol/L), or ketoconazole (25–75 μmol/L) and apoptosis was determined after 24 hours by Hoechst 33342 assay. Mean percentage of apoptosis from four independent experiments in Jeko-1, Grant-519, and SP49 cells are shown in the drug dose matrix data in 3-color scale, where green, black, and red indicate lowest, midpoint, and highest apoptosis, respectively (see also Supplementary Table S1 for raw data and statistical analysis). **C,** Percentage of apoptosis in response to bortezomib and drug-like OGA or OGT inhibitor cotreatment is plotted. Data are mean ± SD ($n = 4$). *, $P < 0.05$ versus bortezomib-treated cells; two-sided Student *t* test.

Published OnlineFirst November 22, 2017; DOI: 10.1158/1535-7163.MCT-17-0390

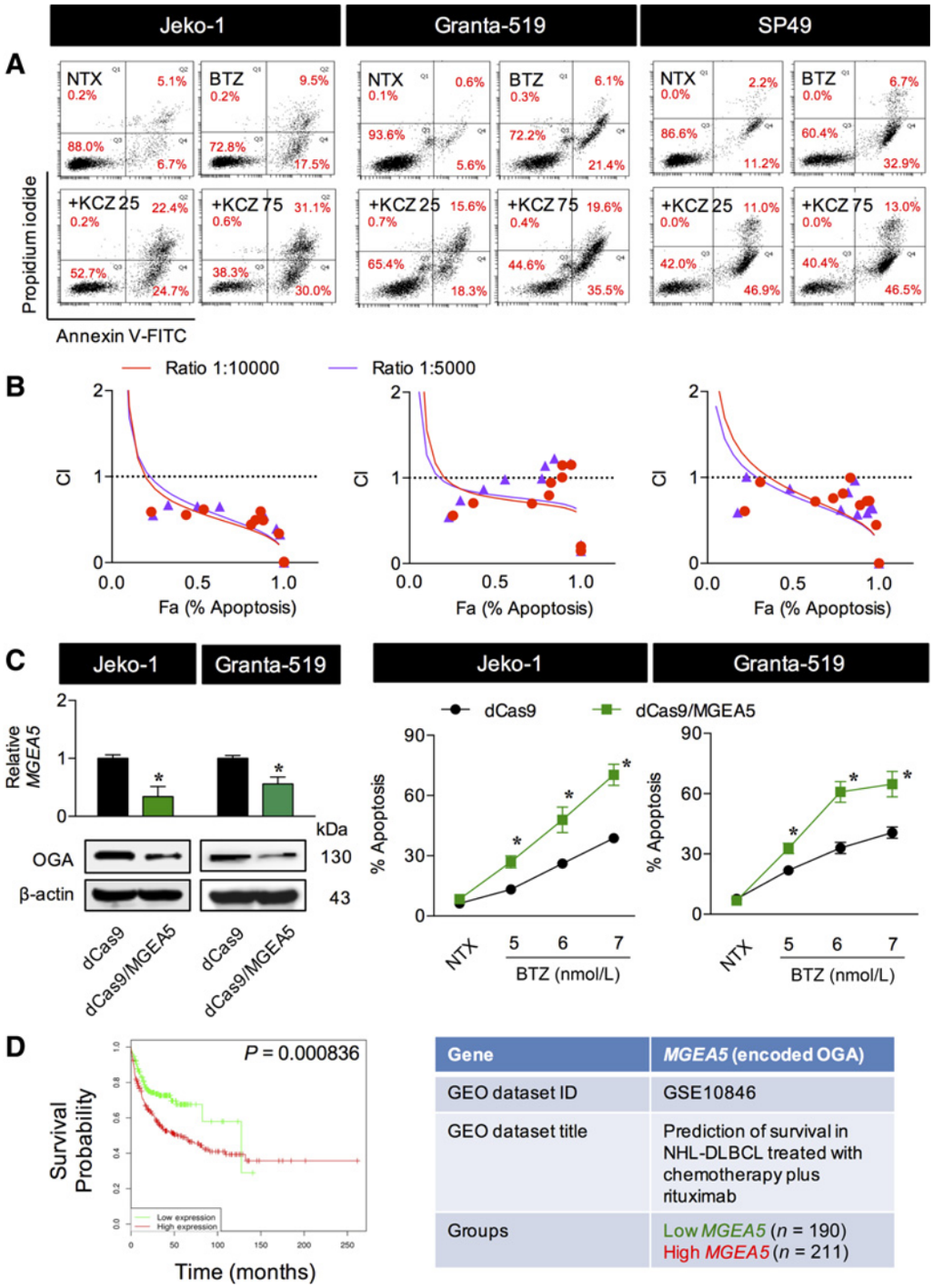

Figure 2.

Drug-like OGA inhibitor ketoconazole (KCZ) sensitizes MCL cells to bortezomib (BTZ)-induced apoptosis. **A,** MCL cells were treated with bortezomib (6 nmol/L) in the presence of increasing concentrations of ketoconazole (0–75 μmol/L) for 24 hours and analyzed for apoptosis and necrosis by flow cytometry using Annexin V and propidium iodide (PI) as probes. Representative dot plots of Annexin V (*x*-axis) and PI (*y*-axis) are shown. Early and late apoptotic cells are in the lower and upper right quadrants with Annexin V positive. NTX, nontreatment. **B,** Combination index (CI) analysis by the fixed-ratio model. MCL cells were treated with bortezomib and ketoconazole at the ratio of 1 to 10,000 and 1 to 5,000 and CI values were calculated and predicted (trendlines) using CompuSyn software. CI = 1, additivity; CI > 1, antagonism; CI < 1, synergy. **C,** Transcriptional repression of *MGEA5* (encoding OGA) was performed using CRISPR interference. (left) Quantitative real-time PCR of *MGEA5* mRNA expression and Western blot analysis of OGA protein level in control (dCas9) and OGA-knockdown (dCas9/MGEA5) Jeko-1 and Granta-519 cells. (right) Effect of OGA inhibition on bortezomib-induced apoptosis. Cells were treated with bortezomib (0–7 nmol/L) for 24 hours and apoptosis was determined by Hoechst 33342 assay. Data are mean ± SD ($n = 3$). *, $P < 0.05$ versus bortezomib-treated dCas9 control cells; two-sided Student *t* test. **D,** Kaplan–Meier survival curve of patients with DLBCL, segregated according to high (red) or low (green) expression of *MGEA5* (encoding OGA), obtained from public database through a bioinformatics analysis using PPISURV (www.bioprofiling.de).

Published OnlineFirst November 22, 2017; DOI: 10.1158/1535-7163.MCT-17-0390

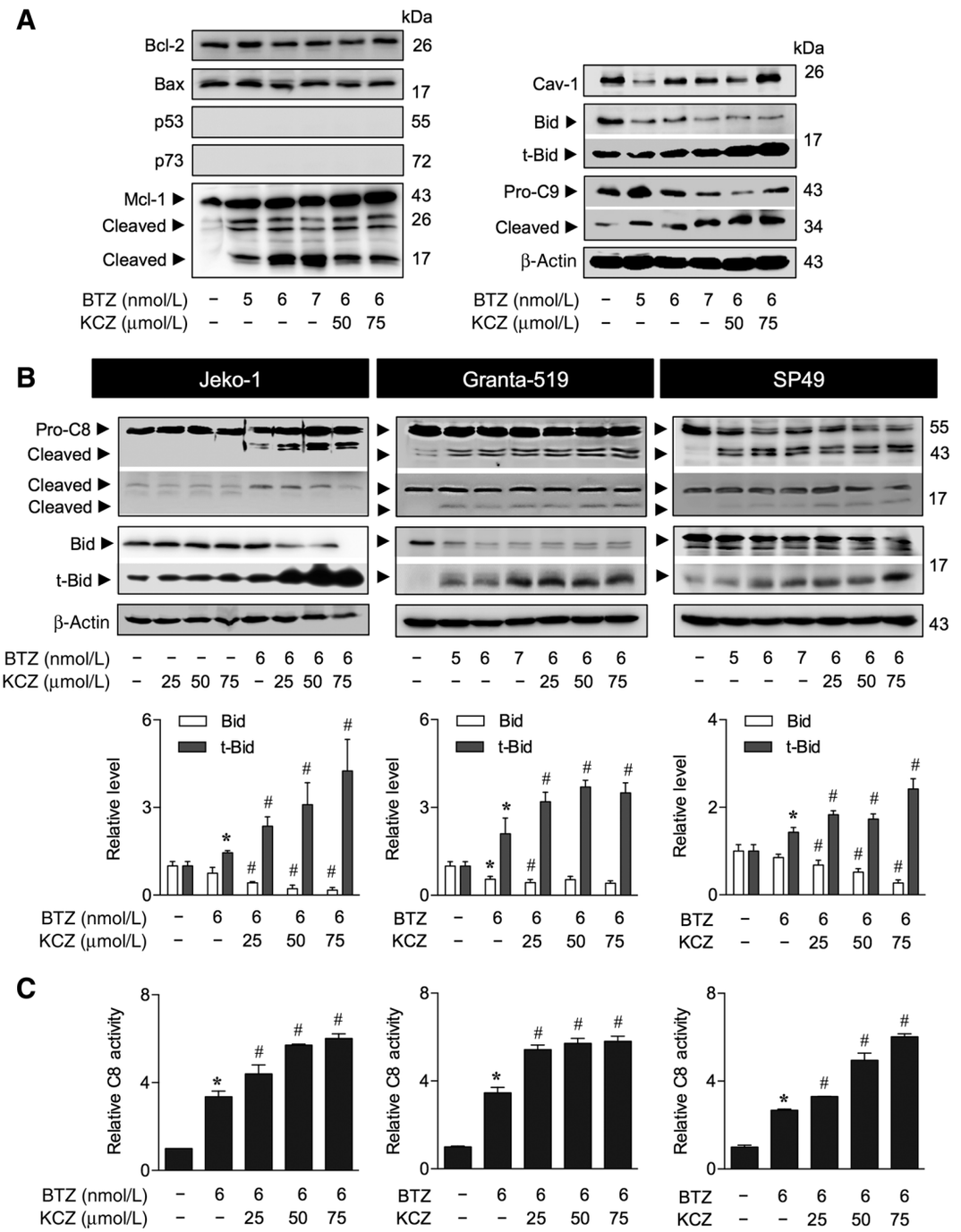

Figure 3.

Drug-like OGA inhibitor ketoconazole (KCZ) cleaves Bid to its truncated active form tBid. **A,** Analysis of apoptosis-signaling proteins in response to bortezomib (BTZ) and ketoconazole cotreatment. MCL Jeko-1 cells were treated with various concentrations of bortezomib (0–7 nmol/L) and ketoconazole (25–75 μmol/L) for 24 hours and analyzed for key apoptosis-regulatory proteins, including Bcl-2, Bax, p53, p73, Mcl-1, caveolin-1 (Cav-1), Bid, and caspase-9 (C9) using Western blotting. Blots were reprobed with anti-β-actin antibody to confirm equal loading of the samples. **B,** Ketoconazole potentiates caspase-8 activation and Bid cleavage in bortezomib-treated cells. Cells were treated with various concentrations of bortezomib and ketoconazole for 24 hours and the levels of pro- and activated caspase-8 (C8) as well as Bid and tBid were determined by Western blotting. Quantitative analysis of Bid and tBid by densitometry is shown. Data are mean ± SD ($n = 4$). *, $P < 0.05$ versus nontreated cells; two-sided Student t test. #, $P < 0.05$ versus bortezomib-treated cells; two-sided Student's t test. **C,** C8 activity was evaluated in the cells treated with bortezomib (6 nmol/L) and increasing concentrations of ketoconazole (0–75 μmol/L) for 16 hours using the fluorometric substrate IETD-AFC. Data are mean ± SD ($n = 3$). Data are mean ± SD ($n = 3$). *, $P < 0.05$ versus nontreated cells; two-sided Student t test. #, $P < 0.05$ versus bortezomib-treated cells; two-sided Student t test.

Published OnlineFirst November 22, 2017; DOI: 10.1158/1535-7163.MCT-17-0390

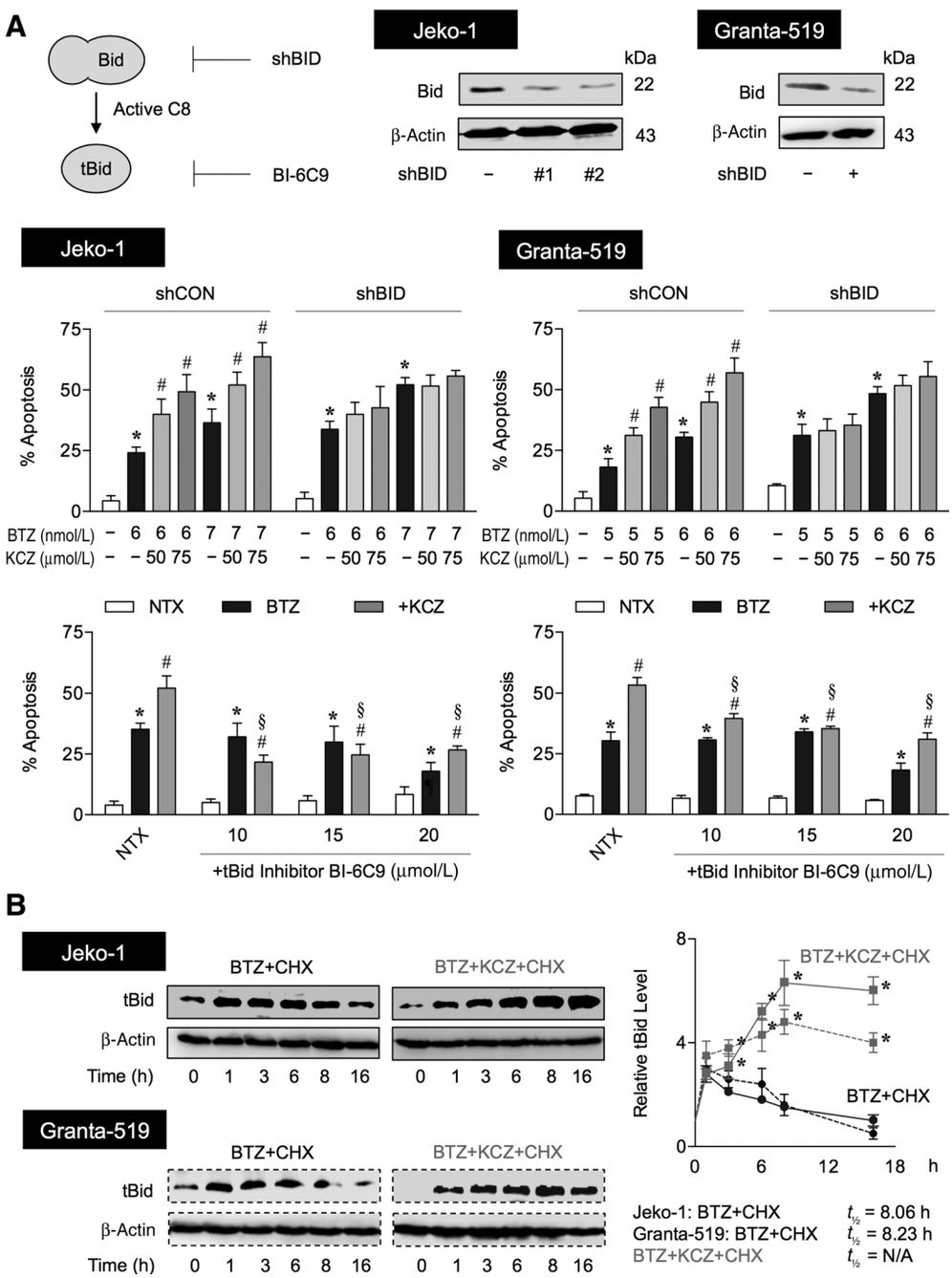

Figure 4.

tBid is a key mediator of ketoconazole (KCZ) sensitization of bortezomib (BTZ)-induced apoptosis. **A,** (upper) A schematic diagram for the inhibition of truncated Bid (tBid) using a small-molecule inhibitor of tBid (BI-6C9) and RNA interference of Bid (shBID) in MCL Jeko-1 and Granta-519 cells. Middle, inhibition of Bid by shBid diminishes the sensitizing effect of ketoconazole on bortezomib-induced apoptosis. shCON and shBID cells were similarly treated with bortezomib (0–7 nmol/L) in the presence or absence of ketoconazole (50–75 μmol/L) for 24 hours and apoptosis was determined by Hoechst 33342 assay. Data are mean ± SD ($n = 3$) *, $P < 0.05$ versus nontreated cells; two-sided Student t test. #, $P < 0.05$ versus bortezomib-treated cells; two-sided Student t test. Bottom, inhibition of tBid reverses the sensitizing effect of ketoconazole on bortezomib-induced apoptosis. Cells were cotreated with bortezomib (6 nmol/L) and ketoconazole (75 μmol/L) in the presence or absence of the tBid inhibitor BI-6C9 (10–20 μmol/L) and analyzed for apoptosis by Hoechst 33342 assay. Data are mean ± SD ($n = 3$). *, $P < 0.05$ versus nontreated cells; two-sided Student t test. #, $P < 0.05$ versus bortezomib-treated cells; two-sided Student t test. §, $P < 0.05$ versus bortezomib-treated cells in the presence of ketoconazole; two-sided Student t test. NTX, nontreatment. **B,** ketoconazole increases tBid stability in bortezomib-treated cells. Jeko-1 and Granta-519 cells were treated with bortezomib and ketoconazole in the presence or absence of the protein translation inhibitor cycloheximide (CHX; 10 μg/mL) for various times (0–16 hours) to follow the degradation of tBid protein. Cell lysates were prepared and tBid expression was determined by Western blotting. Representative immunoblots of tBid and loading control β-actin are shown. Expression–time profiles of tBid in Jeko-1 (solid lines) and Granta-519 (dashed lines) cells treated with CHX and bortezomib alone (circle) or with ketoconazole (square) were plotted and tBid half-lives were calculated and shown. Data are mean ± SD ($n = 3$). *, $P < 0.05$ versus bortezomib and CHX cotreated cells; two-sided Student t test.

Published OnlineFirst November 22, 2017; DOI: 10.1158/1535-7163.MCT-17-0390

PPISURV analysis

PPISURV was used to correlate survival rates in cancer patients to the expression level of *MGEA5*. Samples were separated into low and high expression groups with respect to expression rank of the gene, which reflects relative mRNA expression level, based on the average expression across the dataset. The R statistical package was used to perform survival analyses and to draw Kaplan–Meier plots. Unadjusted *P* values were generated using standard survival analysis package (28).

Caspase-8 activity assay

Caspase-8 activity was determined by detecting the cleavage of specific substrate IETD-AFC using a commercial assay kit (Biovision). After treatments, cell lysates were prepared and incubated with IETD-AFC (50 μmol/L) for 1 hour. Free AFC fluorescence was measured using a fluorescence plate reader (Synergy H1, BioTek) at the 400-nm and 505-nm excitation and emission wavelengths. Caspase-8 activity was expressed as the ratio of signals from the treated and control samples.

Western blot analysis

After specific treatments, cells were incubated in a commercial lysis buffer (Cell Signaling Technology) and a protease inhibitor mixture (Roche Molecular Biochemicals) at 4°C for 30 minutes. Protein content was analyzed using BCA protein assay (Pierce Biotechnology) and 50–150 μg of proteins were resolved under denaturing conditions by SDS-PAGE as described previously (29).

Retrovirus production and short hairpin RNA–mediated gene knockdown

Retroviral plasmids carrying short hairpin (sh) RNA sequence against human *BID* were obtained from Origene and shBID retroviral production was performed using Platinum-A packaging cells (Cell Biolabs, Inc). Cells were incubated with shBID viral particles in the presence of hexadimethrine bromide (8 μg/mL) for 48 hours and were cultured and selected for puromycin (1 μg/mL) resistance.

Overexpression plasmid and transfection

Cells were transfected with tBID (Addgene, #21149; ref. 30) or GFP (Invitrogen) plasmid by nucleofection using 4D-Nucleofector (Lonza) with EW113 device program. The transfected cells were cultured with G418-containing medium (400 μg/mL) and stable transfectants (clone #1 and #2) were selected and identified by Western blotting.

Coimmunoprecipitation, ubiquitination, and *O*-GlcNAcylation

Cell lysates (200 μg protein) were immunoprecipitated using Dynabeads magnetic beads (Invitrogen). Briefly, the beads were conjugated with anti-tBid (h71) antibody for 10 minutes at room temperature. The conjugated beads were then resuspended with cell lysates for 30 minutes at room temperature. The immune complexes were washed four times and resuspended in 2× Laemmli sample buffer. They were then separated by SDS-PAGE and analyzed for ubiquitination or *O*-GlcNAcylation using anti-ubiquitin or anti-*O*-GlcNAc (RL2) antibody, respectively.

Cycloheximide-chase assay

Cells were treated with cycloheximide (10 μg/mL) to inhibit new protein synthesis for various times (0–16 hours) to follow the degradation of protein by Western blot analysis (29). tBid expression profile was plotted and tBid half-life was calculated using GraphPad Prism software.

Generation of *de novo* bortezomib-resistant cells

Bortezomib-resistant cell lines were generated by stepwise selection method as described previously with slight modifications (31). Parental MCL-derived Jeko-1 (Jeko/Parent) and Granta-519 (Granta/Parent) cells were continuously exposed to increasing concentrations of bortezomib to the maximum concentration of 500 nmol/L in Jeko/Parent cells and 150 nmol/L in Granta/Parent cells, and resistant cells were selected using Dead Cell Removal Kit (Miltenyi Biotec) and designated as Jeko/BTZ500R and Granta/BTZ150R.

Statistical analysis

The data represent means ± SD from three or more independent experiments as indicated. Statistical analysis was performed by Student *t* test at a significance level of $P < 0.05$. An ANOVA followed by Mann–Whitney *U* test was used for a multiple pairwise comparison.

Results

O-GlcNAcase inhibitors increase bortezomib sensitivity in MCL cells

To investigate the potential role of *O*-GlcNAcylation in bortezomib sensitivity, we modulated intracellular *O*-GlcNAcylation level using various known small-molecule inhibitors of specific enzymes in the hexosamine pathway, as schematically depicted in Fig. 1A (left). First, we determined the subtoxic concentrations of these inhibitors in the tested cell systems to ensure that the observed effects are not due to the cytotoxicity of the inhibitors. MCL Jeko-1, Granta-519, and SP49 cells were treated with well-known inhibitors of OGA (PugNAc and thiamet G), drug-like OGA inhibitor (ketoconazole), and OGT inhibitor (alloxan), and their effect on cell apoptosis was determined by Hoechst 33342 assay. We identified the appropriate noncytotoxic concentrations of these inhibitors, that is, up to 50 μmol/L for PugNAc, 15 μmol/L for thiamet G, 1.5 mmol/L for alloxan, and 75 μmol/L for ketoconazole (Fig. 1A, right; see also Supplementary Figs. S1 and S2). To evaluate their effect on bortezomib sensitivity, cells were pretreated with the inhibitors for 1 hour, followed by bortezomib treatment and apoptosis was determined after 24 hours. Figure 1B and Supplementary Table S1 show that the OGA inhibitors PugNAc and thiamet G significantly enhanced the sensitivity of MCL cells to bortezomib (5–7 nmol/L). In contrast, the OGT inhibitor alloxan abrogated bortezomib-induced apoptosis, suggesting the role of *O*-GlcNAcylation in MCL apoptotic response.

We also investigated the effect of drug-like OGA inhibitor ketoconazole on bortezomib sensitivity due to its potential clinical application. Similar to the well-known small-molecule OGA inhibitors, ketoconazole (25–75 μmol/L) dose dependently promoted the apoptotic effect of bortezomib in all MCL cell lines tested (Fig. 1C; Supplementary Table S1). Flow cytometric analysis using Annexin V-FITC and PI double staining further confirmed the observed sensitizing effect of ketoconazole on bortezomib apoptosis, as indicated by an increase in the proportion of Annexin V–positive cells (Fig. 2A). To strengthen that the combination of bortezomib and ketoconazole would have added benefits, CI values were calculated based on the fixed-ratio model using CompuSyn software to define whether the two drugs are

Published OnlineFirst November 22, 2017; DOI: 10.1158/1535-7163.MCT-17-0390

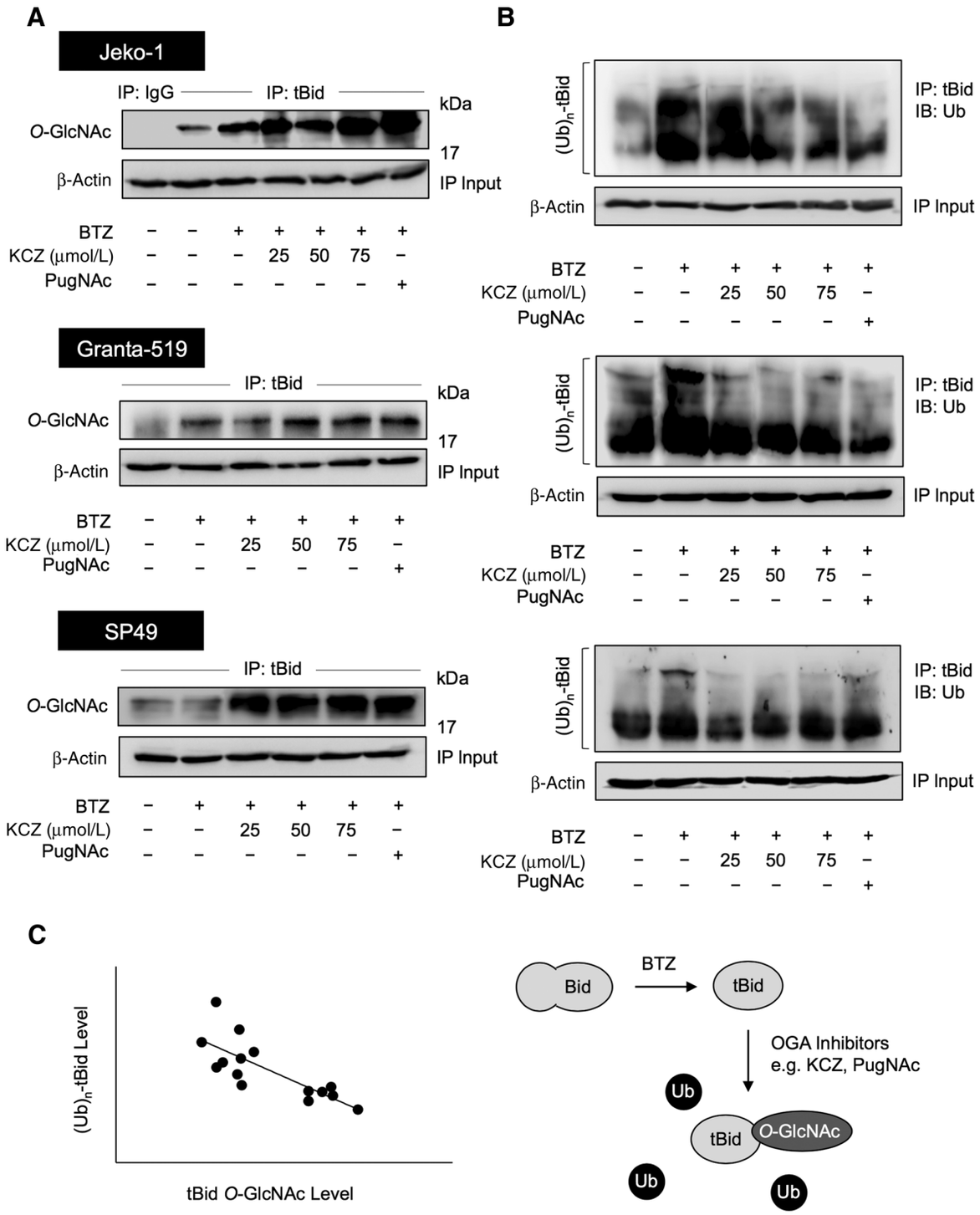

Figure 5.

Drug-like OGA inhibitor ketoconazole (KCZ) increases the *O*-GlcNAcylation but decreases the ubiquitination of tBid. **A,** Analysis of *O*-GlcNAcylation of tBid in response to bortezomib (BTZ) and ketoconazole cotreatment. MCL cells were cotreated with bortezomib (6 nmol/L) and increasing concentrations of KCZ (25–75 μmol/L) or PugNAc (50 μmol/L) for 3 hours. Cell lysates were prepared and immunoprecipitated using control IgG or anti-tBid (h71) antibody and probed with anti-*O*-GlcNAc antibody. Immunoblots were performed on cell lysates used as IP input using anti-β-actin antibody to confirm equal loading of the samples. **B,** Analysis of tBid ubiquitination in response to bortezomib and ketoconazole cotreatment. Cells were cotreated with bortezomib (6 nmol/L) and ketoconazole (25–75 μmol/L) or PugNAc (50 μmol/L) in the presence of MG132 (50 μmol/L) for 3 hours. Cell lysates were immunoprecipitated using anti-tBid (h71) antibody and analyzed for ubiquitin by Western blotting. **C,** Correlation analysis of tBid *O*-GlcNAcylation and ubiquitination in bortezomib-treated cells in the presence or absence of ketoconazole and PugNAc ($r = -0.7760$; left). A schematic diagram showing the interfering effect of O-GlcNAc on tBid ubiquitination (right).

Published OnlineFirst November 22, 2017; DOI: 10.1158/1535-7163.MCT-17-0390

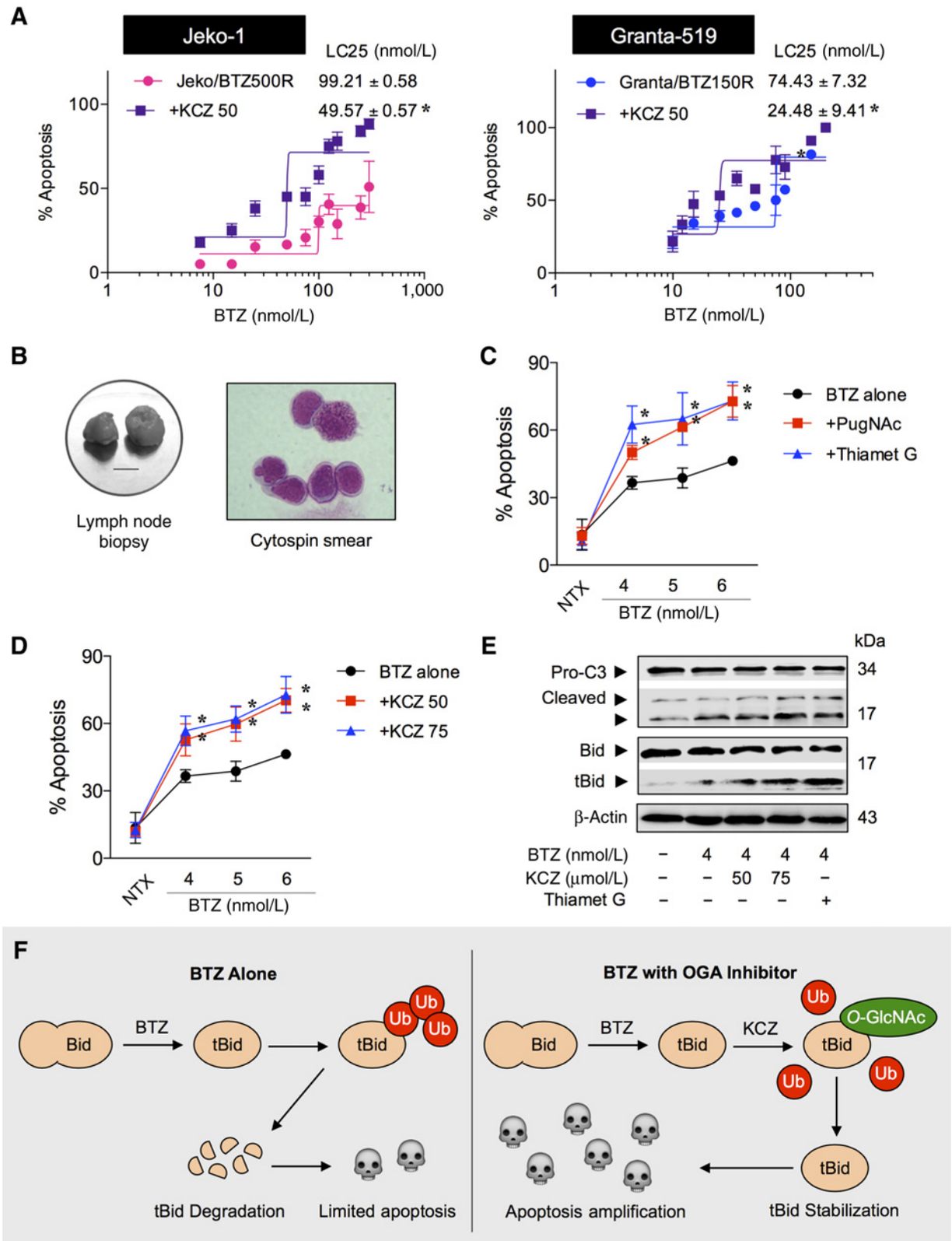

Published OnlineFirst November 22, 2017; DOI: 10.1158/1535-7163.MCT-17-0390

synergistic (CI < 1), additive (CI = 1), or antagonistic (CI > 1). Strong synergy was observed along the magnitude of apoptosis in all cell tested (Fig. 2B), indicating the potential application of ketoconazole.

Next, CRISPR interference (CRISPR/dCas9) targeting *MGEA5* (encoding OGA) was used to repress *MGEA5* expression. The OGA-knockdown (dCas9/MGEA5) cells were established and their apoptotic response to bortezomib was examined in comparison with control (dCas9) cells. Figure 2C shows that bortezomib induced more apoptosis in the knockdown cells than control cells, thus confirming the apoptosis sensitization by *O*-GlcNAcylation and OGA inhibition. Using PPISUV bioinformatics tool, we analyzed the association between *MGEA5* (encoding OGA) expression and clinical outcomes of patients with NHL, diffuse large B-cell lymphoma (DLBCL) subtype (due to the availability of data) and found that high expression of *MGEA5* correlates well with low survival rates of patients (Fig. 2D). These clinical data support the involvement of *O*-GlcNAcylation in controlling of aggressive lymphoma.

Cleavage of Bid contributes to ketoconazole-mediated sensitization to bortezomib

To characterize the apoptotic response to bortezomib and ketoconazole, MCL Jeko-1, Granta-519 and SP49 cells were treated with bortezomib (0–6 nmol/L) alone or in combination with ketoconazole (75 μmol/L) in the presence or absence of caspase inhibitor z-DEVD-fmk (10–15 μmol/L). z-DEVD-fmk significantly but not completely suppressed bortezomib-induced apoptosis, suggesting that bortezomib induces both caspase-dependent and -independent apoptotic process. On the other hand, the inhibition of apoptosis by z-DEVD-fmk was more prominent in bortezomib and ketoconazole cotreatment, indicating that apoptosis sensitization by ketoconazole is associated with caspase activation (Supplementary Fig. S3A and S3B). Western blot analysis shows a dose-dependent increase in caspase-3 activation and PARP cleavage by bortezomib, which was further increased by the addition of ketoconazole, in concomitant with the observed changes in caspase-3 activity (Supplementary Fig. S3C). Caspase-9 serves as the apical caspase of the intrinsic apoptosis pathway, while caspase-8 represents the apical caspase of the extrinsic pathway (32, 33). Caspase-8 inhibitor (z-LEHD-fmk) and to a lesser extent caspase-9 inhibitor (z-IETD-fmk) significantly inhibited caspase-3 activation induced by the cotreatment, suggesting that the sensitizing effect of ketoconazole involves both intrinsic and extrinsic pathways.

To elucidate the underlying mechanisms of ketoconazole -mediated sensitization, we monitored the expression levels of various apoptosis-regulatory proteins, including Bcl-2, Bax, Bid, Mcl-1, p53, p73, and Cav-1 following the ketoconazole and bortezomib treatment. The results show that Bcl-2/Bax ratio was relatively unchanged, while p53 and p73 were undetectable, and Cav-1 level was fluctuated after the treatment with bortezomib alone or with ketoconazole (Fig. 3A), suggesting their nondominant role in the apoptotic process. While bortezomib alone caused a marked increase in the apoptotic fragments of Mcl-1, addition of ketoconazole did not potentiate this effect, suggesting its unlikely involvement in the ketoconazole sensitization process. Remarkably, we observed a downregulation of Bid and a striking upregulation of transcated Bid (tBid; Bid cleavage) in the bortezomib and ketoconazole cotreated cells along with an increase in caspase-9 activation. These results suggest the potential involvement of tBid in the sensitization process.

Because tBid links the extrinsic to intrinsic apoptosis pathway (34, 35), we evaluated and found an increase in caspase-8 activation in parallel with tBid induction in all MCL cell lines tested following their treatment with bortezomib and ketoconazole (Fig. 3B). We confirmed by qPCR analysis that *BCL2*, *BAX*, *TP53*, *MCL1*, *CAV1*, and *BID* showed no appreciable changes in their expression in a way that would promote apoptosis (Supplementary Fig. S4), except for *TP53* in response to ketoconazole at 75 μmol/L. We postulate that although p53 was not a likely target of *O*-GlcNAcylation in the current setting, due to its undetectable protein level, ketoconazole at higher doses might induce apoptosis in part through an upregulation of *TP53*. To validate the role of tBid in the ketoconazole-sensitizing effect, tBid was inhibited directly and indirectly by small-molecule inhibitor of tBid (BI-6C9) and RNA interference using shRNA against *BID*. Consistent with a recent report on the antiapoptotic function of full-length Bid in mouse embryonic fibroblasts (36), we observed that knockdown of Bid slightly promoted bortezomib-induced apoptosis, but abolished the sensitizing effect of ketoconazole (Fig. 4A, middle), suggesting the role of Bid/tBid in the sensitizing process. Specific inhibition of tBid by BI-6C9 effectively reversed the ketoconazole-sensitizing effect (Fig. 4A, bottom), indicating that tBid is a key mediator in this process. Notably, the inhibition of BI-6C9 on bortezomib-induced apoptosis was observed only at a high dose (20 μmol/L), suggesting that other regulators are likely to be involved in the apoptosis induced by bortezomib alone.

tBid degradation is mediated by ubiquitin-mediated proteasomal degradation

The stability of tBid is an important factor in determining its apoptotic activity (37, 38). We tested whether tBid stability is

Figure 6.

Drug-like OGA inhibitor ketoconazole (KCZ) enhances bortezomib (BTZ) sensitivity in *de novo* bortezomib-resistant cells and patient-derived primary cells. **A,** Ketoconazole reduces the LC_{25} of bortezomib-resistant MCL cells. Bortezomib-resistant Jeko/500R and Granta/150R cells were generated by stepwise selection method (Supplementary Fig. S6) and treated with various concentrations of bortezomib in the presence or absence of ketoconazole (50 μmol/L). Dose–response curves were generated and LC_{25} of bortezomib in cells treated with bortezomib alone or in combination with ketoconazole were determined and compared. Data are mean ± SD ($n = 3$). *, $P < 0.05$ versus LC25 of bortezomib-treated Jeko/BTZ500R or Granta/BTZ150R in the absence of ketoconazole; two-sided Student *t* test. **B,** Primary cells were obtained from fresh biopsy-derived lymphoma tissues (lymph nodes; left; scale bar = 1 cm) of MCL patient and were captured for Wright-stained cytospin (right). Clinical characterization of the cells is shown in Supplementary Table S2. **C** and **D,** MCL patient-derived primary cells were treated with increasing concentrations of bortezomib (0–6 nmol/L) in the presence or absence of OGA inhibitors, PugNAc (50 μmol/L) and thiamet G (10 μmol/L) (**C**) or ketoconazole (50–75 μmol/L) (**D**) for 24 hours and apoptosis was determined by Hoechst 33342 assay. Data are mean ± SD ($n = 3$). *, $P < 0.05$ versus bortezomib-treated cells; two-sided Student *t* test. **E,** Western blot analysis of activated caspase-3 (cleaved C3) and truncated Bid (tBid) in patient-derived primary cells in response to bortezomib (4 nmol/L) and ketoconazole (50–75 μmol/L) cotreatment. **F,** A schematic diagram for the regulation of tBid by bortezomib and ketoconazole. In the presence of ketoconazole and other OGA inhibitors, for example, PugNAc and thiamet G, tBid *O*-GlcNAcylation occurs to inhibit tBid ubiquitination and proteasomal degradation. tBid stabilization intensifies the apoptotic signal and sensitizes MCL to bortezomib-induced apoptosis.

Published OnlineFirst November 22, 2017; DOI: 10.1158/1535-7163.MCT-17-0390

controlled by proteasomal degradation in MCL cells. MCL Jeko-1 cells were treated with the proteasome inhibitor MG132 and tBid expression was determined by Western blotting using specific tBid antibody (h71). The result shows that the MG132 treatment increases the level of tBid, suggesting its regulation by proteasomal degradation (Supplementary Fig. S5A). Ubiquitination is a PTM process that triggers proteasomal degradation (39, 40). With a low basal level of tBid, cells were first induced to overexpress tBid by gene transfection, and its ubiquitination was examined by Western blotting. Supplementary Figure S5C shows that treatment of the cells with the proteasome inhibitor MG132 strongly induced polyubiquitination of tBid, supporting ubiquitin-mediated proteasomal degradation of the protein.

On the basis of the observed sensitizing effect of ketoconazole and the role of tBid in the process, we hypothesized that ketoconazole might cause tBid accumulation by regulating of tBid stability. To test this possibility, we evaluated the expression–time profile of tBid in MCL cells treated with bortezomib with or without ketoconazole. The results show that the combination treatment dramatically shortened tBid induction from 16 to 6 hours compared with bortezomib treatment alone (Supplementary Fig. S6). tBid protein half-life was further evaluated in both treatment groups by a cycloheximide-chase assay. In this assay, the tBid half-life following inhibition of new protein synthesis by cycloheximide was calculated, revealing a gradual decrease in tBid expression over time when the cells were treated with bortezomib alone (Fig. 4B). In contrast, the tBid expression continued to increase when the cells were treated with both bortezomib and ketoconazole even in the absence of new protein synthesis, indicating the stabilization of tBid following the combination treatment.

O-GlcNAcylation of tBid reduces its ubiquitination

PTMs like phosphorylation are known to influence protein stability through ubiquitin-mediated proteasomal degradation (41, 42). As *O*-GlcNAcylation occurs on serine and/or threonine residues of protein similarly to phosphorylation (5, 6), it is conceivable that ketoconazole might induce *O*-GlcNAcylation of tBid, which interferes with its ubiquitination. MCL Jeko-1, Granta-519, and SP49 cells were treated with bortezomib and ketoconazole, and tBid was immunoprecipitated and subjected to Western blot analysis using an *O*-GlcNAc–specific antibody (RL2). The level of tBid *O*-GlcNAcylation was found to increase markedly in the presence of ketoconazole in all tested cells (Fig. 5A). tBid ubiquitination was further analyzed after the bortezomib and ketoconazole cotreatment. Figure 5B shows that ketoconazole indeed reduced tBid ubiquitination, possibly through its induction of tBid *O*-GlcNAcylation. A similar result was observed when the cells were treated with another OGA inhibitor, PugNAc. Further analysis of the correlation between tBid *O*-GlcNAcylation and ubiquitination in the tested cells reveals the inverse relationship of the two events with a correlation coefficient (r) of -0.7760 (Fig. 5C), thus supporting the interfering effect of *O*-GlcNAcylation on tBid ubiquitination.

Ketoconazole enhances bortezomib sensitivity in patient-derived primary cells and *de novo* bortezomib-resistant MCL cells

To investigate the potential clinical application of bortezomib and ketoconazole combination therapy for MCL, we further tested the sensitizing effect of ketoconazole in acquired bortezomib-resistant MCL cells and in patient-derived primary cells. Drug resistance remains a major clinical challenge for MCL treatment; we thus established *de novo* bortezomib-resistant cells by continuous exposure of MCL Jeko-1 and Granta-519 cells to increasing concentrations of bortezomib over time. Dose–response curve of the parental and bortezomib-resistant cells was generated and LC_{25} was calculated from the plot. Bortezomib-resistant Jeko/BTZ500R and Granta/BTZ150R cells exhibited an LC_{25} approximately 20-fold and 10-fold higher than that of their parental cells, respectively (Supplementary Fig. S7). Treatment of bortezomib-resistant Jeko/BTZ500R and Granta/BTZ150R cells with ketoconazole reduced their LC_{25} by approximately 50%–65% (Fig. 6A).

MCL patient-derived primary cells were obtained from fresh patient-derived lymphoma tissues (Fig. 6B; see Supplementary Table S2 for their clinical characterization) and treated with bortezomib in the presence or absence of two well-known small-molecule inhibitors, PugNAc and thiamet-G, or drug-like OGA inhibitor ketoconazole for 24 hours. Figure 6C and D shows that the addition of either small-molecule inhibitor or drug-like inhibitor ketoconazole similarly sensitized the cells to bortezomib-induced apoptosis. Western blot analysis reveals a marked increase in caspase-3 activation in response to the cotreatment of bortezomib and ketoconazole or thiamet G (Fig. 6E). A parallel increase in tBid expression and a reduction in Bid were also observed in the treated cells, thus validating the role of tBid in the apoptosis sensitization in MCL cell lines. Importantly, the combination treatment of bortezomib and ketoconazole had no significant cytotoxic effect on normal PBMCs and hepatocytes at a similar dosing condition (Supplementary Fig. S8). Taken together, our results support the potential clinical application of bortezomib and ketoconazole combination therapy for MCL.

Discussion

Aberrant hexosamine metabolism and *O*-GlcNAcylation have been linked to various aggressive behaviors of solid tumors (6, 7), as yet relatively little is known about their roles in hematologic malignancies, particularly MCL. Here, we provide compelling evidence that *O*-GlcNAcylation of tBid promotes apoptosis of MCL cells in response to its frontline therapeutic agent bortezomib. This finding is in line with a previous report showing reduced doubling time and enhanced cytogenetic abnormalities in CLL cells with a low level of *O*-GlcNAcylation (RL2 index < 1) relative to those with a higher index (RL2 > 1; ref. 11) and with the survival analyses of DLBCL patients showing better clinical outcomes with low *MGEA5* (encoding OGA) expression (Fig. 2D). We further demonstrate that inhibition of OGA and subsequent *O*-GlcNAcylation by either small-molecule inhibitors or drug-like inhibitor ketoconazole potentiates bortezomib sensitivity in MCL. We highlight for the first time the potential clinical application and molecular mechanism of bortezomib and ketoconazole combination therapy for MCL.

Ketoconazole is a conventional antifungal drug that was recently found to be one of the most potent inhibitors of human and *C. perfringen* OGAs based on high-throughput screening assays of OGA proteins against a commercial library of 880 off-patent small molecules (20). In this study, we found that ketoconazole, like well-known OGA inhibitors including

Published OnlineFirst November 22, 2017; DOI: 10.1158/1535-7163.MCT-17-0390

PugNAc and thiamet G, was able to sensitize MCL cells to bortezomib-induced apoptosis, albeit at approximately 5 times higher molar concentration (Figs. 1 and 2). To our knowledge, this is the first demonstration of the sensitizing effect of OGA inhibitors, specifically ketoconazole, on MCL apoptosis induced by chemotherapeutic agent. Ketoconazole, which sensitizes MCL cells for bortezomib-induced apoptosis, markedly induces Bid cleavage (tBid) with no or minimal effects on other major apoptosis-regulatory proteins (Fig. 3). We herein validate the role of tBid in ketoconazole sensitizing effect and demonstrate that ketoconazole stabilizes tBid, which is generated on stimulation of bortezomib itself and greatly potentiated by ketoconazole cotreatment (Fig. 4). This finding suggests that bortezomib and ketoconazole cooperatively cause tBid accumulation, linking the extrinsic and intrinsic apoptosis pathway and intensifying the death signal.

O-GlcNAcylation is a PTM process that regulates the expression and function of several proteins and has a ubiquitous role in many types of cancer (6, 7). In pancreatic carcinoma MiaPaCa-2 and PANC-1 cells, a decrease in *O*-GlcNAcylation triggers the intrinsic apoptosis pathway by reducing Bcl-xL, while its upregulation in BxPC-3 cells promotes anoikis resistance in part through NFκB signaling (43). On the other hand, an accumulation of *O*-GlcNAcylation reduces the viability of breast cancer MCF-7 cells likely through the accumulation of p53 (44). Thus, the role of *O*-GlcNAcylation in cell death and survival remains unclear and appears to be cell type- and context-dependent. In this study, we found that *O*-GlcNAcylation of tBid renders MCL cells more susceptible to bortezomib-induced apoptosis. Previous studies have shown that tBid undergoes ubiquitination and subsequently degrades by 26s proteasome (36, 45). The crosstalk between *O*-GlcNAcylation and ubiquitination are also reported, for example, the counteraction of *O*-GlcNAcylation and ubiquitination was earlier found to regulate circadian clock proteins, BMAL1 and CLOCK (46), as yet their precise interplay is unclear as enhanced ubiquitination was observed upon increasing of *O*-GlcNAcylation in the other report (47). Our data indicate that *O*-GlcNAcylation of tBid interferes with its ubiquitination, as supported by their inverse correlation in all cell systems tested and under various treatment conditions (Fig. 5). Degradation of tBid is known to limit the extent of apoptosis (35, 37), thereby tBid accumulation and stabilization would aid in the amplification and maintenance of apoptosis signal. It is worth noting that the reported sensitizing effect of ketoconazole on bortezomib-induced apoptosis was also seen in patient-derived primary cells and in bortezomib-resistant MCL cells (Fig. 6).

Taken together, the evidence presented here demonstrates the role of tBid *O*-GlcNAcylation in the regulation of apoptosis in MCL cells. Such PTM improves the stability of tBid by blocking its ubiquitination and subsequent proteasomal degradation, leading to sustained apoptosis, as schematically summarized in Fig. 6F. Our findings not only point to the involvement of hexosamine metabolic pathway and *O*-GlcNAcylation in MCL response to chemotherapy, but also advise the potential clinical application of drug-like OGA inhibitor ketoconazole in combination therapy to battle against drug-resistant MCL and other malignancies whose development and apoptosis is dependent on tBid dysregulation.

Disclosure of Potential Conflicts of Interest

No potential conflicts of interest were disclosed.

Authors' Contributions

Conception and design: S. Luanpitpong, S. Issaragrisil
Development of methodology: S. Luanpitpong
Acquisition of data (provided animals, acquired and managed patients, provided facilities, etc.): S. Luanpitpong, M. Janan, J. Poohadsuan, P. Samart, Y. U.-Pratya, S. Issaragrisil
Analysis and interpretation of data (e.g., statistical analysis, biostatistics, computational analysis): S. Luanpitpong, Y. Rojanasakul
Writing, review, and/or revision of the manuscript: S. Luanpitpong, Y. Rojanasakul, S. Issaragrisil
Administrative, technical, or material support (i.e., reporting or organizing data, constructing databases):
Study supervision: S. Issaragrisil
Other (research assistant): N. Chanthra

Acknowledgments

S. Issaragrisil is a Senior Research Scholar of Thailand Research Fund. We would like to acknowledge Dr. S. Jirawatnotai from Systems Pharmacology, Department of Pharmacology, Faculty of Medicine Siriraj Hospital, Mahidol University for his technical assistance and Profs. D. Solter and B. Knowles for their comments on the manuscript. This work was supported by grants from Thailand Research Fund (RTA 488-0007, to S. Issaragrisil; TRG5980013, to S. Luanpitpong), the Commission on Higher Education (CHE-RES-RG-49, to S. Issaragrisil), and NIH (R01-ES022968, to Y. Rojanasakul).

The costs of publication of this article were defrayed in part by the payment of page charges. This article must therefore be hereby marked *advertisement* in accordance with 18 U.S.C. Section 1734 solely to indicate this fact.

Received May 1, 2017; revised September 29, 2017; accepted November 14, 2017; published OnlineFirst November 22, 2017.

References

1. Hanahan D, Weinberg RA. Hallmarks of cancer: the next generation. Cell 2011;144:645–74.
2. Cheong H, Lu C, Lindsten T, Thompson CB. Therapeutic targets in cancer cell metabolism and autophagy. Nat Biotechnol 2012;30:671–8.
3. Perez-Galan P, Dreyling M, Wiestner A. Mantle cell lymphoma: biology, pathogenesis, and the molecular basis of treatment in the genomic era. Blood 2011;117:26–38.
4. Shah BD, Martin P, Sotomayor EM. Mantle cell lymphoma: a clinically heterogeneous disease in need of tailored approaches. Cancer Control 2012;19:227–235.
5. Bond MR, Hanover JA. A little sugar goes a long way: the cell biology of O-GlcNAc. J Cell Biol 2015;208:869–80.
6. Jóźwiak P, Forma E, Brys´ M, Krzes´lak A. O-GlcNAcylation and metabolic reprogramming in cancer. Front Endocrinol 2014;5:145.
7. de Queiroz RM, Carvalho E, Dias WB. O-GlcNAcylation: the sweet side of the cancer. Front Oncol 2014;4:132.
8. Champattanachai V, Netsirisawan P, Chaiyawat P, Phueaouan T, Charoenwattanasatien R, Chokchaichamnankit D, et al. Proteomic analysis and abrogated expression of O-GlcNAcylated proteins associated with primary breast cancer. Proteomics 2013;13:2088–99.
9. Lynch TP, Ferrer CM, Jackson SR, Shahriari KS, Vosseller K, Reginato MJ. Critical role of O-Linked β-N-acetylglucosamine transferase in prostate cancer invasion, angiogenesis, and metastasis. J Biol Chem 2012;287:11070–81.
10. Mi W, Gu Y, Han C, Liu H, Fan Q, Zhang X, et al. O-GlcNAcylation is a novel regulator of lung and colon cancer malignancy. Biochim Biophys Acta 2011;1812:514–9.

Published OnlineFirst November 22, 2017; DOI: 10.1158/1535-7163.MCT-17-0390

11. Shi Y, Tomic J, Wen F, Shaha S, Bahlo A, Harrison R, et al. Aberrant O-GlcNAcylation characterizes chronic lymphocytic leukemia. Leukemia 2010;24:1588–98.
12. Kouroukis CT, Fernandez LA, Crump M, Gascoyne RD, Chua NS, Buckstein R, et al. A phase II study of bortezomib and gemcitabine in relapsed mantle cell lymphoma from the National Cancer Institute of Canada Clinical Trials Group (IND 172). Leuk Lymphoma 2011;52: 394–9.
13. Hegde GV, Nordgren TM, Munger CM, Mittal AK, Bierman PJ, Weisenburger DD, et al. Novel therapy for therapy-resistant mantle cell lymphoma: multipronged approach with targeting of hedgehog signaling. Int J Cancer 2012;131:2951–60.
14. Ma Z, Vosseller K. Cancer metabolism and elevated O-GlcNAc in oncogenic signaling. J Biol Chem 2014;289:34457–65.
15. Chou TY, Hart GW, Dang CV. c-Myc is glycosylated at threonine 58, a known phosphorylation site and a mutational hot spot in lymphomas. J Biol Chem 1995;270:18961–65.
16. Hurtado-Guerrero R, Dorfmueller HC, van Aalten DM. Molecular mechanisms of O-GlcNAcylation. Curr Opin Struct Biol 2008;18:551–7.
17. Yuzwa SA, Macauley MS, Heinonen JE, Shan X, Dennis RJ, He Y, et al. A potent mechanism-inspired O-GlcNAcase inhibitor that blocks phosphorylation of tau in vivo. Nat Chem Biol 2008;4:483–90.
18. Konrad RJ, Zhang F, Hale JE, Knierman MD, Becker GW, Kudlow JE. Alloxan is an inhibitor of the enzyme O-linked N-acetylglucosamine transferase. Biochem Biophys Res Commun 2002;293: 207–12.
19. Dehennaut V, Lefebvre T, Sellier C, Leroy Y, Gross B, Walker S, et al. O-linked N-acetylglucosaminyltransferase inhibition prevents G2/M transition in *Xenopus laevis* oocytes. J Biol Chem 2007;282: 12527–36.
20. Dorfmueller HC, van Aalten DMF. Screening-based discovery of drug-like O-GlcNAcase inhibitor scaffolds. FEBS Lett 2010;584:694–700.
21. Becattini B, Sareth S, Zhai D, Crowell KJ, Leone M, Reed JC, et al. Targeting apoptosis via chemical design: inhibition of bid-induced cell death by small organic molecules. Chem Biol 2004;11:1107–17.
22. Amin HM, McDonnell TJ, Medeiros LJ, Rassidakis GZ, Leventaki V, O'Connor SL, et al. Characterization of 4 mantle cell lymphoma cell lines. Arch Pathol Lab Med 2003;127:424–31.
23. Kridel R, Meissner B, Rogic S, Boyle M, Telenius A, Woolcock B, et al. Whole transcriptome sequencing reveals recurrent NOTCH1 mutations in mantle cell lymphoma. Blood 2012;119:1963–71.
24. Drexler HG. Establishment and culture of leukemia-lymphoma cell lines. Methods Mol Biol 2011;731:181–200.
25. Zhang N, Fu JN, Chou TC. Synergistic combination of microtubule targeting anticancer fludelone with cytoprotective panaxytriol derived from panax ginseng against MX-1 cells in vitro: experimental design and data analysis using the combination index method. Am J Cancer Res 2016;6:97–104.
26. Qi LS, Larson MH, Gilbert LA, Doudna JA, Weissman JS, Arkin AP, et al. Repurposing CRISPR as an RNA-guided platform for sequence-specific control of gene expression. Cell 2013;152:1173–83.
27. Larson MH, Gilbert LA, Wang X, Lim WA, Weissman JS, Qi LS. CRISPR interference (CRISPRi) for sequence-specific control of gene expression. Nat Protoc 2013;8:2180–96.
28. Antonov AV, Krestyaninova M, Knight RA, Rodchenkov I, Melino G, Barlev NA. PPISURV: a novel bioinformatics tool for uncovering the hidden role of specific genes in cancer survival outcome. Oncogene 2014;33:1621–8.
29. Luanpitpong S, Li J, Manke A, Brundage K, Ellis E, McLaughlin SL, et al. SLUG is required for SOX9 stabilization and functions to promote cancer stem cells and metastasis in human lung carcinoma. Oncogene 2016;35:2824–33.
30. Li H, Zhu H, Xu CJ, Yuan J. Cleavage of BID by caspase 8 mediates the mitochondrial damage in the Fas pathway of apoptosis. Cell 1998;94: 491–501.
31. Pérez-Galán P, Mora-Jensen H, Weniger MA, Shaffer AL III, Rizzatti EG, Chapman CM, et al. Bortezomib resistance in mantle cell lymphoma is associated with plasmacytic differentiation. Blood 2011;117:542–52.
32. Tait SWG, Green DR. Mitochondria and cell death: outer membrane permeabilization and beyond. Nat Rev Mol Cell Biol 2010; 11:621–32.
33. Guicciardi ME, Gores GJ. Life and death by death receptors. FASEB J 2009;23:1625–37.
34. Unterkircher T, Cristofanon S, Vellanki SH, Nonnenmacher L, Karpel-Massler G, Wirtz CR, et al. Bortezomib primes glioblastoma, including glioblastoma stem cells, for TRAIL by increasing tBid stability and mitochondrial apoptosis. Clin Cancer Res 2011;17:4019–30.
35. Wei MC, Lindsten T, Mootha VK, Weiler S, Gross A, Ashiya M, et al. tBID, a membrane-targeted death ligand, oligomerizes BAK to release cytochrome c. Genes Dev 2000;14:2060–71.
36. Luo W, Li J, Zhang D, Cai T, Song L, Min X-M, et al. Bid mediates anti-apoptotic COX-2 induction through the IKKβ/NFκB pathway due to 5-MCDE exposure. Curr Cancer Drug Targets 2010;10:96–106.
37. Breitschopf K, Zeiher AM, Dimmeler S. Ubiquitin-mediated degradation of the proapoptotic active form of bid. A functional consequence on apoptosis induction. J Biol Chem 2000;275:21648–52.
38. Ying S, Seiffert BM, Häcker G, Fischer SF. Broad degradation of proapoptotic proteins with the conserved Bcl-2 homology domain 3 during infection with Chlamydia trachomatis. Infect Immun 2005;73:1399–1403.
39. Mani A, Gelmann EP. The ubiquitin-proteasome pathway and its role in cancer. J Clin Oncol 2005;23:4776–89.
40. Lam YA, Lawson TG, Velayutham M, Zweier JL, Pickart CM. A proteasomal ATPase subunit recognizes the polyubiquitin degradation signal. Nature 2002;416:763–7.
41. Swaney DL, Beltrao P, Starita L, Guo A, Rush J, Fields S, et al. Global analysis of phosphorylation and ubiquitylation cross-talk in protein degradation. Nat Methods 2013;10:676–82.
42. Hunter T. The age of crosstalk: phosphorylation, ubiquitination, and beyond. Mol Cell 2007;28:730–8.
43. Ma Z, Vocadlo DJ, Vosseller K. Hyper-O-GlcNAcylation is anti-apoptotic and maintains constitutive NF-κB activity in pancreatic cancer cells. J Biol Chem 2013;288:15121–30.
44. Yang WH, Kim JE, Nam HW, Ju JW, Kim HS, Kim YS, et al. Modification of p53 with O-linked N-acetylglucosamine regulates p53 activity and stability. Nat Cell Biol 2006;8:1074–83.
45. Azakir BA, Desrochers G, Angers A. The ubiquitin ligase Itch mediates the antiapoptotic activity of epidermal growth factor by promoting the ubiquitylation and degradation of the truncated C-terminal portion of Bid. FEBS J 2010;277:1319–30.
46. Li MD, Ruan HB, Hughes ME, Lee JS, Singh JP, Jones SP, et al. O-GlcNAc signaling entrains the circadian clock by inhibiting BMAL1/CLOCK ubiquitination. Cell Metab 2013;17:303–10.
47. Guinez C, Mir AM, Dehennaut V, Cacan R, Harduin-Lepers A, Michalski JC, et al. Protein ubiquitination is modulated by O-GlcNAc glycosylation. FASEB J 2008;22:2901–11.

SCIENTIFIC REPORTS

OPEN

Hyper-*O*-GlcNAcylation induces cisplatin resistance via regulation of p53 and c-Myc in human lung carcinoma

Received: 11 April 2017
Accepted: 15 August 2017
Published online: 06 September 2017

Sudjit Luanpitpong[1], Paweorn Angsutararux[1], Parinya Samart[1,2], Nawin Chanthra[1], Pithi Chanvorachote[3] & Surapol Issaragrisil[1,4,5]

Aberrant metabolism in hexosamine biosynthetic pathway (HBP) has been observed in several cancers, affecting cellular signaling and tumor progression. However, the role of *O*-GlcNAcylation, a post-translational modification through HBP flux, in apoptosis remains unclear. Here, we found that hyper-*O*-GlcNAcylation in lung carcinoma cells by *O*-GlcNAcase inhibition renders the cells to apoptosis resistance to cisplatin (CDDP). Profiling of various key regulatory proteins revealed an implication of either p53 or c-Myc in the apoptosis regulation by *O*-GlcNAcylation, independent of p53 status. Using co-immunoprecipitation and correlation analyses, we found that *O*-GlcNAcylation of p53 under certain cellular contexts, i.e. high p53 activation, promotes its ubiquitin-mediated proteasomal degradation, resulting in a gain of oncogenic and anti-apoptotic functions. By contrast, *O*-GlcNAcylation of c-Myc inhibits its ubiquitination and subsequent proteasomal degradation. Gene manipulation studies revealed that *O*-GlcNAcylation of p53/c-Myc is in part a regulator of CDDP-induced apoptosis. Accordingly, we classified CDDP resistance by hyper-*O*-GlcNAcylation in lung carcinoma cells as either p53 or c-Myc dependence based on their molecular targets. Together, our findings provide novel mechanisms for the regulation of lung cancer cell apoptosis that could be important in understanding clinical drug resistance and suggest *O*-GlcNAcylation as a potential target for cancer therapy.

Cancer cells increase nutrient consumption leading to deregulating cellular metabolism, an emerging characteristic hallmark of cancer[1,2]. The hexosamine biosynthetic pathway utilizes major essential nutrients and metabolic intermediates including glucose, glucosamine, amino acid, fatty acid and nucleotide into an end product of nucleotide sugar uridine diphosphate N-acetyl-glucosamine (UDP-GlcNAc)[3]. *O*-linked-β-*N*-acetylglucosomaine (*O*-GlcNAc) is subsequently transferred from UDP-GlcNAc to serine (Ser) and/or threonine (Thr) residues in substrate proteins by the enzyme *O*-GlcNAc transferase (OGT) causing a post-translational modification (PTM) called *O*-GlcNAcylation. This PTM which can be removed by the enzyme *O*-GlcNAcase (OGA; encoded by *MGEA5*) can alter protein functions and stability directly and indirectly, e.g. by competing with phosphorylation sites. Increasing evidence has shown that PTM dynamic regulates gene transcription and cellular signaling in response to changes in microenvironment triggered by altered nutrients and stress[4,5].

In recent years, elevated *O*-GlcNAcylation (hyper-*O*-GlcNAcylation) has been observed in various cancers, including breast, colon, pancreas, liver and lung[6,7], and its roles in oncogenesis and tumor progression have been increasingly reported. *O*-GlcNAcylation was found to modulate cell proliferation and anchorage-independent growth of pancreatic cancer cells through NF-κB activation[8], whilst induce cell invasion and metastasis of breast cancer cells through the modulation of FOXM1 transcription factor[9]. In lung carcinoma, *O*-GlcNAcylation induced tumor growth by increasing glucose metabolic flux through

[1]Siriraj Center of Excellence for Stem Cell Research, Faculty of Medicine Siriraj Hospital, Mahidol University, Bangkok, 10700, Thailand. [2]Department of Immunology, Faculty of Medicine Siriraj Hospital, Mahidol University, Bangkok, 10700, Thailand. [3]Department of Pharmacology and Physiology, Faculty of Pharmaceutical Sciences, Chulalongkorn University, Bangkok, 10330, Thailand. [4]Division of Hematology, Department of Medicine, Faculty of Medicine Siriraj Hospital, Mahidol University, Bangkok, 10700, Thailand. [5]Bangkok Hematology Center, Wattanosoth Hospital, BDMS Center of Excellence for Cancer, Bangkok, 10310, Thailand. Correspondence and requests for materials should be addressed to S.I. (email: surapol.iss@mahidol.ac.th)

pentose phosphate pathway[10]. However, the role of *O*-GlcNAcylation in apoptosis and detailed mechanisms by which protein-specific *O*-GlcNAcylation contributes to the apoptotic response to chemotherapy remain largely unknown.

Here we present evidence that hyper-*O*-GlcNAcylation by OGA inhibitors renders human lung carcinoma cells to apoptosis resistance induced by cisplatin (CDDP) via two distinct pathways that are either p53- or c-Myc-dependent, depending on cellular context, independent of p53 status. Specifically, *O*-GlcNAcylation of CDDP-induced p53 promotes ubiquitin-mediated proteasomal degradation, causing p53 instability. On the contrary, when *O*-GlcNAcylation of c-Myc occurs, it inhibits c-Myc ubiquitination and degradation. Our findings unveil a previously unknown mechanism for the regulation of lung tumor cell apoptosis that could be important in understanding clinical drug resistance and may have clinical utility for targeted drug therapy of lung and other cancers whose etiology is dependent on *O*-GlcNAcylation.

Results

Expression of *O*-GlcNAc cycling enzymes in human lung carcinoma. Hyper-*O*-GlcNAcylation might be attributable to high OGT and/or low OGA levels. We performed mRNA expression analysis of *OGT* and *MGEA5* (encoded OGA) in human clinical specimens available on Oncomine™ bioinformatics database. An elevated *OGT* expression was observed in the majority of human lung adenocarcinoma tissues compared with normal lung tissues in 7 out of 8 analyzed datasets − one remaining dataset (Bhattachajee) revealed a remarkable decrease in *MGEA5* expression (Fig. 1A). Lung carcinoma tissues in Su, Okayama and Landi datasets were found to have both high *OGT* and low *MGEA5* levels as compared with normal tissues (Fig. 1B,C). These analyses support the previous finding on hyper-*O*-GlcNAcylation in lung carcinoma[11].

Hyper-*O*-GlcNAcylation renders cisplatin resistance in human lung carcinoma. To investigate the role of *O*-GlcNAcylation in apoptosis of human lung carcinoma, we treated a panel of National Cancer Institute (NCI) lung cancer cell lines, including NCI-H460, NCI-H292, NCI-H23 and A549 cells, with a known apoptosis inducer CDDP in the presence or absence of small molecule inhibitors of OGA (removal of *O*-GlcNAc) that cause an increase in global *O*-GlcNAcylation, including PugNAc and KCZ. After a 24 h post-treatment, cell apoptosis was determined by Hoechst 33342 assay. CDDP treatment (0–50 μM in A549; 0–75 μM in NCI-H460 and NCI-H23; and 0–125 μM in NCI-H292 cells) caused a dose-dependent increase in apoptosis in all tested cell lines, the effect that was inhibited by co-treatment of the cells with OGA inhibitors PugNAc (0–75 μM) and KCZ (0–75 μM) (Fig. 2A,B,E and F). The apoptotic cells exhibited condensed and/or fragmented nuclei with intense nuclear fluorescence (Fig. 2C,D,G and H). The inhibitory effect of OGA inhibitors suggests that hyper-*O*-GlcNAcylation plays a critical role in the protection against CDDP-induced apoptosis, which is confirmed by subsequent cell diameter and DNA content analyses (Supplementary Figure S1). As KCZ displays a higher selectivity for human OGA over its closely related lysosomal hexosamidases (HexA/B) than PugNAc[12], we used KCZ in subsequent molecular studies.

To strengthen the role of hyper-*O*-GlcNAcylation in apoptosis inhibition and CDDP resistance, we further inhibited or repressed cellular OGA by a novel selective inhibitor thiamet G or by genetic manipulation using CRISPR/Cas9 system. Figure 3A–D shows that apoptosis induction by CDDP was substantially reduced after co-treatment of the cells with thiamet G. This effect was observed in all four cell lines tested and in a dose-dependent manner. For CRISPR-mediated repression of *MGEA5* (encoded OGA), we used two *MGEA5*-targeting guide RNAs (gRNA #1 and #2) to create double-stranded breaks near the promoter region, which resulted in a decrease in *MGEA5* expression in the cell population (Fig. 3E). The OGA-knockdown (Cas9/MGEA5) cells were significantly less responsive to CDDP when compared to control (WT) cells (Fig. 3F,G), thus confirming the inhibitory effect of hyper-*O*-GlcNAcylation on CDDP-induced apoptosis.

***O*-GlcNAcylation suppresses cisplatin-induced apoptosis through a caspase-dependent pathway.** To understand how *O*-GlcNAcylation regulates apoptosis, we first characterized the pathway of apoptosis in response to CDDP and KCZ co-treatment. NCI-H460 and NCI-H292 cells were treated with CDDP (50 or 75 μM) alone or in combination with increasing concentrations of KCZ (25–75 μM) in the presence or absence of caspase inhibitor z-DEVD-fmk (10 μM). KCZ was found to suppress caspase-3 activity, the central execution event of apoptosis[13], in a dose-dependent manner (Supplementary Figure S2) in concomitant with the observed nuclear morphological changes (Fig. 2). The caspase inhibitory effect of KCZ was similar to and synergistic with that of z-DEVD-fmk, suggesting that *O*-GlcNAcylation inhibits apoptosis induced by CDDP through caspase inhibition. Western blot analysis further confirmed the inhibitory effect of KCZ on caspase-3 activation and its downstream event PARP cleavage (Fig. 4A,B), thus substantiating that *O*-GlcNAcylation prevents caspase-dependent apoptosis.

Bcl-2 family proteins regulate apoptosis along the intrinsic mitochondrial apoptosis pathway that is activated in response to various apoptotic stimuli, including CDDP[14,15]. To determine whether Bcl-2 family proteins involve in the inhibitory effect of *O*-GlcNAcylation on caspase activation and apoptosis, we co-treated the cells with CDDP and KCZ and analyzed for Bcl-2 and Bax expression in correlation to hyper-*O*-GlcNAcylation by Western blotting. Figure 4C,D shows that although CDDP was able to tilt the balance between pro-apoptotic Bax and anti-apoptotic Bcl-2 in favor of apoptosis, i.e. a decrease in Bcl-2/Bax ratio, KCZ did not exert its effect through the Bcl-2/Bax balance since we observed no significant changes in the ratio after co-treating the cells with KCZ compared to CDDP treatment alone. Further analysis of other Bcl-2 family members revealed insignificant changes of anti-apoptosis proteins (e.g. Bcl-xL and Mcl-1) and pro-apoptotic proteins (Bak and Bid) in relation to the apoptotic responses (Supplementary Figure S3).

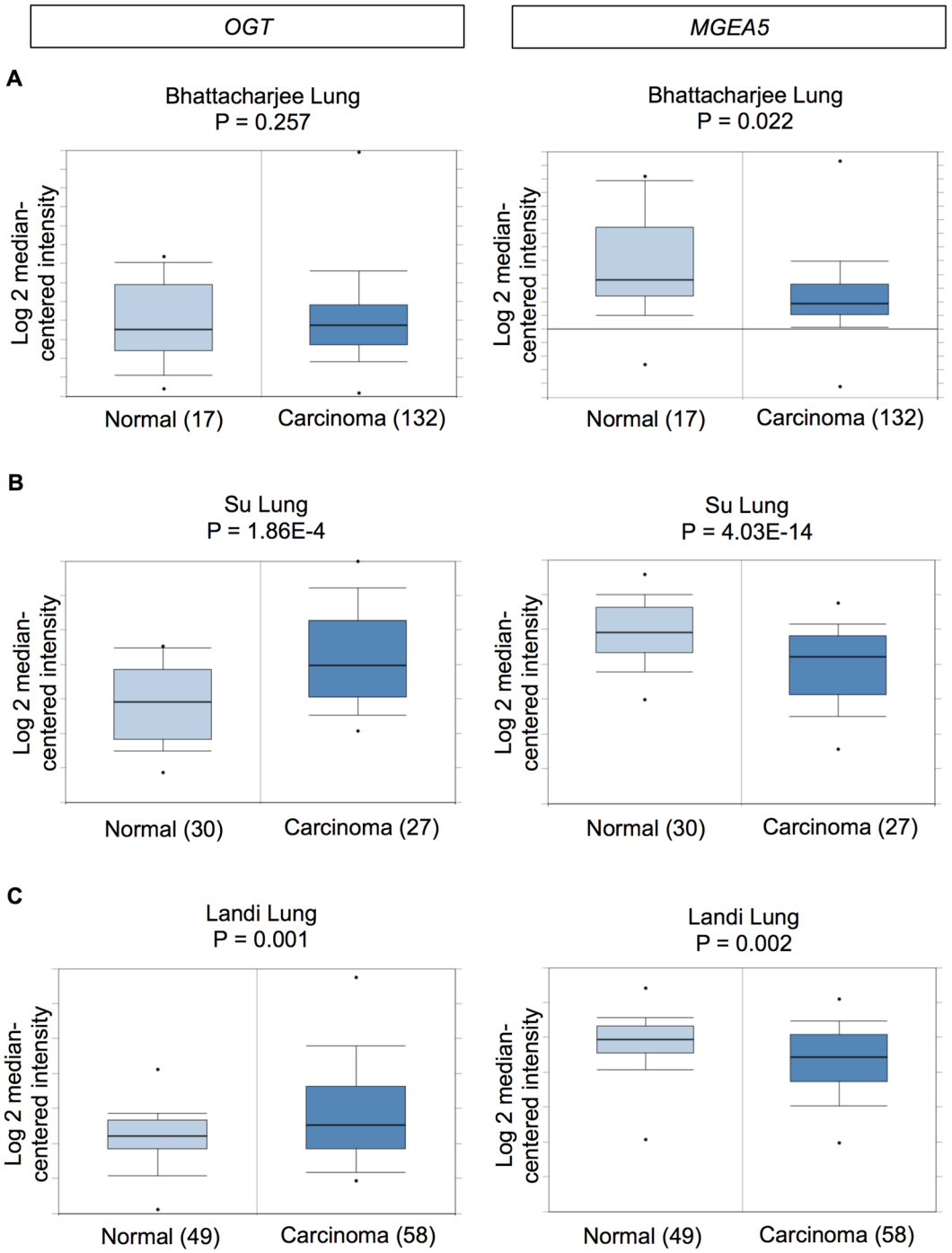

Figure 1. mRNA expression of *O*-GlcNAc cycling enzymes *OGT* and *MGEA5* in clinical lung carcinoma samples in comparison to normal lung tissues on Oncomine™ bioinformatics database. (**A**,**B**,**C**) Differential expression of *OGT* and *MGEA5* (encoded OGA) in the Bhattacharjee Lung, Su Lung and Landi Lung datasets.

Distinct effects of *O*-GlcNAcylation on p53 and c-Myc in wild-type and mutant p53 lung cancer cells. Having demonstrated that *O*-GlcNAcylation has minimal effects on the regulation and/or expression of critical Bcl-2 family proteins, we next tested its effect on the central oncogenic switch of c-Myc oncogene and p53 tumor suppressor, both of which are known targets of *O*-GlcNAcylation[16–19]. Figure 5A–D shows that although CDDP induced p53 activation in all wild-type (NCI-H460, NCI-H292 and A549)[20,21] and mutant p53 (NCI-H23) cells[22], the level of activation differs substantially among these cells independent of their p53 status. We also observed that CDDP unexpectedly induced c-Myc in the cells with high p53 activation (>5-fold), i.e. NCI-H460 and A549 cells, but reduced c-Myc in the cells with low p53 activation (<5-fold), i.e. NCI-H292 and NCI-H23 cells.

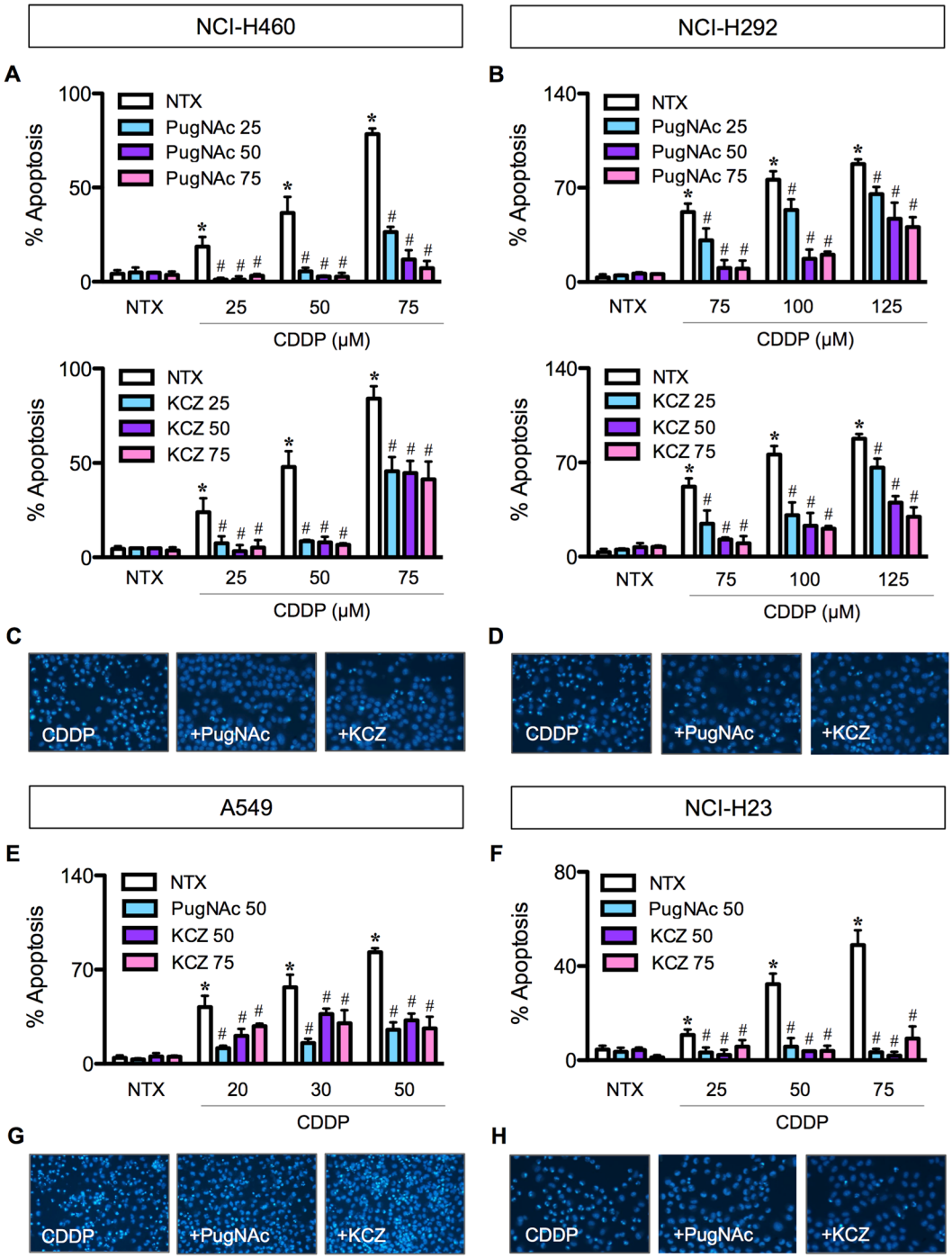

Figure 2. *O*-GlcNAcase inhibitors prevent cisplatin-induced apoptosis in lung carcinoma cells. Multiple human lung carcinoma cell lines, including NCI-H460 (**A**), NCI-H292 (**B**), A549 (**E**) and NCI-H23 (**F**) cells were treated with cisplatin (CDDP; 0–75 μM in NCI-H460 and NCI-H23, 0–125 μM in NCI-H292, and 0–50 μM in A549 cells) for 24 in the presence or absence of *O*-GlcNAcase inhibitors, including PugNAc (25–75 μM) (*upper*) and ketoconazole (KCZ; 25–75 μM) (*lower*), before analysis for apoptosis by Hoechst 33342 assay. (**C**,**D**,**G**,**H**) Fluorescence micrographs of the treated cells stained with Hoechst dye. Plots are means ± S.D. ($n = 4$). *$p < 0.05$ versus non-treated control. $^{\#}p < 0.05$ versus CDDP-treated cells.

We further found that KCZ dose-dependently rendered CDDP-induced p53 activation only in NCI-H460 and A549 cells where high p53 activation was detected, but not in NCI-H292 and NCI-H23 cells. In cells with low p53 activity, the protective effect of KCZ on CDDP-induced apoptosis appears to be dependent on c-Myc level based on the observations that (i) KCZ hampered CDDP-driven c-Myc reduction in concomitant with the increase in cell survival in a dose-dependent manner, and (ii) KCZ had minimal effect on p53 protein level, suggesting that the target proteins of *O*-GlcNAcylation may vary depending on cellular context, i.e. the presence of active p53.

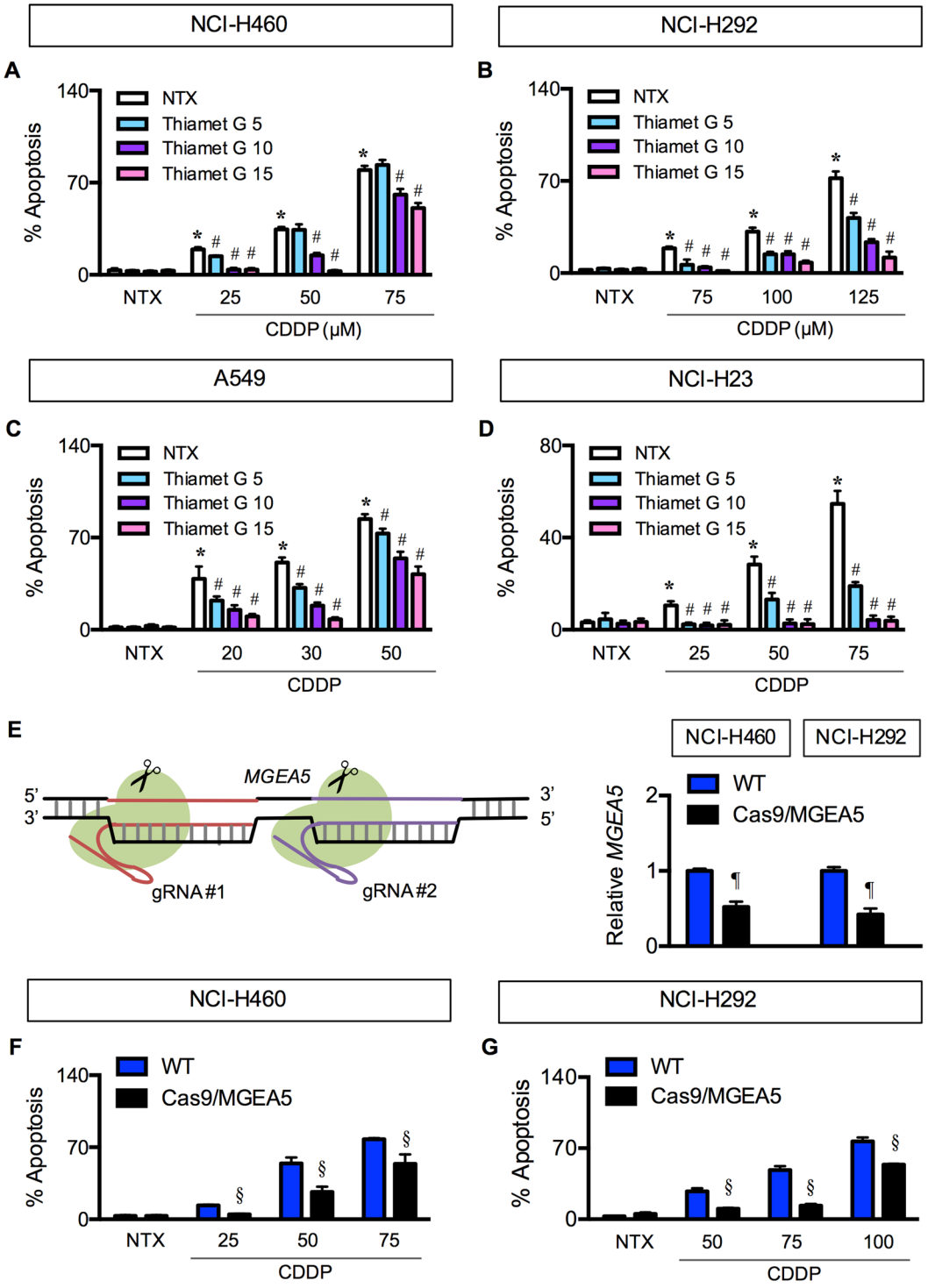

Figure 3. Validation of apoptosis blockage by *O*-GlcNAcase inhibition and repression. (**A**–**D**) Multiple human lung carcinoma cell lines, including NCI-H460 (**A**), NCI-H292 (B), A549 (**C**) and NCI-H23 (**D**) cells were treated with cisplatin (CDDP; 0–75 μM in NCI-H460 and NCI-H23, 0–125 μM in NCI-H292, and 0–50 μM in A549 cells) for 24 h in the presence or absence of a potent and selective *O*-GlcNAcase inhibitor thiamet G (5–15 μM). Apoptosis was determined by Hoechst 33342 assay at 24 h post-treatment. Plots are means ± S.D. (n = 3). *$p < 0.05$ versus non-treated control. $^{\#}p < 0.05$ versus CDDP-treated cells. (**E**) (*left*) A schematic diagram for a transcriptional repression of *MGEA5* (encoding OGA) using CRISPR/Cas9 system. (*right*) Quantitative real-time PCR of *MGEA5* mRNA expression in NCI-H460 and NCI-H292 cells. Plots are means ± S.D. (n = 3). $p < 0.05$ versus control (WT) cells. (**F**) Effect of *MGEA5* repression on CDDP-induced apoptosis. OGA-knockdown (Cas9/MGEA5) and control (WT) cells were treated with CDDP for 24 h and analyzed for apoptosis using Hoechst 33342 assay. Plots are means ± S.D. (n = 3). $^{\S}p < 0.05$ versus cisplatin-treated control (WT) cells.

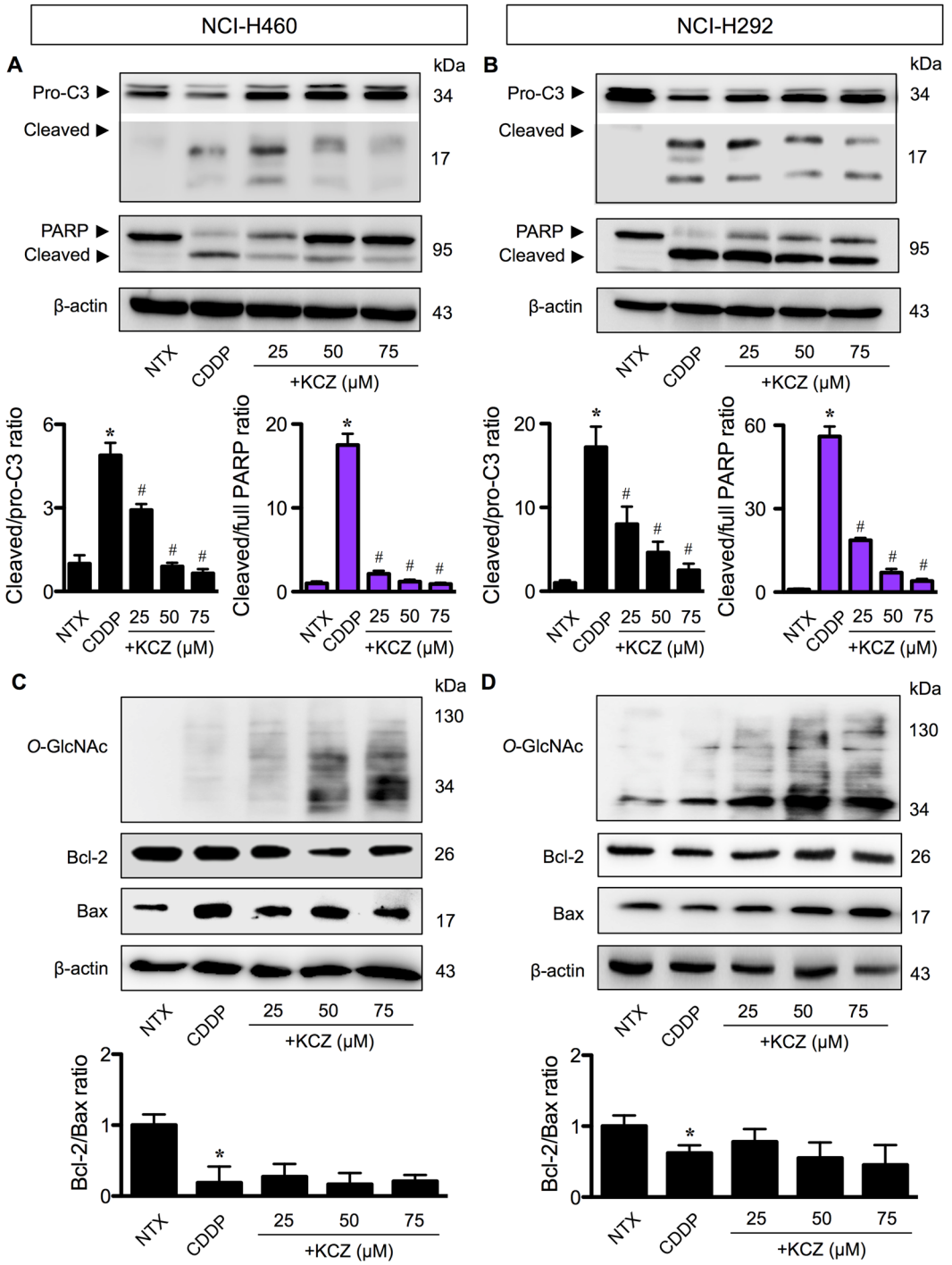

Figure 4. *O*-GlcNAcylation had minimal effect on Bcl-2 and Bax imbalance caused by cisplatin. (**A**,**B**) Human lung carcinoma NCI-H460 and NCI-H292 cells were co-treated with cisplatin (CDDP; 50 or 75 μM) and a highly selective *O*-GlcNAcase inhibitor ketoconazole (KCZ; 25–75 μM) for 24 h and cell lysates were prepared and analyzed for cleaved (active) caspase-3 (C3) and cleaved PARP by Western blotting. Blots were reprobed with anti-β-actin antibody to confirm equal loading of the samples. Immunoblot signals were quantified by densitometry and mean data from three independent experiments (one of which is shown here) were normalized to the loading control, calculated as the fold difference relative to non-treated control and presented as cleaved/pro-C3 and cleaved/full PARP ratios. Cleaved and pro-C3 were cropped from different parts of the same gel and exposure was adjusted to aid the visualization of cleaved C3. (**C**,**D**) Cells were similarly treated with CDDP and KCZ, and Bcl-2 and Bax protein levels were evaluated along with global *O*-GlcNAcylation by Western blotting. Quantitative analysis of Bcl-2 and Bax by densitometry is shown as Bcl-2/Bax ratio. Plots are means ± S.D. ($n = 3$). *$p < 0.05$ versus non-treated control. $^{\#}p < 0.05$ versus CDDP-treated cells.

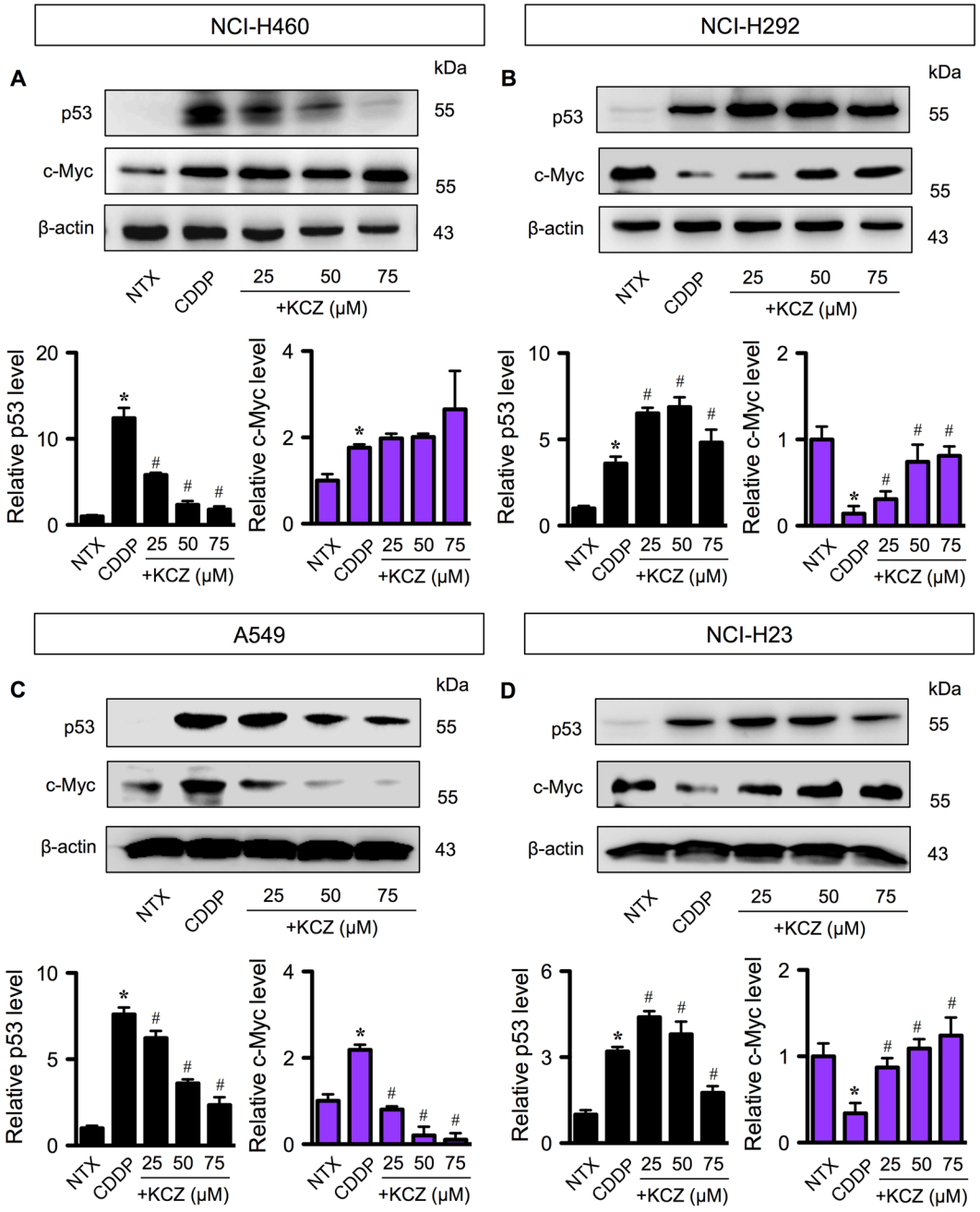

Figure 5. *O*-GlcNAcylation targets p53 or c-Myc in cisplatin-induced apoptosis independent of p53 status. Multiple human lung carcinoma cell lines, including NCI-H460 (**A**), NCI-H292 (**B**), A549, (**C**) and NCI-H23 (**D**) cells were treated with cisplatin (CDDP; 50 μM in NCI-H460 and NCI-H23, 30 μM in A549, and 100 μM in NCI-H292 cells) for 24 in the presence or absence of increasing concentrations of *O*-GlcNAcase inhibitor ketoconazole (KCZ; 25–75 μM). Cell lysates were then prepared and analyzed for p53 and c-Myc by Western blotting. Plots are means ± S.D. ($n = 3$). $^{*}p < 0.05$ versus non-treated control. $^{\#}p < 0.05$ versus CDDP-treated cells.

Cisplatin resistance by hyper-*O*-GlcNAcylation is regulated by p53 or c-Myc. To test whether *O*-GlcNAcylation of p53/c-Myc is a potential regulator of CDDP-induced apoptosis in lung cancer cells under specified context, NCI-H460 and NCI-H292 cells were ectopically transfected with p53 and c-Myc, respectively, and apoptosis in response to CDDP and KCZ co-treatment was determined. Figure 6A shows that p53-overexpressing NCI-H460 cells were more susceptible to CDDP-induced apoptosis than control transfected cells, yet they were protected by KCZ. On the other hand, c-Myc-overexpressing NCI-H292 cells were less susceptible to CDDP-induced apoptosis and had strengthening protective effect of KCZ compared to control cells (Fig. 6B). The effects of p53 and c-Myc overexpression in A549 and NCI-H23 cells are shown in Supplementary Figure S4.

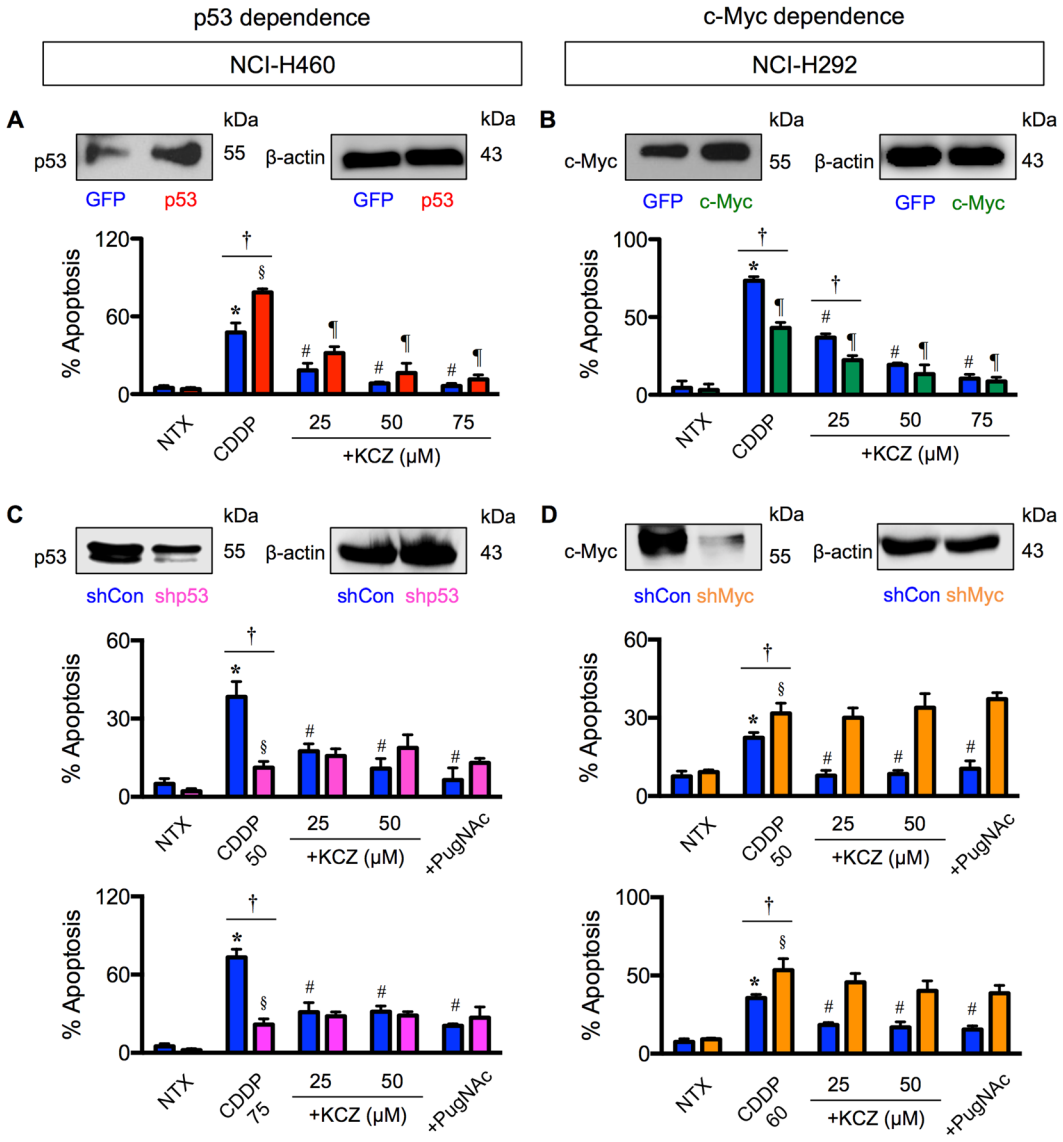

Figure 6. p53/c-Myc is crucial for *O*-GlcNAc-mediated cisplatin resistance. (**A**,**B**) Human lung carcinoma NCI-H460 and NCI-H292 cells were transfected with p53 or c-Myc expression plasmid, co-treated with cisplatin (CDDP; 50 μM in NCI-H460 and 100 μM in NCI-H292 cells) and ketoconazole (KCZ; 25–75 μM), and analyzed for apoptosis by Hoechst 33342 assay at 24 h. (**C**,**D**) p53 and c-Myc knockdown experiments were performed using NCI-H460 or NCI-H292 cells treated with retroviral particles carrying shp53 or with lentiviral particles carrying shMyc. Cells were co-treated CDDP (50–75 μM in NCI-H460 and 50–60 μM in NCI-H292 cells) and KCZ (25–50 μM), and similarly analyzed for apoptosis at 24 h post-treatment. Plots are means ± S.D. ($n = 3$). $^{*,§}p < 0.05$ versus non-treated GFP or p53/c-Myc-overexpressed cells and non-treated shCon or shp53/shMyc cells. $^{\#}p < 0.05$ versus CDDP-treated GFP or p53/c-Myc-overexpressed cells and CDDP-treated shCon cells. $^{\dagger}p < 0.05$ versus CDDP-treated GFP cells and CDDP-treated shp53/shMyc cells.

To verify that p53/c-Myc is required for *O*-GlcNAc-mediated cisplatin resistance, p53 and c-Myc expression were inhibited by RNA interference using short hairpin RNAs against *TP53* (shp53) and *MYC* (shMyc) in NCI-H460 and NCI-H292 cells, and their effects on apoptosis inhibition by OGA inhibitor were examined. Figure 6C,D shows that knockdown of p53 rendered NCI-H460 cells to CDDP resistance, while knockdown of c-Myc sensitized NCI-H292 cells to CDDP. KCZ noticeably failed to protect cells from CDDP-induced apoptosis in both NCI-H460-shp53 cells and NCI-H292-shMyc cells, the results that were confirmed by another OGA inhibitor PugNAc, indicating that p53/c-Myc is critical for the apoptosis inhibition by *O*-GlcNAcylation. Altogether, these results indicate that CDDP-induced apoptosis was regulated in part by *O*-GlcNAcylation of p53 or c-Myc. Accordingly, we classified CDDP resistance by hyper-*O*-GlcNAcylation in lung carcinoma cells as either p53 or c-Myc dependence based on the target of *O*-GlcNAcylation.

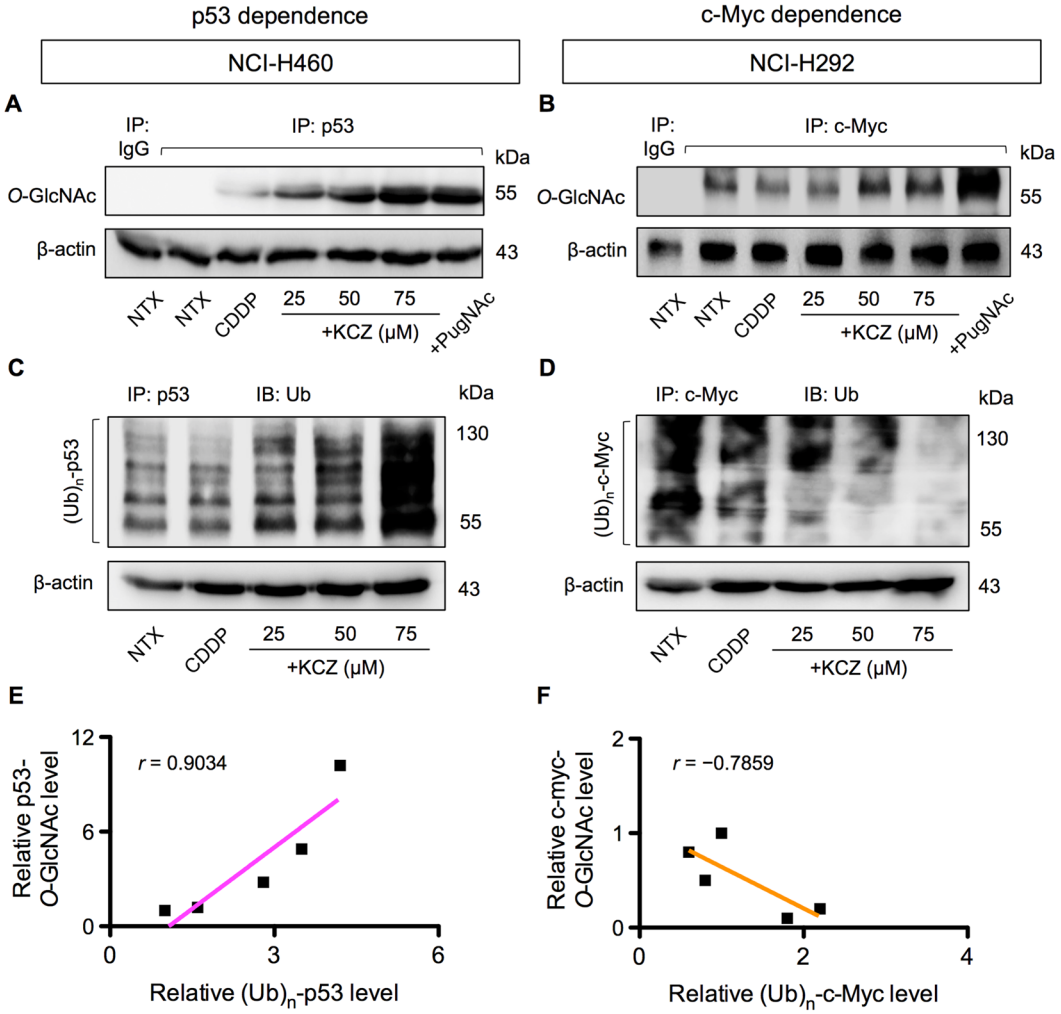

Figure 7. *O*-GlcNAcylation of p53 and c-Myc interferes with their ubiquitin-proteasomal degradation in cisplatin-treated cells. NCI-H460 cells and NCI-H292 cells were treated with CDDP and KCZ for 3 h, and cell lysates were prepared and immunoprecipitated using anti-p53 and anti-c-Myc antibodies. The immune complexes were analyzed for *O*-GlcNAcylation (**A**,**B**) or ubiquitination (Ub) (**C**,**D**) by Western blotting. Immunoblots were performed on cell lysates served as IP input using anti-β-actin antibody to confirm equal loading of the samples. (**E**,**F**) Correlation analysis of *O*-GlcNAcylation and ubiquitination of p53 and c-Myc in CDDP-treated cells in the presence or absence of KCZ.

Effects of *O*-GlcNAcylation on ubiquitination of p53 and c-Myc. PTMs are the key mechanism that diversifies the proteome complexity and are known to influence protein stability and function[23,24]. Ubiquitination is a major PTM that occurs on Ser and/or Thr residues and controls protein degradation and stability via ubiquitin-proteasomal pathway[25]. As *O*-GlcNAcylation similarly occurs on Ser and/or Thr residues of protein, it is conceivable that *O*-GlcNAcylation of p53 and c-Myc might interfere with their ubiquitination and subsequent expression. NCI-H460 and NCI-H292 cells were treated with CDDP and KCZ, and p53 or c-Myc was immunoprecipitated and subjected to Western blot analysis using an *O*-GlcNAc-specific antibody (RL2). Figure 7A,B shows that while CDDP had a minimal effect on *O*-GlcNAcylation of p53 in NCI-H460 cells and of c-Myc in NCI-H292 cells, KCZ indeed stimulated hyper-*O*-GlcNAcylation of p53 and c-Myc. Similar results were observed when the cells were treated with another OGA inhibitor, PugNAc, thus confirming the inductive effect of OGA inhibitor on *O*-GlcNAcylation of p53 and c-Myc. Ubiquitination of p53 and c-Myc was further analyzed after the cells were similarly exposed to CDDP and KCZ. Figure 7C shows that KCZ significantly increased p53 ubiquitination in NCI-H460 cells in a dose-dependent manner in parallel with the observed increase in p53 *O*-GlcNAcylation (Fig. 7A) and the decrease in its expression (Fig. 5A). Further analysis of the correlation between p53 *O*-GlcNAcylation and ubiquitination revealed the positive relationship of the two events with a correlation coefficient (r) of 0.9034 (Fig. 7E), supporting the notion that ubiquitin-mediated p53 degradation was strengthen by its *O*-GlcNAcylation. By contrast, KCZ remarkably decreased c-Myc ubiquitination in NCI-H292 cells in concomitant with the observed decrease in *O*-GlcNAcylation (Fig. 7D), an inverse relationship with an r value of −0.7859 (Fig. 7F), and with the increase in its expression (Fig. 5B), thus substantiating the interfering

effect of *O*-GlcNAcylation on c-Myc ubiquitination. Taken together, our findings support that *O*-GlcNAcylation of certain target proteins, e.g. p53 and c-Myc, interferes with their ubiquitination, affecting protein stability and apoptotic responses of lung carcinoma cells to chemotherapy.

Discussion

Lung cancer is one of the leading causes of cancer-related death worldwide, partly due to an innate and acquired resistance to chemotherapy that critically limits the outcome of treatments[26,27]. Comprehensive understanding of the molecular basis of apoptosis resistance would facilitate in the identification of potential novel therapeutic targets. The present study identifies the previously unknown role of hyper-*O*-GlcNAcylation in lung carcinoma cells in regulating a distinct set of target proteins that involve in apoptosis resistance to CDDP, the frontline chemotherapy for both non-small cell lung carcinoma (NSCLC) and small cell lung carcinoma (SCLC)[28,29].

Reprogramming in glucose metabolism and energy production in cancers has been substantiated for decades, known as the Warburg effect, in which cancer cells increase glucose uptake and rely preferentially on aerobic glycolysis instead of oxidative phosphorylation for ATP production, even under normoxic conditions[30,31]. The HBP is a branch of glucose metabolism that consumes approximately 5% of total glucose, and thus the abundance of glucose in cancer cells may also drive this pathway and ultimately elevate *O*-GlcNAcylation. Immunohistochemical analysis of tissue microarrays revealed an increase in global *O*-GlcNAcylation in lung cancer tissues compared with their corresponding normal adjacent tissues[11]. Additionally, we analyzed the mRNA expression of *OGT* and *MGEA5* (encoded OGA) using Oncomine™ bioinformatics database and found a remarkable increase in the *OGT* and/or a decrease in the *MGEA5* in lung carcinoma tissues compared with normal lung tissues in many datasets (Fig. 1).

To investigate the role of *O*-GlcNAcylation in the apoptosis response of lung carcinoma to CDDP, we used small molecule inhibitors of OGA and CRISPR-mediated repression of *MGEA5* to elevate the level of global *O*-GlcNAcylation. We observed that in all lung carcinoma cell lines examined hyper-*O*-GlcNAcylation protects the cells from CDDP-induced apoptosis (Figs 2 and 3). To address the potential mechanisms of how *O*-GlcNAcylation rendered lung carcinoma cells to apoptosis resistance, we first identified the changes in apoptosis-regulatory proteins during hyper-*O*-GlcNAcylation. We found that although CDDP disrupted the balance of Bcl-2/Bax ratio in favor of apoptosis, hyper-*O*-GlcNAcylation had minimal effect on the disrupted balance (Fig. 4), indicating that *O*-GlcNAcylation did not protect against CDDP-induced apoptosis through the Bcl-2/Bax axis.

Aberrant p53 tumor suppressor and/or c-Myc oncogene expression is a common feature in the majority of human cancers. p53 mutations, i.e. missense mutations, frameshift insertions and deletions, and point mutations, were reported to occur in approximately 50% of NSCLC and 80% of SCLC[32,33], while c-Myc mutations, i.e. DNA amplification overexpression, were more common in SCLC in up to 40% of all cases[33]. Here, we found that hyper-*O*-GlcNAcylation could render lung carcinoma cells to apoptosis resistance through distinct mechanisms that involve p53 or c-Myc, depending on cellular context, i.e. the presence of active p53. In lung carcinoma cells with high CDDP-induced p53 activation, hyper-*O*-GlcNAcylation targets p53, promotes its ubiquitination and subsequent p53 degradation, resulting in the gain of oncogenic and anti-apoptotic functions (Figs 5–7). By contrast in lung carcinoma cells with low p53 activation, hyper-*O*-GlcNAcylation has minimal effect on p53 and instead regulates c-Myc stability by interfering with its ubiquitin-mediated degradation. These notions are supported by the correlation analysis between *O*-GlcNAcylation and ubiquitination of p53 or c-Myc. Based on the observed findings, we proposed two distinct mechanisms of CDDP resistance in lung carcinoma that are either p53 dependence or c-Myc dependence, as schematically summarized in Fig. 8. It is worth noting that our finding on the induction of p53 degradation by hyper-*O*-GlcNAcylation is inconsistent with a previous study in breast cancer cells that reported the stabilization of p53 by *O*-GlcNAcylation at Ser 149 through the weakening of phosphorylation at Thr 155[18]. We postulate that this discrepancy may be due to the distinct effect of site-specific *O*-GlcNAcylation that is supported by the previous reports showing: (i) p53 contains multiple sites for *O*-GlcNAcylation[18]; and (ii) the major target of CDDP-induced phosphorylation is Ser 15[34,35].

In conclusion, our findings unveil a novel mechanism of chemoresistance in lung cancer cells that involves *O*-GlcNAcylation of p53 and c-Myc, which in turn interferes with their ubiquitin-proteasomal degradation. As hyper-*O*-GlcNAcylation is one of the initial events for lung cancer cells to escape from apoptosis, suppression of this PTM may serve as a novel therapeutic strategy for resistant lung cancers.

Materials and Methods

Oncomine™ bioinformatics database analysis. mRNA expression of *OGT* and *MGEA5* in lung adenocarcinoma tissues were analyzed in comparison to normal lung tissues from 8 available datasets in Oncomine™ bioinformatics database (https://www.oncomine.org/resource/login.html). The reporter ID (#) and platform for each analyzed dataset were as follows: Bhattachajee Lung #38614_s_at on Human Genome U95A-Av2 Array; Garber Lung #IMAGE:143790 (not Oncomine™ pre-defined platform); Hou Lung 207563_s_at on Human Genome U133 Plus 2.0 Array; Landi Lung #207563_s_at on Human Genome U133A Array; Okayama Lung #207563_s_at on Human Genome U133 Plus 2.0 Array; Selamat Lung #ILMN_1697639 on Illumina HumanWG-6 v3.0 Expression Beadchip; Stearman Lung #38614_s_at on Human Genome U95A-Av2 Array; and Su Lung #207563_s_at on Human Genome U133A Array. The P value for statistical significance was set up as 0.05, while the fold change was defined as all.

Cell culture. Human lung carcinoma cell lines, including NCI-H460, NCI-H292, NCI-H23 and A549 cells, were obtained from American Type Culture Collection (ATCC; Manassas, VA). A549 cells were cultured in DMEM medium supplemented with 10% fetal bovine serum (FBS), 2 mM L-glutamine, 100 U/ml penicillin and 100 μg/ml streptomycin, while all other cells were cultured in RPMI 1640-based medium in 5% CO_2 environment at 37 °C.

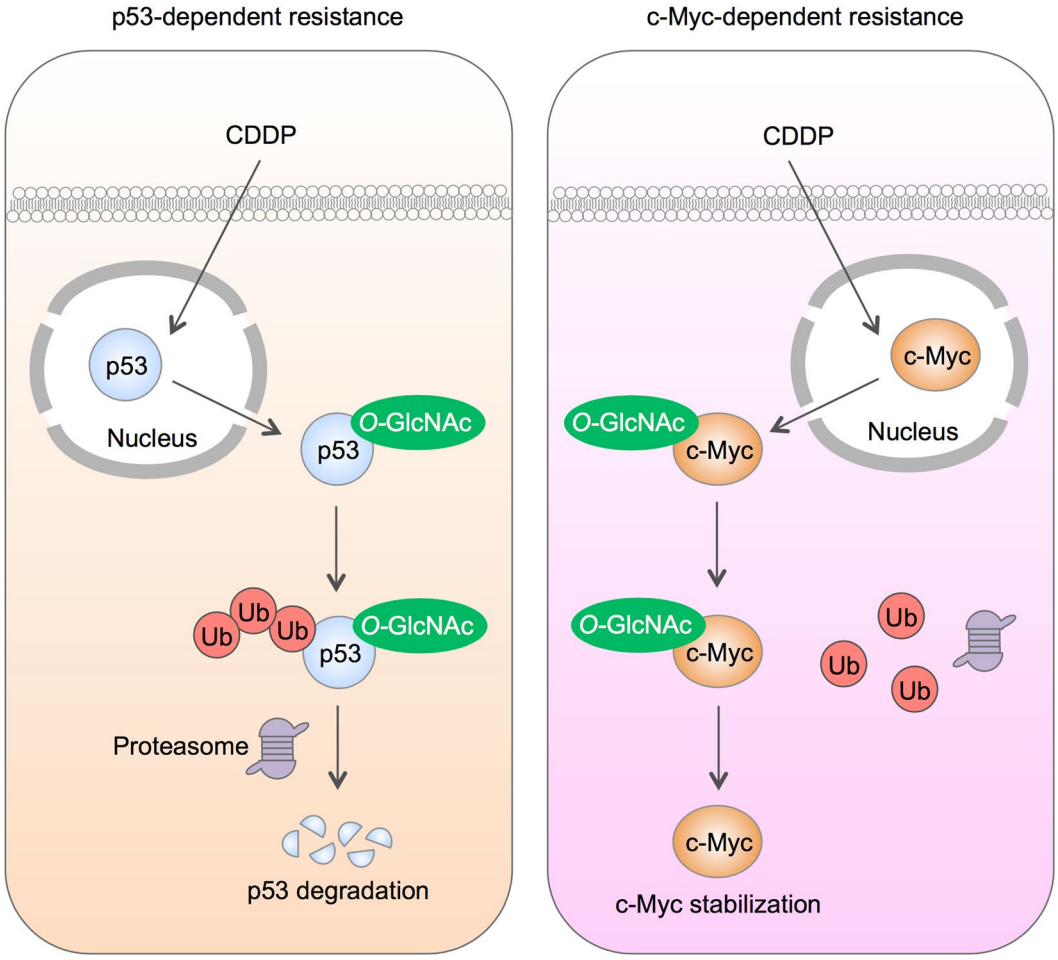

Figure 8. A schematic working model for the mechanisms of cisplatin resistance mediated by *O*-GlcNAcylation. Depending on the cellular context, *O*-GlcNAcylation targets either p53 or c-Myc in cisplatin-treated cells and interferes with its ubiquitin-mediated proteasomal degradation that causes either p53 degradation or c-Myc stabilization.

Reagents. Small molecule inhibitors of OGA PugNAc and thiamet G were obtained from Abcam (Cambridge, UK), while ketoconazole (KCZ)[12] was from Crosschem Intercontinental Company, Derb & Co. (Lugano, Switzerland). *Cis*-diamminedichloroplatinum II (cisplatin, CDDP) was obtained from Sigma-Aldrich (St. Louis, MO). Hoechst 33342 and propidium iodide (PI) were obtained from Molecular Probes (Eugene, OR). Antibodies for *O*-GlcNAc and ubiquitin were obtained from Abcam, while antibody for p53 was from Santa Cruz Biotechnology (Dallas, Texas). All other antibodies and proteasome inhibitor MG132 were from Cell Signaling Technology (Beverly, MA).

CRISPR guide RNA design, vector construction and lentivirus production. CRISPR/Cas9 system containing Cas9 nuclease (Addgene #52962, Cambridge, MA) and two gRNAs was used to induce transcriptional repression of *MGEA5*. Briefly, gRNAs targeting *MGEA5* (sequence #1: CACAGCCTCGCTCTCCGCTT and #2: CGCAAGCGCAGTGCGGATAAAC) were designed using CRISPR Design tool (http://crispr.mit.edu/) and cloned into human gRNA expression vector containing a mouse U6 promoter and a constitutive CMV promoter driving an *mCherry* gene (Addgene plasmid #44248)[36], as described previously[37]. Lentivirus production was performed using HEK293T packaging cells (ATCC) in conjunction with pCMV.dR8.2 dvpr lentiviral packaging and pCMV-VSV-G envelope plasmids (Addgene plasmids #8454 and 8455)[38]. Cells were incubated with Cas9 and gRNA viral particles in the presence of hexadimethrine bromide (HBr) for 48 h. The transfection efficiency was determined by using an mCherry reporter and was found to be ~80%.

Short hairpin RNA-mediated gene knockdown. Retroviral and lentiviral plasmids carrying short hairpin RNA sequences against human *TP53* and *MYC* were obtained from Addgene (plasmids #10672 and 29435)[39,40]. Retrovirus production was performed using Platinum-A packaging cell lines and lentivirus production was performed using HEK293T packaging cells as described above. Cells were incubated with shp53 or shMyc viral particles in the presence of HBr for 36 h and p53 and c-Myc knockdown was analyzed prior to use by Western blotting.

Plasmids and transfection. Control GFP and p53 plasmids were obtained from Invitrogen (Carlsbad, CA), while c-Myc plasmid was a gift from Wafik El-Diery (Addgene plasmid #16011)[41]. Briefly, 1×10^6 cells were suspended in 100 μl nucleofection solution SF and transfected with 2 μg of plasmid by nucleofection using 4D Nucleofector™ (Lonza, Cologne, Germany) with EH-158 device program. The transfected cells were checked for GFP fluorescence, and p53 and c-Myc expression levels were identified by Western blotting.

Apoptosis assay. Apoptosis was determined by Hoechst 33342 assay and by cell diameter and DNA content analyses. In the Hoechst assay, cells were incubated with 10 μg/ml Hoechst 33342 for 30 min and analyzed for apoptosis by scoring the percentage of cells having condensed chromatin and/or fragmented nuclei by fluorescence microscopy (Eclipse Ti-U with NiS-Elements, Nikon, Tokyo, Japan). The apoptotic index was calculated as the percentage of cells with apoptotic nuclei over total number of cells. For DNA content analysis, cells were harvested, fixed with ice cold 70% ethanol overnight and stained with propidium iodide (PI) solution (50 μg/ml; Molecular Probes) containing 0.2% Tween 20 and 1 μg/ml RNase at room temperature for 30 min. PI fluorescence was analyzed using flow cytometry (BD LSRII; Becton Dickinson, Rutherford, NJ) at the excitation and emission wavelengths of 535 nm and 617 nm and fragmented DNA (sub-G0 cell cycle phase) was determined. Cell diameter was measured using an automated cell counter (Sceptor™ 2.0, Merck Millipore, Billerica, MA), which is an impedance-based particle detection system employing the Coulter principle that enables the discrimination of apoptotic cells[42].

RNA isolation and RT-PCR. Total RNA was prepared using TRIzol reagent (Invitrogen) and cDNA was prepared using SuperScript III first-strand synthesis system and oligo (dT) primers (Invitrogen). qPCR analysis was carried out on a 7500 Fast real-time PCR using a Power SYBR Green PCR master mix (Applied Biosystems, Foster City, CA). Initial enzyme activation was performed at 95 °C for 10 min, followed by 40 cycles of denaturation at 95 °C for 15 sec and primer annealing/extension at 60 °C for 1 min. Relative expression of each gene was normalized against the housekeeping *GAPDH* gene product.

Caspase-3 activity assay. Caspase activity was determined by detecting the cleavage of specific substrate DEVD-AFC using a commercial assay kit (Biovision, Milpitas, CA). After specific treatments, cell lysates were prepared and incubated with DEVD-AFC (50 μM) for 1 h. AFC fluorescence was measured using a fluorescence plate reader (Synergy H1, BioTek, Winooski, VT) at the 400-nm and 520-nm excitation and emission wavelengths. Caspase-3 activity was expressed as the ratio of signals from the treated and control samples.

Western blot analysis. After specific treatments, cells were incubated in a commercial lysis buffer (Cell Signaling Technology) and a protease inhibitor mixture (Roche Molecular Biochemicals, Indianapolis, IN) at 4 °C for 30 min. Protein content was analyzed using BCA protein assay (Pierce Biotechnology, Rockford, IL) and 50 μg of proteins were resolved under denaturing conditions by SDS–PAGE and transferred onto PVDF membranes. Membranes were blocked with 5% nonfat dry milk, incubated with appropriate primary antibodies at 4 °C overnight, and subsequently incubated with peroxidase-conjugated secondary antibodies for 1 h at room temperature. The immune complexes were analyzed by enhanced chemiluminescence detection system on a digital imager (ImageQuant LAS, GE Healthcare, Pittsburgh, PA).

Co-immunoprecipitation, ubiquitination, and *O*-GlcNAcylation. Cell lysates (200 μg protein) were immunoprecipitated using Dynabeads Protein G magnetic beads (Invitrogen). Briefly, the beads were conjugated with anti-p53 or anti-c-Myc antibody for 10 min at room temperature. The conjugated beads were then resuspended with cell lysates for 30 min at room temperature. The immune complexes were washed four times and resuspended in 2x Laemmli sample buffer. They were then separated by SDS-PAGE and analyzed for ubiquitination or *O*-GlcNAcylation using anti-ubiquitin or anti-*O*-GlcNAc (RL2) antibody respectively.

Statistical analysis. The data represent means ± s.d. from three or more independent experiments as indicated. Statistical analysis was performed by Student's *t*-test at a significance level of $p < 0.05$.

References

1. Hanahan, D. & Weinberg, R. A. Hallmarks of cancer: the next generation. *Cell* **144**, 645–674 (2011).
2. Cheong, H., Lu, C., Lindsten, T. & Thompson, C. B. Therapeutic targets in cancer cell metabolism and autophagy. *Nat. Biotechnol.* **30**, 671–678 (2012).
3. Bond, M. R. & Hanover, J. A. A little sugar goes a long way: the cell biology of O-GlcNAc. *J. Cell Biol.* **208**, 869–880 (2015).
4. Hu, P., Shimoji, S. & Hart, G. W. Site-specific interplay between O-GlcNAcylation and phosphorylation in cellular regulation. *FEBS Lett.* **585**, 2526–2538 (2010).
5. Hart, G. W., Slawson, C., Ramirez-Correa, G. & Lagerlof, O. Cross talk between O-GlcNAcylation and phosphorylation: roles in signaling, transcription, and chronic disease. *Annu. Rev. Biochem.* **80**, 825–858 (2011).
6. de Queiroz, R. M., Carvalho, E. & Dias, W. B. O-GlcNAcylation: the sweet side of the cancer. *Front. Oncol.* **4**, 132 (2014).
7. Ma, Z. & Vosseller, K. Cancer metabolism and elevated O-GlcNAc in oncogenic signaling. *J. Biol. Chem.* **289**, 34457–34465 (2014).
8. Ma, Z., Vocalldo, D. J. & Voseller, K. Hyper-O-GlcNAcylation is anti-apoptotic and maintains constitutive NF-κB activity in pancreatic cancer cells. *J. Biol. Chem.* **288**, 15121–15130 (2013).
9. Caldwell, S. A. *et al.* Nutrient sensor O-GlcNAc transferase regulates breast cancer tumorigenesis through targeting of the oncogenic transcription factor FoxM1. *Oncogene* **29**, 2831–2842 (2010).
10. Rao, X. *et al.* O-GlcNAcylation of G6PD promotes the pentose phosphate pathway and tumor growth. *Nat. Commun.* **6**, 8468 (2015).
11. Mi, W. *et al.* O-GlcNAcylation is a novel regulator of lung and colon cancer malignancy. *Biochim. Biophys. Acta* **1812**, 514–519 (2011).
12. Dorfmueller, H. C. & van Aalten, D. M. F. Screening-based discovery of drug-like O-GlcNAcase inhibitor scaffolds. *FEBS Lett.* **584**, 694–700 (2010).
13. Li, J. & Li, Y. Caspases in apoptosis and beyond. *Oncogene* **27**, 6194–6206 (2008).

14. Chanvorachote, P. *et al*. Nitric oxide regulates cell sensitivity to cisplatin-induced apoptosis through S-nitrosylation and inhibition of Bcl-2 ubiquitination. *Cancer Res.* **66**, 6353–6360 (2006).
15. Wu, H. M., Jiang, Z. F., Ding, P. S., Shao, L. J. & Liua, R. Y. Hypoxia-induced autophagy mediates cisplatin resistance in lung cancer cells. *Sci. Rep.* **5**, 12291 (2015).
16. Chou, T. Y., Dang, C. V. & Hart, G. W. Glycosylation of the c-Myc transactivation domain. *Proc. Natl. Acad. Sci. U. S. A.* **92**, 4417–44121 (1995).
17. Itkonen, H. M. *et al*. O-GlcNAc transferase integrates metabolic pathways to regulate the stability of c-MYC in human prostate cancer cells. *Cancer Res.* **73**, 5277–5287 (2013).
18. Yang, W. H. *et al*. Modification of p53 with O-linked N-acetylglucosamine regulates p53 activity and stability. *Nat. Cell Biol.* **8**, 1074–1083 (2006).
19. de Queiroz, R. M., Madan, R., Chien, J., Dias, W. B. & Slawson, C. Changes in O-linked N-acetylglucosamine (O-GlcNAc) homeostasis activate the p53 pathway in ovarian cancer cells. *J. Biol. Chem.* **291**, 18897–18914 (2016).
20. Yoshikawa, H. *et al*. Mutational analysis of p73 and p53 in human cancer cell lines. *Oncogene* **18**, 3415–3421 (1999).
21. Jia, L. Q. *et al*. Screening the p53 status of human cell lines using a yeast functional assay. *Mol. Carcinogen.* **19**, 243–253 (1997).
22. Takahashi, T. *et al*. Wild-type but not mutant p53 suppresses the growth of human lung cancer cells bearing multiple genetic lesions. *Cancer Res.* **52**, 2340–2343 (1992).
23. Duan, G. & Walther, D. The roles of post-translational modifications in the context of protein interaction networks. *PLoS Comput. Biol.* **11**, e1004049 (2015).
24. Swaney, D. L. *et al*. Global analysis of phosphorylation and ubiquitylation cross-talk in protein degradation. *Nat. Methods* **10**, 676–682 (2013).
25. Mani., A. & Gelmann, E. P. The ubiquitin-proteasome pathway and its role in cancer. *J. Clin. Oncol.* **23**, 4776–4789 (2005).
26. Shanker, M., Willcutts, D., Roth, J. A. & Ramesh, R. Drug resistance in lung cancer. *Lung Cancer: Targets and Therapy* **1**, 23–36 (2010).
27. Tsvetkova, E. & Goss, G. D. Drug resistance and its significance for treatment decisions in non-small-cell lung cancer. *Curr. Oncol.* **19**, S45–S51 (2012).
28. Sculier, J. P. & Moro-Sibilot, D. First- and second-line therapy for advanced nonsmall cell lung cancer. *Eur. Respir. J.* **33**, 915–930 (2009).
29. Rossi, A. *et al*. Carboplatin- or cisplatin-based chemotherapy in first-line treatment of small-cell lung cancer: the COCIS meta-analysis of individual patient data. *J. Clin. Oncol.* **30**, 1692–1698 (2012).
30. Elstrom, R. L. *et al*. Akt stimulates aerobic glycolysis in cancer cells. *Cancer Res.* **64**, 3892–3899 (2004).
31. Lv, X. B. *et al*. SUN2 exerts tumor suppressor functions by suppressing the Warburg effect in lung cancer. *Sci. Rep.* **5**, 17940 (2015).
32. Salgia, R. & Skarin, A. T. Molecular abnormalities in lung cancer. *J. Clin. Oncol.* **16**, 1207–1217 (1998).
33. Mogi, A. & Kuwano, H. TP53 mutations in nonsmall cell lung cancer. *J. Biomed. Biotechnol.* **2011**, 583929 (2011).
34. Mujoo, K., Watanabe, M., Nakamura, J., Khokhar, A. R. & Siddik, Z. H. Status of p53 phosphorylation and function in sensitive and resistant human cancer models exposed to platinum-based DNA damaging agents. *J. Cancer Res. Clin. Oncol.* **129**, 709–718 (2003).
35. Damia, G. *et al*. Cisplatinum and taxol induce different patterns of p53 phosphorylation. *Neoplasia* **3**, 10–16 (2001).
36. Qi, L. S. *et al*. Repurposing CRISPR as an RNA-guided platform for sequence-specific control of gene expression. *Cell* **152**, 1173–1183 (2013).
37. Larson, M. H. *et al*. CRISPR interference (CRISPRi) for sequence-specific control of gene expression. *Nat Protoc* **8**, 2180–2196 (2013).
38. Stewart, S. A. *et al*. Lentivirus-delivered stable gene silencing by RNAi in primary cells. *RNA* **9**, 493–501 (2003).
39. Masutomi, K. *et al*. Telomerase maintains telomere structure in normal human cells. *Cell* **114**, 241–253 (2003).
40. Lin, C. H., Jackson, A. L., Guo, J., Linsley, P. S. & Eisenman, R. N. Myc-regulated microRNAs attenuate embryonic stem cell differentiation. *EMBO J.* **28**, 3157–3170 (2009).
41. Ricci, M. S. *et al*. Direct repression of FLIP expression by c-myc is a major determinant of TRAIL sensitivity. *Mol. Cell. Biol.* **24**, 8541–8555 (2004).
42. Tahara, M. *et al*. Cell diameter measurements obtained with a handheld cell counter could be used as a surrogate marker of G2/M arrest and apoptosis in colon cancer cell lines exposed to SN-38. *Biochem. Biophys. Res. Commun.* **434**, 753–759 (2013).

Acknowledgements

This work was supported by grants from Thailand Research Fund [RTA 488-0007] (to S. I.) and [TRG5980013] (to S. L.) and the Commission on Higher Education [CHE-RES-RG-49] (to S. I.). S. Issaragrisil is a Senior Research Scholar of Thailand Research Fund. We would like to thank Prof. Yon Rojanasakul for his comments on the manuscript.

Author Contributions

S.L. designed research, coordinated the project, and analyzed the data. S.L., P.A., P.S. and N.C. carried out experiments. P.C. participated in the design of the study. S.I. conceived the project. S.L. and S.I. prepared the manuscript. All authors read and approved the final manuscript.

Additional Information

Supplementary information accompanies this paper at doi:10.1038/s41598-017-10886-x

Competing Interests: The authors declare that they have no competing interests.

Publisher's note: Springer Nature remains neutral with regard to jurisdictional claims in published maps and institutional affiliations.

Redox Status Dictates the Susceptibility of Mantle Cell Lymphoma to Bortezomib

Sudjit Luanpitpong[1], Nawin Chanthra[1], Paweorn Angsutararux[1], Surapol Issaragrisil[1]

[1]Siriraj Center of Excellence for Stem Cell Research, Faculty of Medicine Siriraj Hospital, Mahidol University, Bangkok 10700, Thailand.

ABSTRACT

Mantle cell lymphoma (MCL) is an aggressive non-Hodgkin B-cell lymphoma with disappointing 5-year survival rate. While proteasome inhibitor bortezomib (BTZ) has remarkably improved therapeutic outcome of relapsed and refractory MCL, substantial numbers of MCL patients are either intrinsic or acquired resistance to BTZ. An increased reactive oxygen species (ROS) is observed in the microenvironment of various aggressive tumors, including B-cell lymphoma, but how ROS affects MCL cellular behaviors is still limit. Superoxide anion ($^{\bullet}O_2^-$) is the primary free radical generated from aerobic cellular metabolism of tumor cells themselves and/or neighboring cells. Here, we investigated the roles of $^{\bullet}O_2^-$ in the regulation of MCL aggressive cancer phenotypes. Using various known small molecule inhibitors and donor of cellular $^{\bullet}O_2^-$, we revealed for the first time an inverse correlation between the level of $^{\bullet}O_2^-$ and aggressive phenotypes. $^{\bullet}O_2^-$ inhibits MCL clonal expansion, cell proliferation and sensitizes MCL apoptosis induced by BTZ. We further observed that expression of anti-apoptotic Mcl-1 is a favorable target of $^{\bullet}O_2^-$. Using pharmacological inhibition and gene manipulation, we verified that Mcl-1 is responsible for apoptosis sensitizing effect by $^{\bullet}O_2^-$. These findings identify an important role of redox status of the cells in determining their aggressive phenotypes, which are imperative to a better understanding of therapeutic resistance and pathophysiology of aggressive B-cell lymphoma.

BACKGROUND

- MCL is an aggressive form of non-Hodgkin B-cell lymphoma that is typically incurable, due to intrinsic drug resistance.
- $^{\bullet}O_2^-$ is a major initial ROS found in tumor microenvironment.

$$^{\bullet}O_2^- \xrightarrow[\text{SOD}]{} H_2O_2 \xrightarrow[Fe^{2+}]{} {}^{\bullet}OH$$

METHODOLOGY

Small molecule inducer and inhibitors: Intracellular $^{\bullet}O_2^-$ was induced by DMNQ and inhibited by an SOD mimetic MnTBAP and SOD enzyme. Mcl-1 was inhibited by MIM1 and Mcl-1 inhibitor II.
Cell proliferation: Cell count was performed by Sceptor™.
Apoptosis assay: Apoptosis was evaluated by Hoechst assay.
Clonal expansion: Clonal expansion was performed using methylcellulose clonogenicity assay (Stem Cell Technologies).

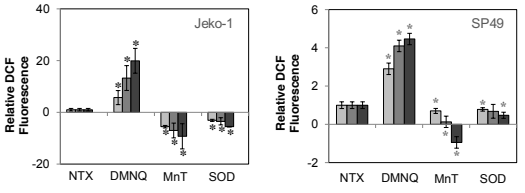

Figure 1. Effect of $^{\bullet}O_2^-$ modulators on cellular ROS. MCL Jeko-1 and SP49 cells were treated with various concentrations of DMNQ (2.5-7.5 μM), MnTBAP (MnT; 10-25 μM) and SOD (50-100 U/mL) and intracellular ROS was analyzed by fluorescence reader using H_2DCF-DA as an oxidative probe. *P < 0.05 vs NTX cells.

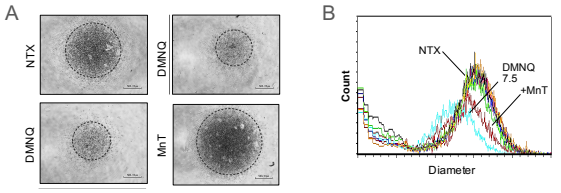

Figure 2. $^{\bullet}O_2^-$ inhibits MCL clonal expansion and cell proliferation. MCL Jeko-1 cells were treated with DMNQ (7.5 μM) and/or MnTBAP (MnT; 25 μM) for 3 days. (A) Representative tumor spheres of treated cells after 10 days in methylcellulose culture. (B) Representative histograms of cell size and count using Scepter™ automated Coulter counter.

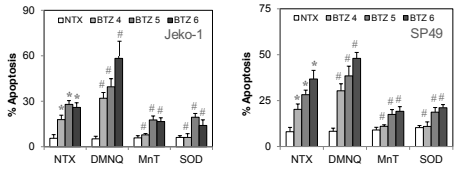

Figure 3. $^{\bullet}O_2^-$ sensitizes MCL cells to BTZ-induced apoptosis. MCL Jeko-1 and SP49 cells were treated with DMNQ (5 μM), MnTBAP (MnT; 25 μM) or SOD (100 U/mL) for 3 days, following by BTZ (0-6 nM) for 24 hours and apoptosis was determined. *P < 0.05 vs NTX. #P < 0.05 vs BTZ-treated NTX cells.

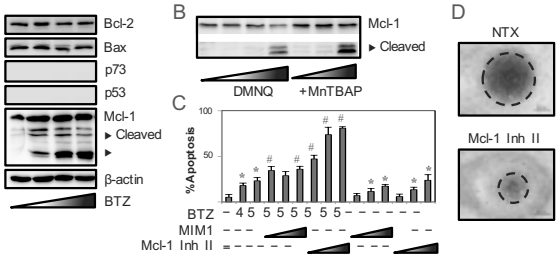

Figure 4. Mcl-1 is a favorable target of $^{\bullet}O_2^-$ in MCL. (A) BTZ induces Mcl-1 fragment, suggesting that BTZ-induced apoptosis is mediated through Mcl-1. (B) $^{\bullet}O_2^-$ downregulates Mcl-1 in a dose-dependent manner. (C, D) Inhibition of Mcl-1 potentiates BTZ-induced apoptosis (C) and suppresses MCL clonal expansion (D). *P < 0.05 vs NTX. #P < 0.05 vs BTZ-treated NTX cells.

CONCLUSIONS

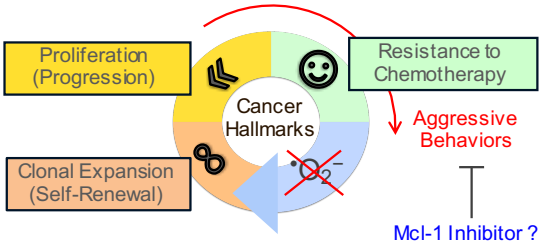

Zeb-1 contributes to the development of chemotherapeutic resistance in mantle cell lymphoma

Sudjit Luanpitpong[1], Jirarat Poohadsuan[1], Montira Janan[1], Kanjana Thumanu[2], Yon Rojanasakul[3], Surapol Issaragrisil[1]

[1]Siriraj Center of Excellence for Stem Cell Research, Faculty of Medicine Siriraj Hospital, Mahidol University, Bangkok 10700, Thailand; [2]Synchrotron Light Research Institute, Nakhon Ratchasima 30000, Thailand; [3]WVU Cancer Institute, Morgantown, West Virginia 26506, USA.

BACKGROUND

- Mantle cell lymphoma (MCL) is an aggressive form of non-Hodgkin B-cell lymphoma, that is typically incurable due to the inevitable development of drug resistance.
- MCL complete response is still limit and relapse rates hover around 50%.
- Understanding how MCL cells acquire resistance at the molecular level may be a key innovation to targeted therapy.
- Previous study identified Zeb-1 as a central transcription component of adipogenic cell differentiation[1].

METHODOLOGY

- Model: *De novo* bortezomib (BTZ)-resistant MCL Jeko-1 cell lines at various levels, i.e. up to 500 nM, as determined by magnitute of apoptosis using Hoechst 33342 assay.
- Gene/protein profiling: PCR array or Western blot analysis of genes/proteins related to drug resistance, drug metabolism, apoptosis, cell growth, cell cycle, Hippo signaling and pluripotency.
- Biosynthesis profiling: Synchrotron-based FTIR microscopy.
- Lipid storage: Oil red O staining.
- Cancer stem cell (CSC) detection: 3D lymphoma spheroids and ALDH activity and.

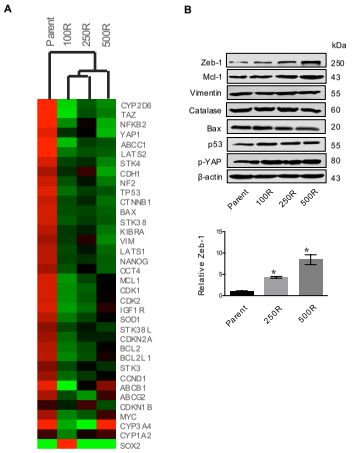

Fig. 1. (A) Gene profiling using PCR array reveals a down-regulation of most of the candidate genes in BTZ-resistant cells when compared to parental MCL cells. **(B)** Western blot analysis reveals a remarkably increase of Zeb-1, an EMT activator earlier shown to be important in MCL cell proliferation and tumor growth[2], in BTZ-resistant cells.

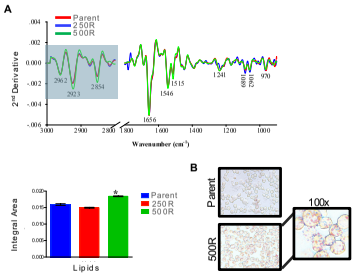

Fig. 2. (A) Synchrotron-based FTIR analysis at single cell level shows an aberrant lipid content in BTZ-resistant cells in correlation with **(B)** an increase in intracellular lipid droplets.

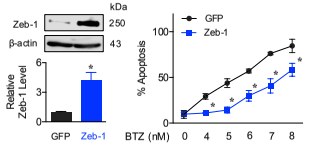

Fig. 3. Ectopic expression of Zeb-1 in parental MCL Jeko-1 cells render the cells to acquire apoptosis resistance to BTZ.

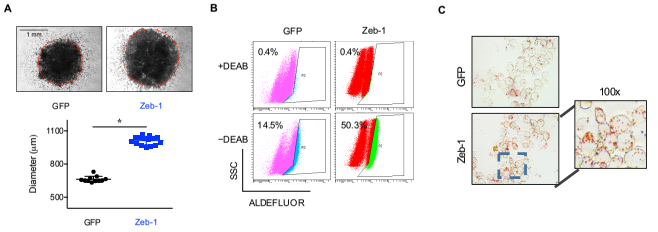

Fig. 4. (A) Ectopic expression of Zeb-1 results in an enlargement of 3D lymphoma spheroids. The relative apoptosis resistant levels are as follows: Zeb-1 spheroids > GFP spheroids > Zeb-1 suspension > GFP suspension (not shown). **(B)** Analysis of ALDH activity reveals a greater proportion of ALDH-positive cells in Zeb-1-overexpressing cells. **(C)** Oil red O staining shows an increase in intracellular lipid droplets in Zeb-1-overexpressing cells.

CONCLUSION

Our results unveils a novel role of Zeb-1 in MCL chemotherapeutic resistance via two possible encompassing mechanisms.

- Zeb-1 induces CSC-like cells.
- Zeb-1 induces lipid reprogramming.

Further studies are needed to validate the role of lipid in BTZ sensitivity.

References:

1. Gublemann et al. eLife 2014;3:e03346.
2. Sánchez-Tilló et al. Cell Death Differ 2014;21:247–257.

*This work was supported by grants from Thailand Research Fund (TRG5980013) and Faculty of Medicine Siriraj Hospital.